Groundwater and Surface Water Conceptual Flow from Environmental Tracer Signatures in the Pukekohe and Bombay Area

U Morgenstern
K Johnson
M Moreau
DB Townsend
MA Coble

GNS Science Report 2022/63
March 2023

GNS SCIENCE
TE PŪ AO

DISCLAIMER

BIBLIOGRAPHIC REFERENCE

Morgenstern U, Moreau M, Coble MA, Johnson K, Townsend DB. 2023. Groundwater and surface water conceptual flow from environmental tracer signatures in the Pukekohe and Bombay area. Lower Hutt (NZ): GNS Science. 97 p. (GNS Science report; 2022/63). doi:10.21420/VNBF-3X96.

U Morgenstern, GNS Science, PO Box 30368, Lower Hutt 5040, New Zealand

M Moreau, GNS Science, Private Bag 2000, Taupō 3352, New Zealand

MA Coble, GNS Science, PO Box 30368, Lower Hutt 5040, New Zealand

K Johnson, Auckland Council, Private Bag 92300, Victoria Street West, Auckland 1142, New Zealand

DB Townsend, GNS Science, PO Box 30368, Lower Hutt 5040, New Zealand

www.gns.cri.nz

ISSN 2350-3424 (online)
ISBN 978-1-99-105801-0 (online)
http://dx.doi.org/10.21420/VNBF-3X96

CONTENTS

FIGURES

TABLES

APPENDICES

APPENDIX FIGURES

ATTACHMENTS

(Attached to PDF)

GNS SR2022-63 – Data Output

GNS SR2022-63 Appendix 2 – CFC Analysis

GNS SR2022-63 Appendix 2 – Radon Analysis

GNS SR2022-63 Appendix 2 – SF_6 Analysis

GNS SR2022-63 Appendix 2 – Tritium Analysis

ABSTRACT

Better understanding of the following is needed to inform improved nutrient-management tools and water-take limits in the Pukekohe–Bombay area:

- Conceptual groundwater flow
- Connection with surface water
- Nitrate pathways
- Potential risk of nitrate contamination of deeper aquifers
- 'Future nitrate loads to come'
- Connections within the aquifer system.

Refined groundwater ages, together with hydrochemistry, water isotopes and atmospheric gas concentrations, enabled detailed understanding of groundwater flow processes.

Groundwaters in the aquifers underlaying the Pleistocene deposits and in the deep basalt aquifers are all old, implying very little active circulation through these deeper systems. Rain onto the Pleistocene deposits therefore drains, mainly during the wet season, through shallow, fast-flow paths, without sufficient storage reservoir to sustain significant stream flow during baseflow in the dry season.

Active subsurface drainage through large groundwater reservoirs only occurs through the basalt lava of the Pukekohe and Bombay volcanoes and, to a lesser extent, through the unconsolidated volcanic materials, including tuff and tephra. The active groundwater flow systems in the basalt lava have sufficient storage to maintain significant stream baseflow over the course of years.

Three main streams drain the basalt lava of the Pukekohe and Bombay volcanoes on their northern perimeters: Whangamaire Stream, Whangapouri Creek and Hingaia Stream. These streams have a combined groundwater storage of approximately 350 Mm^3. On the south-western flanks of these volcanoes, the upper reaches of the Mauku and Ngakoroa streams also receive discharge from the basalt lava. They have a combined groundwater storage of approximately 37 Mm^3.

Three main spring systems drain the basalt lava groundwater systems: Hickey, Hillview and Patumahoe springs. The average groundwater flow rates to these springs are approximately 190, 160, and 65 m/y, respectively.

Whangamaire Stream and Whangapouri Creek drain the Pukekohe basalt lava at the northern perimeter of the plateau, where they receive most of their flow. Groundwater age, isotopes and hydrochemistry match those of the water in these streams, including high nitrate concentrations. There is no significant flow gain north of the basalt lava within the Pleistocene deposits, indicating absence or insignificance of deep groundwater flux to these streams. This implies that these areas drain only via shallow flow paths that are depleted during summer baseflow conditions.

Hingaia Stream receives water in its upper reaches partially from impermeable greywacke basement rock catchments and partially from the north-eastern perimeter of the basalt lava. The mixing of water from the essentially pristine greywacke catchment with water recharged in areas of high nitrate leaching activities results in medium nitrate concentrations. At the northern perimeter of the volcanic cone, where Hillview Spring discharges into Hingaia Stream,

flow more than doubles, as does nitrate concentration. Groundwater ages, isotopes and hydrochemistry match those of the water discharging from Hillview Spring, including high nitrate concentrations.

In the upper reaches of Ngakoroa Stream, isotopes and nitrate indicate flow contribution from the south-western, low-altitude flanks of the Bombay basalt lava. North of the basalt, the stream does not gain any significant flow. However, nitrate concentration decreases significantly, probably due to in-stream processes.

Mauku Stream gains flow in its upper reaches from the Pukekohe basalt lava along its south-western perimeter. Groundwater ages, isotopes and hydrochemistry match those of the water in the upper reaches of the stream. From the north-western flanks of the Pukekohe basalt lava, the stream receives water from a groundwater system recharged at lower altitudes and likely to be anoxic. Stream flow more than doubles, while nitrate concentrations become diluted.

Oira Creek, having very low flow, discharges locally recharged, relatively old, groundwater with low nitrate concentrations. Similarly, Waitangi Stream discharges locally recharged groundwater with low nitrate concentrations. Both streams are likely to drain anoxic groundwater systems.

The most active groundwater drainage flow with the youngest water feeding the springs occurs near the surface of the water tables. Slightly deeper groundwater is older than expected for the upstream position in the active flow path towards the springs. Recharge to the deeper groundwater system is estimated to be 280 mm/y. As indicated by calculated recharge temperatures, recharge to the deeper groundwater system appears to be preferential flow through fractures, allowing fast flow to beneath the water table. This contrasts with the groundwater providing the spring discharges, which is recharged through matrix flow through the bulk material of the unsaturated zone.

Fracture flow in the shallow basalt lava appears to be unstable. In all four basalt lava wells in the Pukekohe and upper Waikato area with long-term monitoring data, hydrochemistry parameters (indicative of land use and geologic sources) have changed drastically over recent decades. These changes were permanent, usually from older to younger water, with raising water tables. This indicates changing capture zones for these wells, with each well changing at a different time.

Weathered basalts form rich horticultural soils. Since the 1950s, high-intensity market gardening, associated with high nitrate leaching, has resulted in high nitrate loads into the transmissive basalt lava of the Pukekohe and Bombay volcanoes. These basalt lavas discharge oxic groundwater into streams, indicating absence of organic matter and inorganic electron donors in the aquifer, which would be required for facilitation of microbial reactions, including denitrification. Without denitrification occurring, the nitrate load is expected to discharge from this basalt lava without any nitrate attenuation, with a lag time equal to the travel time (age) of the water through the aquifer.

On average, it takes 18 years for the nitrate load to travel through the Pukekohe basalt lava and 36 years to travel through the Bombay basalt lava. Assuming approximately constant nitrate load for circa 65 years since the onset of industrial agriculture in around 1955, these groundwater discharges from the basalt have essentially adjusted to the high land-use nitrate loads in the recharge areas. However, nitrate concentrations in the deeper groundwater are still increasing and adjusting to the high nitrate loads in the recharge areas. Due to the relatively

long lag times noted above, reducing land-use nitrate loads will take decades to manifest in the baseflow spring discharges of the basalt in the Pukekohe–Bombay area.

In contrast to the oxic water discharging from the basalt lava, significant amounts of water (approximately 60 L/s) discharge from the north-western flanks of the Pukekohe basalt lava that appear to be anoxic and low in nitrate, despite discharging from areas with land use associated with high nitrate leaching. There is potential for significant nitrate attenuation in this groundwater system. Denitrification may also be possible in the shallow drainage system of the Pleistocene deposits, near the redox zone.

KEYWORDS

Basalt aquifer, groundwater age, nitrate, lag time, denitrification, fracture flow, groundwater recharge mechanism, flow rates, groundwater storge, conceptual groundwater flow

This page left intentionally blank.

1.0 INTRODUCTION

Horticulture has been an economic mainstay in the Pukekohe–Bombay area for over 100 years, and high-intensity land use since the 1950s (Murphy 1991) has had a detrimental effect on groundwater quality. High nitrate concentrations have been observed in groundwater from the Pukekohe and Bombay basalt lava since the 1970s (Crush et al. 1997; Auckland Regional Council 2010), with some concentrations exceeding New Zealand's Drinking-Water Standards maximum acceptable value of 11.3 mg/L NO_3-N (Water Services … Regulations 2022). Nitrate-loaded groundwater discharges via springs have a negative effect on the health of streams, with observed concentrations for most of the streams in the Pukekohe–Bombay area exceeding 2.4 mg/L NO_3-N (annual median), the national bottom line for nitrate toxicity in rivers set in the National Policy Statement for Freshwater Management 2020 (Ministry for the Environment 2020).

Nitrate mitigation strategies for the Pukekohe Vegetable Growing Exemption Area must be informed by an understanding of the main processes of nitrate transport and transformation from land through groundwater to streams discharging into the Manukau Harbour. Development of improved nutrient-management tools and water-allocation rules requires better conceptual understanding of the groundwater flow, connection with surface water, nitrate pathways, potential risk of nitrate contamination of deeper aquifers, 'future nitrate loads to come' and connections within the aquifer system (Stenger et al. 2022). In 2023, Phase 2 of this project will specifically investigate whether natural nitrate attenuation occurs in groundwater systems in the Pukekohe–Bombay area.

Building on previous hydrogeologic studies, groundwater age distributions within the Pukekohe–Bombay area could significantly contribute to understanding nitrate transport and transformation processes. This report refines groundwater age distribution parameters in the Pukekohe–Bombay area using age-tracer time-series data and provides additional groundwater ages for a wider coverage of the Bombay and Pukekohe aquifers.

This report has been prepared for Auckland Council under service agreements PIN CW9929 (project 900W4167) and CW137092 (project 900W4242) and was co-founded by GNS Science (GNS)'s Endeavour programme, *Te Whakaheke o Te Wai*.

Weathering of basalts – including tephra – forms prime loam soils. Market gardening is the dominant land use in the Bombay area (~60%), accompanied by some orcharding (~20%) and minor use for other agricultural activities (Murphy 1991). In the Pukekohe area, land use is roughly half livestock farming – including dairying and dry stock – and half market gardening, as well as some orchards (Crush et al. 1997). The intensive land use, especially of market gardening and dairying (Abascal et al. 2022), has led to a positive soil nitrogen balance, resulting in nitrate loss from the soil into the groundwater, which subsequently discharges into the streams.

Generally, nitrate (NO_3-N) concentrations are elevated in the Bombay and Pukekohe basalt aquifers and spring-fed streams (Moreau et al. 2016; White et al. 2019, and references therein), with the key source identified as synthetic fertilisers rather than farming effluent, based on dual nitrate isotopic signatures (Rogers and Buckthought 2022).

The overall understanding of groundwater resources in the Auckland region varies between different aquifers. As pressure on the resource increases over time, so does the need to further refine existing conceptual models. For the wider Franklin groundwater system, more robust groundwater age distributions are required to help constrain the conceptual

model of recharge and groundwater movement, particularly for the division between the shallow Pukekohe basalt and deep Kaawa shell aquifers. The current conceptual model of the Franklin multi-aquifer system is based on water-budget analysis. It suggests that recharge to the Kaawa shell aquifer is through both preferential flow through volcanic cones and diffuse vertical infiltration from overlying sedimentary layers of the Puketoka (Takaanini) Formation (Earthtech Consulting Ltd 2013).

Previous groundwater dating includes a recent study in the Pukekohe–Bombay area (van der Raaij 2015), showing an inverse relationship of nitrate concentration with groundwater mean residence time (MRT). For example, in the upper Pukekohe basalt aquifer, NO_3-N concentrations were greater than 13 mg/L and MRTs ranged from 16 to 52 years. In contrast, in the lower Pukekohe basalt aquifer, NO_3-N concentrations were lower than 1 mg/L and MRT was approximately 100 years. No mean transit times for stream discharges were available yet.

van der Raaij (2015) investigated two groundwater transects, one through the Pukekohe and one through the Bombay basalt aquifer, using groundwater age and chemistry. However, with only one age-tracer dataset available at that time, several assumptions in the data interpretation resulted in somewhat ambiguous conclusions. A new sampling round was conducted in 2021. The previous sites were re-sampled to better constrain groundwater mixing parameters using time-series data. More sites were included for increased spatial coverage in both shallow and deep aquifers. In addition, five sites were sampled for radiocarbon to extend the time scale beyond a few hundred years, as covered by tritium.

Groundwater residence times can be established based on the concentrations of specific age tracers such as tritium (^3H), chlorofluorocarbons (CFCs), sulphur hexafluoride (SF_6) and radiocarbon (^{14}C) (Appendix 1). Stream-water transit times can be established based on the tritium concentration of stream water. Groundwater residence time and stream-water transit times indicate the time elapsed from groundwater recharge (when the water fell as rain) to when it discharged either via springs, streams or production wells, or when it was sampled from within an aquifer via a monitoring well. Water ages, and their gradients, provide insights into how groundwater and associated contaminants move through aquifer systems. This enables better understanding of how land use affects water quality over time.

This report presents results and interpretations from 33 groundwater sites. Sample analysis cost was covered by Auckland Council for 17 sites and by GNS for 12 sites. Data from the remaining four sites came from GNS' historic database. Results from an additional 27 stream sites are also presented, with sample analysis cost covered by Auckland Council. Groundwater sites include repeat sampling of 13 wells reported in the van der Raaij (2015) groundwater age and chemistry study in the Pukekohe–Bombay area. The repeat sampling was undertaken to overcome previously ambiguous age interpretation.

The aim of this report is to use the time-series age-tracer data to constrain water mixing parameters, refine groundwater age models and resolve age-tracer ambiguity. Radiocarbon data are used to extend the age range of tritium (circa 0–200 years) and estimate the age of the deeper, older groundwater. Data from extra wells are used to increase coverage, both spatially and in depth, to enable better understanding of the pattern between different geological units. The new and refined age data are used to improve understanding of the chemical evolution of the groundwater system, potential for denitrification and future nitrogen loadings to streams, as well as to refine the conceptual understanding of groundwater flow. Radon measured in stream water was also used to identify areas where groundwater discharges into the streams. Stream water can be linked to specific groundwater sources based on groundwater age, stable isotopes and nitrate concentrations.

2.0 HYDROGEOLOGY

2.1 Geology of the Auckland Region

The Auckland region covers a land area of 4938 km^2. The landscape evolution is dominated by tectonic uplift followed by late Cenozoic extensional faulting, allochthon emplacement and basaltic volcanism. The region is underlain by Late Paleozoic to Mesozoic metasedimentary and metavolcaniclastic 'basement' rocks of the Waipapa and Murihiku terranes, which are exposed mainly in the east (Figure 2.1).

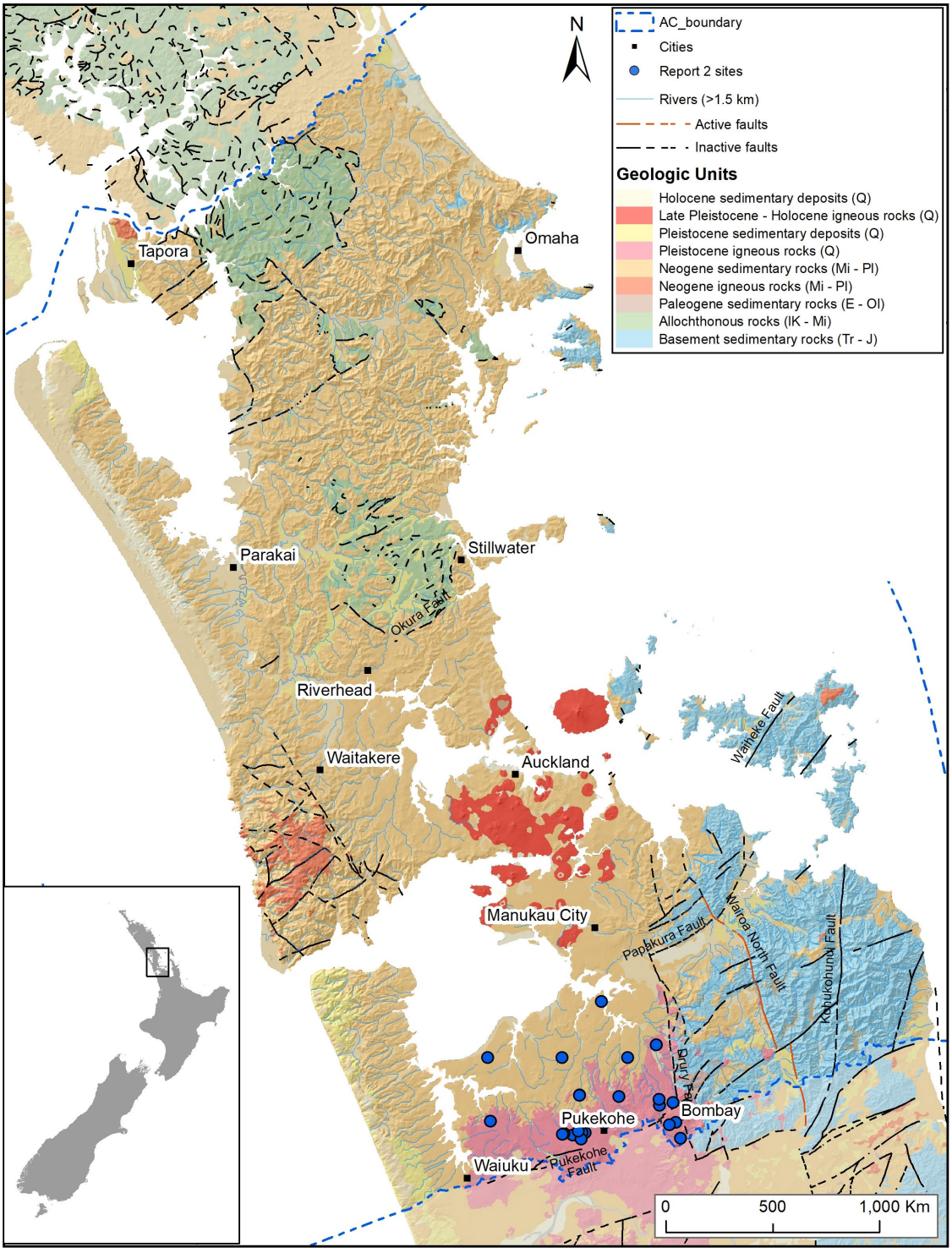

Figure 2.1 Simplified geology of the Auckland region, including major faults and sample site locations of the Pukekohe–Bombay area.

North of about Riverhead, these basement rocks are overlain by Late Cretaceous to Miocene sedimentary and metasedimentary allochthonous terranes of the Mangakahia and Motatau complexes (part of the Northland Allochthon). An overlying succession of Miocene–Pliocene shallow-marine and sub-aerial sedimentary and volcaniclastic sedimentary rocks, including re-worked volcanic deposits, dominates the surface geology of the region (Edbrooke 2001; Barrell et al. 2021). The youngest geologic features include the Auckland Volcanic Field (AVF) and South Auckland Volcanic Field (SAVF), which are comprised of predominantly basaltic lavas erupted as lava flows and tephra from numerous vents during the Pleistocene and Holocene (Briggs et al. 1994; Edbrooke 2001).

2.2 Geology of the Pukekohe–Bombay Area

The geology of the Pukekohe–Bombay area has been described in detail previously (Auckland Regional Water Board 1989; Murphy 1991; Barrell et al. 2021; Jones et al. 2022; Bland et al. 2023). The focus of the current study, following on from van der Raaij (2015), is the aquifer systems within the basalt rocks of the Pukekohe–Bombay area that are part of the SAVF. Eruptive activity in the SAVF was nearly continuous between 1.59 ± 0.13 and 0.51 ± 0.03 Ma, with peaks at ca. 1.3 and 0.6 Ma (Briggs et al. 1994). The basalts consist of dense, fractured lava flows, scoria cones and fine-grained tuff deposits. Lavas are fine- to medium-grained, vesicular and contain porphyritic olivine ± clinopyroxene ± plagioclase (Cook et al. 2004). Scoria cones are generally small, up to about 1 km wide, but typically less than 700 m in diameter. Tuff, a type of tephra deposit formed by explosive activity due to interaction between ascending magma and groundwater, forms constructional rings up to about 2 km wide surrounding their smaller source craters (Bland et al. 2023; Townsend et al., in prep). Though only locally deposited around source craters, tuff is probably more permeable than lava. Erupted tephra contributes finer-grained material to landscape-mantling deposits beyond this.

Basalt lavas are distributed widely in the Pukekohe area, with cumulative flow thicknesses up to 200 m (Viljevac et al. 2002). At the Bombay volcano, basalt lava flows are smaller in areal extent, with flows separated from one another by clay and silt-rich sediments (Murphy 1991). Although originally subdivided into the Bombay basalt and Franklin basalt by Schofield (1958) based on physical characteristics, this classification was revised by Cook et al. (2004) based on mineralogy and geochemical compositions.

In the Pukekohe area, the basalts generally overlie, intrude and interfinger with the Takaanini Formation (Barrell et al. 2021), which includes Pliocene–Holocene sedimentary strata (Figure 2.2). In the Bombay area, basalts may also overlie Jurassic greywacke, or Te Kuiti or Waitemata Group sedimentary rocks, depending on location. The volcanoes are generally the landscape-forming features, but in places they are partly overlain by sediments of the Tauranga Group. Where present, these include pumiceous sands, gravels, silty-clays, peats, and basaltic and silicic tephras (Auckland Regional Water Board 1989). These materials are generally less than 10 m thick. Basalts at or near the surface are deeply weathered and, along with the tephra, form rich horticultural soils. To the west, near Waiuku, the Takaanini Formation is differentiated from the coastal sand deposits flanking the west coast (Āwhitu Group and Karioitahi Group). Recent mapping by Bland et al. (2023) and Townsend et al. (in prep) has recognised that these sand deposits extend much further inland than previously thought, forming thin mantling dunes and intervening flats over much of the low-lying area to the north of the main Pukekohe–Bombay volcanic plateau (Townsend et al., in prep). However, these surficial wind-blown deposits are generally too thin to appear on the Bland et al. (2023) map, and this area is mapped as Takaanini Formation.

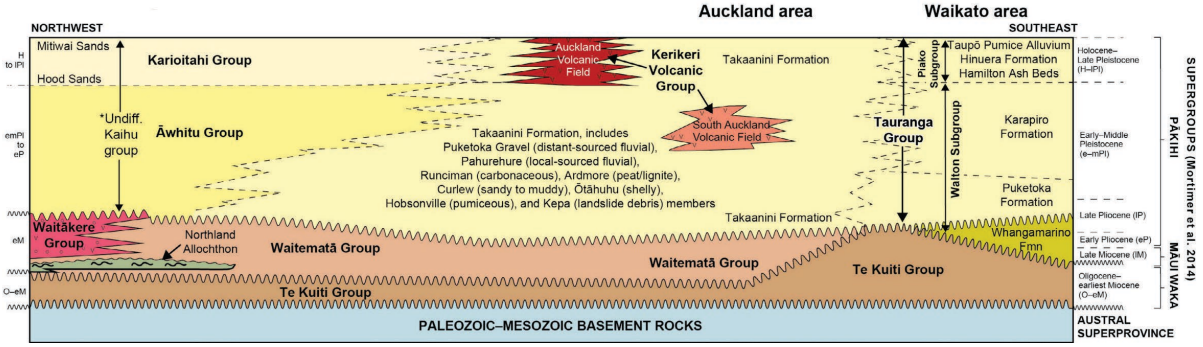

Figure 2.2 Generalised stratigraphic framework for the Auckland and Pukekohe area (South Auckland Volcanic Field) from Barrell et al. (2021). No stratigraphic thicknesses are implied by the illustration.

White et al. (2019) show several lithological cross-sections for the Pukekohe area. van der Raaij (2015) summarised the sequence of the various geologic units for the Pukekohe area (Figure 2.3, left) according to the Auckland Regional Water Board (1989) and for the Bombay area (Figure 2.3, right) according to Murphy (1991), with the approximate well locations of the 2014 sampling sites shown in red.

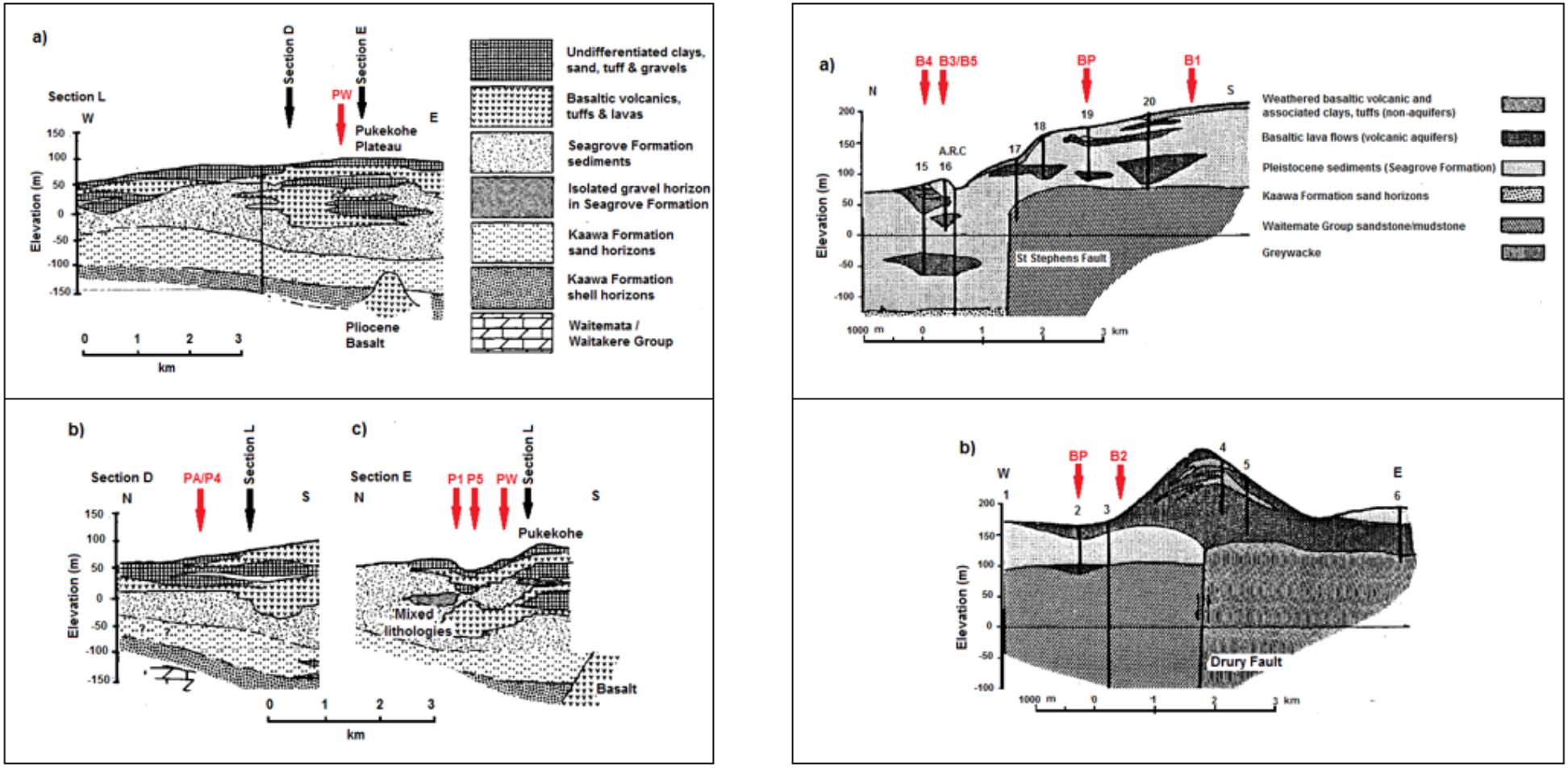

Figure 2.3 Left: Geological cross-sections of the Pukekohe area from the Auckland Regional Water Board (1989). (a) W–E-trending cross-section 'L'. (b) N–S-trending cross-section 'D'. (c) N–S-trending cross-section 'E'. Approximate locations of the wells and their identification numbers (IDs) from the van der Raaij (2015) study are shown in red. Right: Geological cross-sections of the Bombay area from Murphy (1991). (a) N–S-trending cross-section '2'. (b) W–E-trending cross-section 'C'. Approximate locations of the wells and their IDs from the van der Raaij (2015) study are shown in red. Their locations are also shown in Figure 2.4, with ID cross-reference provided in Table 2.1.

2.3 Hydrogeology of the Pukekohe–Bombay Area

The Waitemata Group comprises alternating sandstones, mudstones and conglomerates that record a progression between deep-water turbidity flow deposits (flysch) to shallow-water sequences. Groundwater flows mostly through fractures and joints. Hydraulic properties within the Waitemata Group vary spatially, depending on the thickness of sandstone and mudstone beds (ranging from a few metres to over 1000 m) and the amount of jointing and fracturing. The Waitemata Group is regarded as an aquiclude for most of the region, except in limited areas where it is regarded as an aquitard. Groundwater wells are generally drilled to depths of 200–400 m and cased to 100–200 m depth, with yields ranging from a few cubic metres per day to over 1000 m^3/day (Kalbus et al. 2017). Most recharge occurs during autumn and winter, resulting in peak groundwater levels from September to October.

Pleistocene and Holocene deposits consist of sandy alluvial sediments, generally less than 60 m thick. They are regarded as aquitards, which are an important source of small water supply for farm holdings and rural domestic use. Water wells drilled into these sediments are comparatively low-yielding, and the water quality is poor due to elevated iron concentrations. These wells are also susceptible to rural run-off and septic tank and saltwater contamination (Crowcroft and Bowden 2002; Kalbus et al. 2017; Johnson 2021; Foster and Johnson 2021).

The ‘Kaawa Formation’, or Ōtāhuhu Member of the Takaanini Formation (Tauranga Group), is a marine deposit comprising pumiceous shell and sandy shell beds, sands and fine to medium sandstone. Older parts of this member, which may rest unconformably on the Waitemata Group, were previously referred to as the ‘Kaawa Formation’. However, this name was superseded by Barrell et al. (2021) in a revision of the stratigraphy of the south Auckland area, and the formation was re-defined as the ‘Ōtāhuhu Member’. Because of legacy, in this report we retain the use of the name ‘Kaawa’ to refer to this important, relatively confined aquifer in the Manukau Lowlands, from Waiuku and Glenbrook and east towards Pukekohe and Paerata (Kalbus et al. 2017). It is commonly known as the ‘Kaawa shell aquifer’.

The basalt aquifers of the SAVF in the Pukekohe–Bombay area (formerly known as ‘South Auckland Volcanics’ from previous geological name convention in the area) are important sources of groundwater providing baseflow to streams and for municipal and irrigation supply. Groundwater flow is fracture-dominated, and hydraulic properties vary considerably horizontally, vertically and over small distances, with large variations in transmissivity both within and between aquifers. Transmissivities are generally higher in thicker basalt layers and lower in more weathered, thinner layers (Auckland Regional Water Board 1989). The aerial extent of highly permeable basalts is limited in the Bombay area, while, in the Pukekohe area, they are widespread and consist of several unconfined, confined, semi-confined and perched aquifers (Auckland Regional Water Board 1989; Figures 2.3 and 2.4). Water supply wells are typically drilled to depths of 20–150 m.

A simplified geology map of the area with sampling sites and well depth is shown in Figure 2.4, with the data listed in Table 2.1. The geology of the area shown in the following figures is based on Heron (2020), with modifications generalised from Bland et al. (2023). Wells outside the lava flows and cones are generally deep (>100 m). Wells drilled into the lava at Pukekohe have depths between 24 and 42 m. At Bombay, the sampled wells drilled into the lava are generally slightly deeper, with depths between 68 and 79 m.

Recharge to the unconfined shallow basalt aquifers is by direct infiltration of rainfall (Murphy 1991; White et al. 2019), with groundwater levels responding quickly to rainfall events, as well as stormwater soakage in urban areas. Recharge to the hydraulically distinct deeper aquifers

(e.g. Kaawa shell aquifer) has been assumed as both via intrusive fractured basalt (Viljevac et al. 2002) and by vertical (downward) leakage from the upper aquifers (White et al. 2019). This report seeks to better constrain the contributions from these sources.

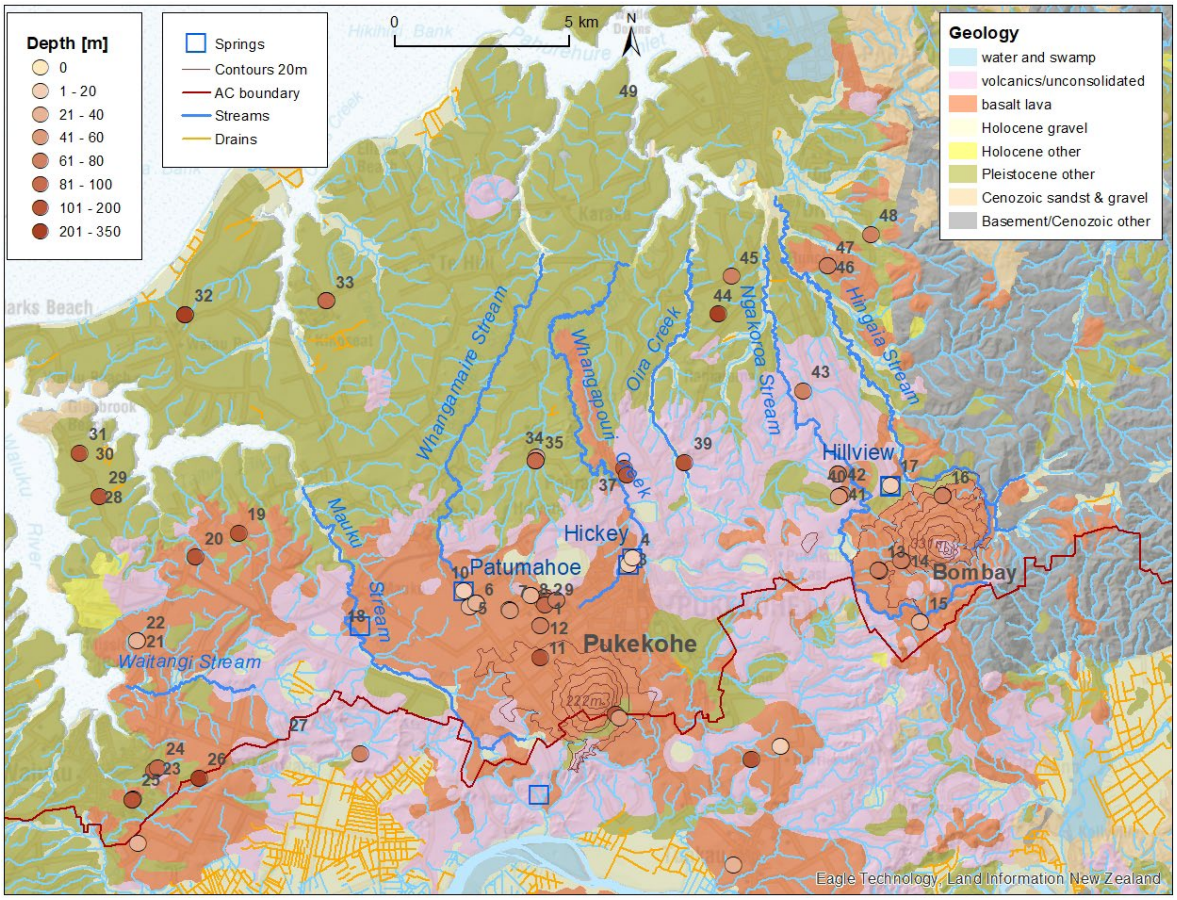

Figure 2.4 Simplified geology, well locations and annotated depth. Labels refer to number in Table 2.1. The springs are indicated by square box outlines.

Piezometric maps in Viljevac et al. (2002) show groundwater elevation in the Pukekohe–Bombay area, with derived groundwater flow in the Bombay area in a north-westerly direction. Water is discharged as springs (e.g. Hillview Spring) at the base of Bombay Hill (Murphy 1991). In the Pukekohe area, the direction of groundwater flow is less consistent. However, there is a general pattern of flow outwards from the higher cone and central recharge area to the periphery, with discharges from springs (Hickey and Patumahoe) occurring at the perimeter of the Pukekohe Plateau.

Water-budget estimates are summarised in White et al. (2019), who estimated long-term rainfall recharge at 485 mm/y (37% of precipitation), with 211 mm/y via shallow flow paths providing the baseflow component to the streams, and a relatively large, deep groundwater flow component of 273 mm/y that is not captured by the streams. Recovery from pumping is quick and sustained in the shallow basalt aquifers, whereas water levels in the deeper basalt aquifers are slightly decreasing over decades (Viljevac 1996).

Groundwater in the Pukekohe–Bombay basalt aquifers is generally low in dissolved solids and generally of high quality overall. However, contamination from agriculture and urban storm water is expressed as elevated concentrations of nitrate, sulphate, potassium, bicarbonate and total hardness (Crowcroft and Bowden 2002). Some groundwater nitrate concentrations exceed the maximum acceptable value of 11.3 mg/L NO_3-N set out in New Zealand's Drinking-Water Standards (Water Services … Regulations 2022).

This report presents results and interpretations from 46 groundwater bores, mostly from the basalt lavas of the Pukekohe and Bombay volcanoes, and from three large springs that drain these volcanoes (Table 2.1). Ten of the bores, all deep, cover the Pliocene Ōtāhuhu Member (Kaawa shell aquifer) and Miocene Waitemata Group north of the volcanoes. Shallow bores screen the basalt lava, while deeper bores screen the underlying, less hydraulically conductive, aquifers.

Table 2.1 Summary of sample sites, locations and well characteristics. Age-tracer data is from various sources (NGMP: National Groundwater Monitoring Programme; TW: Te Whakaheke o Te Wai; AC: Auckland Council; historic data). Springs are shown in blue. NZTM: New Zealand Transverse Mercator projection; WL: water level in metres below ground level (mgbl).

No.	ID 2015	Site ID	Name	NZTM_E	NZTM_N	Depth (mbgl)	Screen Top (mbgl)	Screen Bottom (mbgl)	WL (mbgl)	Aquifer Name	Aquifer Confinement	Project
1	P5	7428105	Rifle Range Shallow NEW	1766295	5880987	42	-	-	16.7	Pukeokohe Volcanic	Confined	NGMP
2	-	7428103	Rifle Range Deep	1766295	5880987	90	-	-	26.2	Pukeokohe Volcanic	Unconfined	NGMP
3	-	7419127	Hickey Spring	1768730	5882046	-	-	-	-	Pukekohe Volcanic	Unconfined	AC
4	-	-	Crisp Ave. Spring	1768830	5882229	-	-	-	-	Pukekohe Volcanic	Unconfined	AC
5	PA	3506	Agrisystems	1764141	5880817	24.4	14	-	-	Upper Pukekohe volc.	-	AC
6	P4	7428031	Wilcox Gun Club	1764324	5880929	27	-	-	-	Pukekohe Volcanic	Unconfined	TW
7	P2	3573	Plant Food Res.	1765290	5880730	40.4	22	-	-	Upper Pukekohe volc.	-	AC
8	P1	3598	Balance Agri	1765891	5881153	37	24.8	-	-	Upper Pukekohe volc.	-	AC
9	P3	3623	Nicholls	1766630	5881015	72	49.7	-	-	Lower Pukekohe volc.	-	AC
10	-	43915	Patumahohe Spring	1763975	5881279	-	-	-	-	Pukekohe Volcanic	Unconfined	TW
11	-	-	Douglas	1766160	5879366	108.2	-	-	-	-	Confined	historic
12	PW	3610	AS Wilcox	1766180	5880280	78	46	-	-	Lower Pukekohe volc.	-	AC
13	BP	7419121	BP Bombay	1775891	5881877	79	62	-	-	Bombay Volcanic	Unconfined	TW
14	B2	4315	Braks	1776568	5882144	68	49.6	-	-	Bombay Volcanic	-	AC
15	B1	21950	Thich Phuoc An	1777100	5880390	26.5	15	-	-	Bombay Volcanic	-	AC
16	BW	4352	Wallath	1777745	5884022	73	45.7	-	-	Bombay Volcanic	-	AC
17	-	7419126	Hillview Spring	1776264	5884330	-	-	-	-	Drury Volcanic	Unconfined	TW
18	-	-	Pilgrim Rd Spring	1760979	5880276	-	-	-	-	-	-	TW

No.	ID 2015	Site ID	Name	NZTM_E	NZTM_N	Depth (mbgl)	Screen Top (mbgl)	Screen Bottom (mbgl)	WL (mbgl)	Aquifer Name	Aquifer Confinement	Project
19	-	-	Coster	1757482	5882952	118	-	-	51.5	Kaawa	-	Historic
20	-	7417001	Glen Hall	1756247	5882259	103.7	-	-	-	Glenbrook Kaawa	Confined	AC
21	-	-	McKenzie Well B	1754565	5879850	139.8	129.3	138	36.6	Kaawa	-	Historic
22	-	-	McKenzie Well A	1754565	5879850	37	-	-	-	Volcanic	-	Historic
23	-	-	Cornwall Rd Well	1755049	5876100	98	89	96	-	-	-	Historic
24	-	8592	STCWR	1755149	5876201	92	85	92	-	-	-	Historic
25	-	92189	STVIC	1754451	5875300	189	92	189	-	-	-	Historic
26	-	174235	STWKU	1756350	5875903	235	174	235	-	-	-	Historic
27	-	28320	Kiwi Broilers	1758942	5877142	unkn.	-	-	-	Glenbrook volcanic	-	AC
28	-	-	Noort Well	1753600	5883900	-	-	-	-	-	-	Historic
29	-	-	Falcon Orchards	1753488	5884003	120	105.12	117.88	16.3	Kaawa	-	Historic
30	-	-	Tucker	1753350	5884980	-	-	-	-	Kaawa	-	Historic
31	-	-	Brundell	1752920	5885260	142	-	-	12.6	Kaawa	-	Historic
32	-	7417021	Seagrove	1755957	5889239	201	-	-	22.5	Waiau Pa Waitemata	Confined	NGMP
33	-	-	Kingseat Well	1760015	5889634	100	-	-	-	-	-	Historic
34	-	7418023	Ostrich Shallow	1766052	5885143	48	46	-	4.2	Pukekohe Kaawa	Confined	NGMP
35	-	7418027	Ostrich Deep	1766043	5885027	84	-	-	2.6	Pukekohe Kaawa	Confined	NGMP
36	-	-	NZ Dairy Co #12	1768578	5884826	104	94	100	29.2	Kaawa	-	Historic
37	-	-	NZ Dairy Co #9	1768654	5884629	121	-	-	39.6	Kaawa	-	Historic
38	-	-	Pukekohe Borough Council	1769120	5879827	-	-	-	-	-	-	Historic
39	-	-	Tuhimata	1770320	5884982	114.2	67.6	-	-	Pukekohe Kaawa	-	AC

No.	ID 2015	Site ID	Name	NZTM_E	NZTM_N	Depth (mbgl)	Screen Top (mbgl)	Screen Bottom (mbgl)	WL (mbgl)	Aquifer Name	Aquifer Confinement	Project
40	B5	4185	Taylor	1774878	5884045	68	-	-	-	-	-	AC
41	B3	4162	Crowe	1774768	5883996	43	21	-	-	Bombay Volcanic	-	AC
42	B4	4133	Martyn	1774740	5884655	77	61.9	-	-	Bombay Volcanic	-	AC
43	-	-	Rainbow Park Nurseries	1773724	5887038	78	67	78.2	30.2	Kaawa	-	Historic
44	-	20424	Underglass	1771294	5889257	350	-	-	-	Paerata Waitemata	-	AC
45	-	-	Harnett Orchards	1771668	5890340	80	76.2	79.2	-	Waitemata	-	Historic
46	-	7419009	Fielding Volc	1774435	5890642	47	16	-	5.9	Drury Volcanic	Unconfined	TW
47	-	7419007	Fielding Sand	1774435	5890642	64	57	-	13.4	Drury Sand	Semi-confined	TW
48	-	-	Oostdam	1775684	5891552	73.6	-	-	-	Sand	-	Historic
49	-	30129	Brink	1768437	5895395	-	-	-	-	Karaka Waitemata	-	AC

2.4 Surface Hydrogeology of the Pukekohe–Bombay Area

The major streams draining the Pukekohe and Bombay volcanoes flow northward towards Manukau Harbour. They include Waitangi Stream, Mauku Stream, Whangamaire Stream, Whangapouri Creek and Oira Creek (Pukekohe volcano) and Ngakoroa Stream and Hingaia Stream (Bombay volcano). Stream sampling sites and measured flows are shown in Figure 2.5, together with the simplified geology of the area. The streams were gauged and sampled at baseflow conditions on 22 February 2022. Table 2.2 lists sample site details and measured flows. Hingaia Stream also drains a significant block of greywacke in its upper reaches.

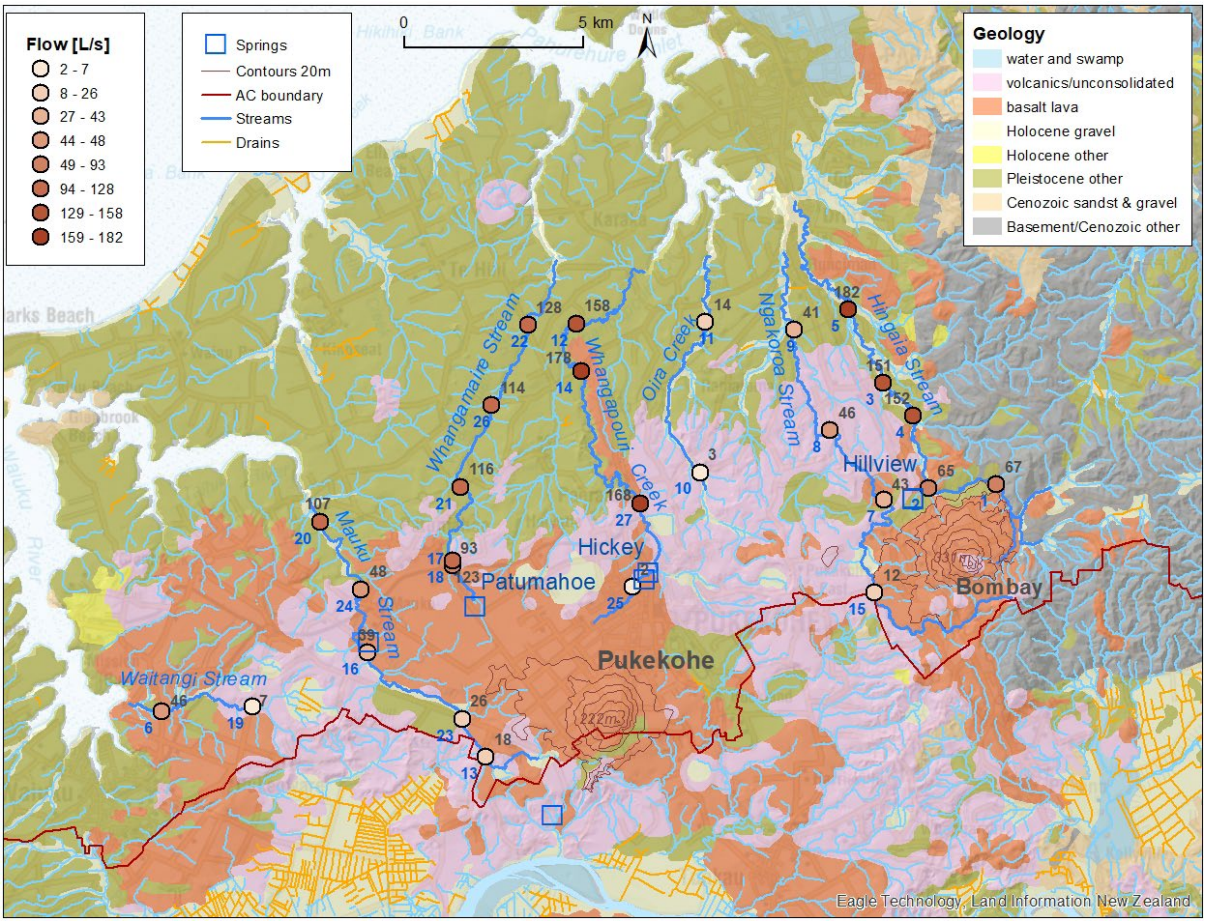

Figure 2.5 Streams and springs draining the Pukekohe and Bombay volcanoes and surrounding lava flows, as well as stream sampling sites, annotated with Auckland Council (AC) ID (blue) and measured stream flows (black) from Table 2.2. To assist understanding of drainage pattern, contours are shown for the volcanic cones, with maximum elevations of Pukekohe Hill at 222 m and Bombay Hill at 331 m.

For the three large streams draining the basalt lavas via the Patumahoe, Hickey and Hillview spring systems, baseflow is the most significant component of stream flow, with an average baseflow index of 0.87, as calculated for streams with continuous flow measurements using various methods (White et al. 2019). The other streams may not be baseflow-dominated. Hydrograph data are summarised in White et al. (2019). The baseflow data, available for sites sampled in February 2022, are also listed in Table 2.2 for comparison. These show that the flows measured on 22 February 2022, which represent late-summer low-flow conditions, were significantly lower than average baseflow throughout the year. Baseflow conditions were chosen for this study because they represent flows during the season when communities need water and want to enjoy their streams most (e.g. for recreation). Improved water management requires an understanding of the parameters of the low baseflow.

The volcanic Pukekohe Plateau and Bombay cone are discharge areas for several streams. The streams receive sizeable flows only at the perimeter of the plateau and cone – the discharge from the basalt aquifers. This discharge includes springs that are predominantly fed by shallow aquifers (Viljevac 1996; Figure 2.5).

Springs in the area provide significant baseflow. Four of the springs on the Pukekohe Plateau have a combined flow of approximately 8.1 Mm^3/y (Viljevac 1996). The total baseflow from the Pukekohe basalt aquifer to streams was estimated by Viljevac et al. (2002) to be approximately 26.1 Mm^3/y, based on flow records from local streams. This equates to a baseflow of 832 L/s. The cumulative discharges from all seven streams at the sampling time of this current study were approximately 700 L/s, suggesting that the results of this report are representative of normal baseflow conditions.

Stream baseflow generally shows no significant trend of decline over time (for Pukekohe: White et al. [2019]), meaning that the hydrologic system is at near steady-state condition. However, nitrate-loaded groundwater discharges via springs have a negative impact on the health of the streams. Observed concentrations exceed 2.4 mg/L NO_3-N (annual median), the national bottom line for nitrate toxicity in rivers (Ministry for the Environment 2020).

Table 2.2 Stream-sample site details and measured flows on 22 February 2022. Annual baseflow for a selection of gauged streams is from White et al. (2019). AC ID: Auckland Council ID at road bridge.

AC ID	Site Name	NZTM_E	NZTM_N	Flow (L/s)	Annual Baseflow
1	Hingaia at Cascades	1778602	5884693	67	-
2	Hingaia at Stones Rd	1776693	5884584	65	-
3	Hingaia at Ararimu Rd Bridge	1775414	5887539	151	-
4	Hingaia at Maxted Rd	1776248	5886629	152	-
5	Hingaia at Quarry Rd	1774433	5889613	182	-
13	Mauku at Puni (Aka Aka Rd Bridge)	1764274	5877049	18	33
23	Mauku at Fallows Bridge (Wiley Rd)	1763615	5878120	26	-
16	Mauku at Titi Rd Bridge	1760951	5879974	39	110
24	Mauku at Wrights Water Gardens	1760776	5881756	48	-
20	Mauku at Swede (Patullo Rd Bridge)	1759628	5883657	107	189
15	Ngakoroa at Mill Rd	1775171	5881667	12	48
7	Ngakoroa at Ingrams	1775433	5884282	43	-
8	Ngakaroa at Kern Rd	1773936	5886216	46	-
9	Ngakaroa at Runciman	1772925	5889040	41	132
10	Oira at Tuhimata Rd	1770289	5885042	3	-
11	Oira at Swing Bridge (Woodlyn Dr)	1770438	5889252	14	-
19	Waitangi at Waiuku Rd	1757721	5878472	7	28
6	Waitangi at SH Bridge	1755185	5878322	46	124
17	Whangamaire at Railway Culvert	1763343	5882414	93	-
18	Whangamaire at D/S Henry's Reserve	1763337	5882558	123	-
21	Whangamaire at Ostrich Rd	1763578	5884630	116	-
26	Whangamaire at Glenbrook Rd	1764431	5886931	114	-
22	Whangamaire at Fantail	1765460	5889182	128	173
25	Whangapouri at Hickey Spring US	1768388	5881820	2	-
27	Whangapouri at Paerata Falls	1768615	5884162	168	-
14	Whangapouri at Glenbrook Rd Bridge	1766944	5887875	178	-
12	Whangapouri at Pukekohe GC	1766821	5889213	158	-

3.0 METHODS

3.1 Sampling and Analytical Methods

Auckland Council and GNS staff collected 29 age-tracer samples (tritium, CFCs, SF_6) from groundwater wells in the Pukekohe–Bombay area between January and March 2021 using standard, New-Zealand-specific, internationally reviewed sampling protocols (Daughney et al. 2006, Daughney 2007). Special care was taken to exclude air from the CFC and SF_6 samples. CFC samples were collected underwater in 125 mL glass bottles and sealed using foil-lined caps to prevent gas exchange with the present-day atmosphere. SF_6 samples were collected in 1 L glass bottles with Polyseal caps that displace headspace. Tritium samples were collected in 1 L Nalgene plastic bottles. Tritium contamination sources, such as luminous watches, were excluded during sampling. Radon samples were collected in 20 mL glass vials with metal foil-lined plastic caps.

On 22 February 2022, five hydrology teams from Auckland Council collected radon, tritium and water-stable isotope samples from Pukekohe–Bombay-area streams at baseflow. At the time of sampling, stream discharge was also gauged using FlowTracker2[1]. On 7 April 2022, Uwe Morgenstern (GNS) and Kolt Johnson (Auckland Council) sampled five streams, all still at baseflow conditions.

CFCs (CFC-11, CFC-12, CFC-113); argon, nitrogen and methane; and SF_6 were analysed at the GNS Water Dating Laboratory by gas chromatograph using an electron capture detector (GC-ECD). The system used to analyse CFCs was similar to that of Busenberg and Plummer (1992). The analytical system for SF_6 is described in van der Raaij (2003). CFC samples were analysed in duplicate for quality control. Dissolved argon, nitrogen and methane were measured simultaneously with CFCs by GC-thermal conductivity detector. Detection limits in terms of gas dissolved in water were 5 x 10^{-14} mol/kg water for CFCs, 1 x 10^{-16} mol/kg water for SF_6 and 3 x 10^{-16} mol/kg for H-1301. Dissolved argon and nitrogen concentrations (analytical accuracy 1% and 3%, respectively) were measured to estimate the temperature at the time of recharge and the excess air concentration (Heaton and Vogel 1981) and to calculate the atmospheric partial pressure (ppt) of CFCs and SF_6 at the time of recharge. CFCs and SF_6 concentrations were subsequently converted to atmospheric equivalents using Ar/N_2-derived temperatures corrected for excess air.

Tritium was measured at the GNS Water Dating Laboratory by liquid scintillation counting using Quantulus™ low-level counters with electrolytic enrichment by a factor of ~90 (Morgenstern and Taylor 2009). The detection limit of this method is approximately 0.02 tritium units (TU; 1 TU is equivalent to $^3H/^1H = 1\times10^{-18}$).

Radon-222 samples from groundwater and surface water were collected in 20 mL glass vials with metal-lined lids. Due to the short half-life of radon, the samples were measured within three days after sampling. Analyses were performed by liquid scintillation spectroscopy, with 10 mL of sample water transferred into counting vials and mixed with a mineral oil-based scintillant and radon absorber, followed by decay counting in a Quantulus™. Detection limits were typically <0.1 Bq/L. This Radon-222 analytical technique was validated by an inter-laboratory comparison organised by Flinders University, Adelaide, in 2018.

1 https://www.xylem.com/en-us/products--services/analytical-instruments-and-equipment/flowmeters-velocimeters/flowtracker2-handheld-adv/

Carbon-14 samples were collected air-free in 250 mL Nalgene or glass bottles, leaving no headspace. Carbon-14 was measured by accelerator mass spectrometry (AMS). CO_2 was extracted from 150 mL of water by adding 4 mL of ortho-phosphoric acid in an evacuated flask. The gas was converted into a graphite target and analysed for ^{14}C by AMS. An aliquot of the CO_2 gas was used for ^{13}C analysis through mass spectrometry. Concentrations and radiocarbon model ages were calculated following the methods described by Morgenstern et al. (2008) and Seltzer et al. (2015).

Stable isotopes of the water molecule (^{18}O and ^{2}H) enable distinguishing between groundwater recharge from climatically different environments, usually between river/stream water from higher altitudes or more inland catchments versus local rain recharge. The stable isotope signature of meteoric water depends on the history of the water masses and temperature-dependent kinetic processes, such as seawater evaporation and re-precipitation. Rivers from colder, higher-altitude catchments usually have a more depleted isotope signature compared to low-altitude rain near the coast. Samples were measured at the GNS Stable Isotope Lab, with measurement errors typically ±0.2‰ for $\delta^{18}O$ and ±2‰ for $\delta^{2}H$.

Together with the isotope and age tracers, groundwater chemistry samples were collected in the Pukekohe–Franklin area during the January–March 2021 sampling campaign. Sampling was conducted following the 2006 standardised sampling protocol for State of the Environment (SOE) monitoring, consistent with the current National Environmental Standards (Daughney et al. 2006; Milne 2019). This sampling was undertaken as part of Auckland SOE programme and the National Groundwater Monitoring Programme (NGMP). Some samples were analysed at the New Zealand Geothermal Analytical Laboratory (GNS Wairakei), the laboratory that has been used for all NGMP samples since 1993. The NGMP analytical suite includes: sodium (Na), calcium (Ca), magnesium (Mg), potassium (K), carbonate (CO_3), bicarbonate (HCO_3), chloride (Cl), sulphate (SO_4), nitrate-nitrogen (NO_3-N), ammonia-nitrogen (NH_3-N), dissolved iron (Fe), manganese (Mn) and dissolved reactive phosphorus (DRP) (Table 3.1). Hydrochemical analysis integrity of the March samples was checked by calculating the charge balance error and/or ionic sum to verify electroneutrality of the samples (Moreau-Fournier and Daughney 2010). Moreau and Daughney (2021) have produced a historical reconstruction (starting from 1993) of changes in analytical methods used for each of the selected parameters monitored as part of NGMP. A temporal map of analytical methods and laboratories used by the SOE network is not currently available, but, upon request, Auckland Council can provide a list of methods used and laboratories where sample analyses were performed as part of the SOE programme.

Table 3.1 Current list of parameters monitored at National Groundwater Monitoring Programme (NGMP) sites. 'APHA' stands for 'American Public Health Association', which is a reference for analytical methods (Baird et al. 2017).

Parameter	Units	NGMP Analytical Method
HCO_3, CO_3	mg/L	Titration, APHA 2320B
Ca, Mg, K, Na, Fe, Mn, SiO_2	mg/L	Induced Coupled Plasma-Optical Emission Spectrometry, APHA 3120B
DRP	mg/L	Flow Injection Analyser, APHA 4500-P G (modified)
Cl, NO_3-N, SO_4, Br, F	mg/L	Ion Chromatography, APHA 4110B
NH_3-N	mg/L	Flow Injection Analyser, APHA 4500-NH_3-N

3.2 Groundwater Age Interpretation

The methodology of groundwater dating using tritium, CFCs and SF_6 is described in detail in Appendix 1. Groundwater dating uses convolution of known time-dependent tracer input concentrations via the rain into and through groundwater systems with a suitable system response function and matching of tracer concentrations measured in the groundwater.

Modelled groundwater MRT is based on lumped-parameter flow models (LPM; Małoszewski and Zuber 1982). Model outputs are matched to measured age-tracer concentrations. Models have been fitted to the data using Microsoft-Excel-based Tracer LPM software from the United States Geological Survey (Jurgens et al. 2012). The exponential piston flow model (EPM) was chosen to account for mixing of groundwaters with different flow-path lengths and, therefore, different ages (Appendix 1). Generally, for wells with long well-screen intervals in unconfined conditions, a high fraction of exponential (mixed) flow of 80–95% was applied. For wells with short screen intervals in confined conditions, a low fraction of exponential flow of 50–60% was applied (see Morgenstern and Daughney [2012]).

Tracer inputs into the groundwater systems were measured tritium concentrations in rain at Kaitoke, 40 km north of Wellington, used with a scaling factor 0.82 to account for the lower input due to lower latitude. CFCs, Halon-1301 and SF_6 concentrations used were representative of southern hemispheric air, which is assumed to be well-mixed and to have uniform gas-tracer concentrations. Pre-1978 CFC data have been reconstructed using the Plummer and Busenberg (2000) methods, scaled to the southern hemisphere by a factor of 0.83 (CFC-11) and of 0.9 (CFC-12). Post-1978 CFC data are from Tasmania. Pre-1970 SF_6 data have been reconstructed (USGS, Reston), 1970–1995 data are from Maiss and Brenninkmeijer (1998) and post-1995 data were measured in Tasmania. Halon-1301 data are from Beyer et al. (2017).

Tritium is produced naturally in the atmosphere through the interaction of cosmic rays with atmospheric particles and subsequently incorporated into meteoric water. Once the water infiltrates into the ground and is separated from the atmosphere, the tritium concentration in the water starts to decrease due to radioactive tritium decay. With its half-life of 12.32 years (Lucas and Unterweger 2000), tritium dating can cover an age range of approximately 1–200 years.

Together with tritium, the complementary gas age-tracers SF_6, Halon 1301 and CFCs were used to date groundwater from wells and springs. Atmospheric concentrations of these age-tracers have increased in recent decades due to human activity. The measured concentration in the groundwater can be related to a certain recharge time (Morgenstern and Daughney 2012). CFCs and SF_6 concentrations were converted to atmospheric equivalents using Henry's law for dissolved gases using an estimated recharge temperature and excess air correction derived from dissolved Ar and N_2 measurements (Busenberg and Plummer 1992; Heaton and Vogel 1981).

To extend the dating range beyond a few hundred years, five sites that were expected to have old groundwater were also analysed using the ^{14}C dating method. Concentrations of atmospherically derived ^{14}C in groundwater are subject to dilution by dissolution of fossil carbonates. Therefore, ^{13}C was used to quantify the dilution by fossil carbonates as described in Morgenstern et al. (2008) and Seltzer et al. (2015).

3.3 Hydrochemistry Data Processing

Hydrochemistry data was available at 16 sites. The dataset consisted of time-series ranging from a single measurement to up to 24 years. State and trend analysis were performed using R software (version 3.6.2), LWP-Trends (version 2101) and NADA (version 1.6-1.1) libraries. The LWP-Trends library was used to compute the Mann-Kendall trend test (seasonally adjusted or not), Sen's slope estimations and Kruskall-Wallis seasonality tests on censored and uncensored time-series that have been processed with NADA (Non-Detects and Data Analysis) methods[2] (Helsel et al. 2020).

To calculate meaningful state and trend metrics, minimum data requirements were set as follows:

- **Descriptive statistics** (indicative of state over the characterised time period): there is no censoring, median or mean absolute deviation (MAD), and percentiles were estimated using statistical formula. For time-series affected by less than 25%, median and MAD were estimated using regression on order statistics (ROS) models, and percentiles were calculated using statistical formula. Above 25% censoring and below 80% censoring, no percentiles were calculated; median and MAD were computed using ROS models. Above 80% censoring, there is no estimate of median, MAD or percentiles; values are shown as below the highest detection limit.
- **Kruskall-Wallis test** (includes seasonal, both trend time periods): four seasons were considered for the analysis (autumn, winter, spring and summer). The annual time period commences on 1 March of the first year (start of autumn). To enable seasonality state and trend assessments, all seasons must have at least one observation, and individual seasons require at least two data points.
- **Mann-Kendall test** and **Sen's slope estimator** (includes seasonal and both trend time periods): the time-series must contain at least 10 data points, the maximum censored values must be smaller than the maximum observed values and at least five unique observations are required for each time-series.

Hierarchical cluster analysis (HCA) is a multivariate statistical method that categorises chemistry data based on similarities in selected characteristics. HCA was undertaken using the calculated site-specific median values of nine different parameters: Ca, Mg, Na, K, HCO_3, Cl, SiO_2, NH_3-N, Mn, and, in addition to field temperature, dissolved oxygen and field electrical conductivity. Data for other parameters, such as Fe and DRP, were not included in the analysis, as most measurements available were for total forms, which include colloidal Fe and Mn. These two forms are not directly comparable, as demonstrated by a significant decrease in Fe concentrations observed following a change in sampling protocol, specifically field-filtering, in the Wellington region in 2004 (Daughney and Randall 2009). NO_3-N in groundwater is mainly a reflection of land use in the recharge area. It is considered separately for assessment of the recharge source. Excluding NO_3-N from the HCA facilitates focusing on groundwater evolutionary processes.

2 The NADA library implements statistical methods to handle censored values (i.e. concentrations measured below the detection limit). It is used here to calculate medians and median absolute deviations for time-series with left-censored values. For heavily censored datasets (i.e. more than 50% of results are recorded below the detection limit for a given parameter), an ROS model was used to calculate the median value. Above 80% censoring (i.e. more than 80% of results for a given parameter are below the detection limit), medians were not estimated. Sites that had been sampled only once were still included in the hydrochemical assessment to maximise the number of sites available.

Approaches for HCA were based on best practise from previous experience in New Zealand and overseas (e.g. Güler et al. 2002; Daughney and Reeves 2005). HCA was initially conducted on log-transformed and normalised median concentrations, temperatures or conductivity using the nearest-neighbour linkage rule. This approach identifies sites where hydrochemistry is most different from other sites. However, no sites were identified as potential outliers in the initial dataset. Next, HCA was conducted using Ward's linkage rule (Ward 1963). Ward's method is based on an analysis of variance. It produces smaller distinct clusters than other linkage rules, in which each site in a cluster is more similar to other sites in the same cluster than to any site assigned to a different cluster. The square of the Euclidean distance was used in HCA as the measure of similarity for both linkage rules.

4.0 TRACER ANALYSIS RESULTS

The entire chemistry and age-tracer dataset used in this report is provided in the attached digital data file '*GNS SR2022-63 – Data Output.xls*', with the worksheets listed below. Age-tracer, gas and isotope data relevant to the figures in this report are also provided in the tables below to allow reference between the text and the figures.

- 'read_me': caveat on the data.
- 'site_information': site details (ID, well depth information, coordinates) for the sample locations. The last column indicates whether chemistry and/or age information is available at each site and corresponding time period.
- 'field_measurements': field measurements collected during the January–March 2021 sampling campaign.
- 'chem_units': detailed information (acronym, units, form) for chemistry parameters.
- 'age_units': detailed information (acronym, units) for age-tracer parameters.
- 'chemistry_data': cleaned and processed analytical results from sources detailed in Section 3.3.
- 'age_data': aggregated age-tracer measurements and interpretations.
- 'state' and 'trend': groundwater chemistry state and trend metrics calculated over the time period available at each site, on a per-site, per-parameter basis. Reported metrics are: median and MAD, percentiles (5^{th}, 25^{th}, 75^{th}, 95^{th}), trend magnitudes and categories and p-values for the Mann-Kendall and Kruskal-Wallis tests (Sections 3.3 and 5.2.5).
- 'clustering': HCA cluster attribution, where applicable (Sections 3.3 and 5.2.3).

4.1 Groundwater

Table 4.1 lists field parameters as measured before sampling, measured gas concentrations and calculated recharge parameters.

The measured age-tracer concentrations for the samples collected in 2021 are provided in the attached results reports noted in Appendix 2. Table 4.2 summarises the age-tracer concentrations relevant for groundwater age modelling, as well as the radon concentrations and stable isotope ratios. Modelled groundwater age-distribution parameters (Section 5.1) are listed in the last two columns of Table 5.1.

4.1.1 Surface Water

Table 4.3 lists the field parameters measured during the sampling campaign on 22 February 2022 and the isotope data for these samples. The last column shows mean transit times (MTT) derived from the tritium concentrations using an EPM with 70% of the flow volume with exponential age distribution within the total flow volume.

Table 4.1 Field parameters as measured before sampling, including electric conductivity (EC), pH, temperature and dissolved oxygen (DO). Further listed are concentrations of methane (CH_4), argon (Ar) and nitrogen (N_2), together with excess air and recharge temperature as calculated from Ar and N_2. 'No.' refers to site IDs listed in Table 2.1.

No.	Date	EC Field (µS/cm)	pH Field	Temperature (°C)	DO (mg/L)	CH_4 (µmol/kg)	±	Ar [mL(STP)/kg]	±	N_2 [mL(STP)/kg]	±	Excess Air [mL(STP)/kg]	±	Recharge Temperature (°C)	±
1	11/01/21	213	6.7	16.5	6.31	0	0	0.45	0.01	19.9	0.8	6.8	2.0	9.9	3.1
2	11/01/21	268	8.5	15.3	0.06	17	0.9	0.50	0.01	23.8	0.6	11.9	1.5	10.3	2.3
3	7/04/22	295	-	16.1	9.59	0	0	0.36	0.01	14.4	0.2	1.9	0.6	16.3	1.6
4	7/04/22	291	-	16.1	8.91	0	0	0.35	0.01	13.7	0.2	1.1	0.6	16.5	1.6
5	9/03/21	-	-	-	-	0	0	0.37	0.01	15.6	0.3	3.3	0.9	15.5	1.8
6	6/01/21	378	6.2	15.7	7.43	0	0	0.38	0.01	15.4	0.4	2.1	1.0	12.8	1.8
7	4/02/21	344	6.2	16.0	7.66	0	0	0.39	0.01	15.7	0.4	2.1	1.1	11.7	1.9
8	26/03/21	311	6.2	18.8	5.07	0	0	0.42	0.01	18.2	0.5	5.1	1.4	11.3	2.2
9	9/03/21	269	-	-	0.83	6	0.3	0.44	0.01	21.9	0.5	11.6	1.3	16.6	2.6
10	7/04/22	358	-	16.2	10.17	0	0	0.36	0.01	14.5	0.2	2.1	0.7	16.4	1.9
11	16/10/09	-	-	-	-	63	4	0.39	0.01	15.5	0.2	2.0	0.5	11.6	1.2
12	26/03/21	253	7.9	15.5	6.36	0	0	0.55	0.02	27.4	1.8	15.7	4.3	8.5	5.5
13	6/01/21	306	7.1	14.8	7.6	0	0	0.40	0.01	16.7	0.8	3.6	2.0	12.3	3.2
14	28/01/21	356	-	-	5.09	0	0	0.39	0.01	16.3	0.5	3.5	1.4	13.5	2.4
15	4/02/21	218	-	-	8.08	0	0	0.40	0.01	16.2	0.4	2.8	1.0	11.8	1.7
16	26/03/21	352	6.5	15.6	8.27	0	0	0.38	0.01	15.3	0.2	1.9	0.6	12.5	1.4
17	7/04/22	290	-	16.0	9.88	0	0	0.34	0.01	13.9	0.2	1.8	0.6	17.8	1.8
18	7/04/22	311	-	17.1	6.42	0	0	0.37	0.01	15.5	0.3	3.1	0.8	15.5	1.7
19	26/02/85	-	-	-	-	-	-	-	-	-	-	-	-	-	-
20	9/03/21	-	-	-	-	14	0.7	0.38	0.01	17.1	0.2	6.0	0.7	18.1	1.8

No.	Date	EC Field (µS/cm)	pH Field	Temperature (°C)	DO (mg/L)	CH_4 (µmol/kg)	±	Ar [mL(STP)/kg]	±	N_2 [mL(STP)/kg]	±	Excess Air [mL(STP)/kg]	±	Recharge Temperature (°C)	±
21	26/02/85	-	-	-	-	-	-	-	-	-	-	-	-	-	-
22	26/02/85	-	-	-	-	-	-	-	-	-	-	-	-	-	-
23	28/08/17	356	8.1	17.1	3.2	0	-	0.41	0.01	17.3	0.4	4.2	1.1	11.9	2.1
24	26/02/15	-	-	-	-	0	-	0.47	0.01	19.7	0.6	5.0	1.5	6.2	1.9
25	26/02/15	-	-	-	-	0	-	0.46	0.01	19.1	0.5	4.3	1.6	6.6	2.4
26	26/02/15	-	-	-	-	0	-	0.47	0.01	19.5	0.5	4.7	1.3	6.0	1.9
27	11/03/21	-	-	-	-	0	0	0.35	0.01	13.1	0.2	-0.4	0.7	14.3	1.5
28	26/02/85	-	-	-	-	-	-	-	-	-	-	-	-	-	-
29	18/03/85	-	-	-	-	-	-	-	-	-	-	-	-	-	-
30	26/02/85	-	-	-	-	-	-	-	-	-	-	-	-	-	-
31	26/02/85	-	-	-	-	-	-	-	-	-	-	-	-	-	-
32	11/01/21	418	8.9	19.1	0.06	2	0.7	0.45	0.01	19.2	0.4	5.2	1.2	8.3	1.8
33	3/11/15	-	-	-	-	0	-	0.46	0.01	20.8	0.5	7.9	1.4	9.7	2.3
34	7/01/21	295	7.1	17.7	0.19	82	50	0.43	0.01	17.6	0.4	3.1	1.0	8.2	1.6
35	11/01/21	301	7.9	18.2	0.11	5	2.1	0.45	0.01	18.7	0.4	4.2	1.2	7.5	1.8
36	6/11/85	-	-	-	-	-	-	-	-	-	-	-	-	-	-
37	6/11/85	-	-	-	-	-	-	-	-	-	-	-	-	-	-
38	6/11/85	-	-	-	-	-	-	-	-	-	-	-	-	-	-
39	11/03/21	-	-	-	-	28	1.8	0.42	0.01	16.7	0.6	2.3	1.5	9	2.2
40	11/06/14	286	-	15.8	1.9	0.2	0	0.42	0.01	16.2	0.3	1.3	0.9	7.6	1.4
41	28/01/21	279	-	-	2.59	0	0	0.43	0.01	18.0	0.5	4.1	1.4	9.6	2.3
42	28/01/21	315	-	-	0.06	17.2	0.9	0.42	0.01	16.7	0.8	2.1	1.8	8.4	4.6

No.	Date	EC Field (µS/cm)	pH Field	Temperature (°C)	DO (mg/L)	CH_4 (µmol/kg)	±	Ar [mL(STP)/kg]	±	N_2 [mL(STP)/kg]	±	Excess Air [mL(STP)/kg]	±	Recharge Temperature (°C)	±
43	6/11/85	-	-	-	-	-	-	-	-	-	-	-	-	-	-
44	4/05/21	-	-	-	-	-	-	-	-	-	-	-	-	-	-
45	6/11/85	-	-	-	-	-	-	-	-	-	-	-	-	-	-
46	7/01/21	319	8.1	18.0	0.15	25	4.3	0.44	0.01	18.4	0.4	4.5	1.1	9.1	1.8
47	7/01/21	351	7.6	18.1	0.16	305	17	0.45	0.01	18.8	0.8	4.7	2.1	8.3	2.9
48	18/12/90	-	-	-	-	-	-	-	-	-	-	-	-	-	-
49	4/05/21	-	-	-	-	-	-	-	-	-	-	-	-	-	-

Table 4.2 Summary of age-tracer concentrations: tritium (TR); calculated atmospheric concentrations of SF_6, Halon-1301 and CFCs; and ^{14}C. Equivalent atmospheric partial pressures of SF_6, Halon-1301 and CFCs were calculated using measured Ar and N_2 concentrations. Data in red are above atmospheric concentrations, indicative of contamination. ^{13}C was used for ^{14}C correction. Groundwater age-distribution parameters are listed in the last two columns of Table 5.1. 'T Code' is the Tritium laboratory code.

No.	Date	T Code	TR	±	SF_6 (pptv)	±	Halon (pptv)	±	CFC-11 (pptv)	±	CFC-12 (pptv)	±	CFC-113 (pptv)	±	^{14}C (pmc)	±	$\delta^{13}C$ (‰)	±	^{14}C Age (y)	Rn (Bq/L)	±	$\delta^{2}H$	$\delta^{18}O$
1	11/01/21	TA287	0.422	0.018	1.77	0.09	1.18	0.10	141	24	343	46	38	7	-	-	-	-	-	17.6	1.7	-28.0	-5.06
2	11/01/21	TA288	0.001	0.014	0.11	0.05	0.02	0.04	4	1	28	3	4	2	58.1	0.3	-22.3	0.2	3540	-	-	-29.7	-5.35
3	7/04/22	TA354	0.732	0.024	8.52	0.32	3.07	0.20	1073	137	768	55	82	7	-	-	-	-	-	25.4	1.5	-27.4	-4.99
4	7/04/22	TA352	0.707	0.024	8.62	0.34	2.98	0.19	797	101	811	59	82	7	-	-	-	-	-	26.8	1.6	-28.5	-5.04
5	9/03/21	TA316	0.818	0.026	80956	3963	2.36	0.15	967	120	522	39	70	7	-	-	-	-	-	-	-	-	-
6	6/01/21	TA293	0.783	0.024	6.30	0.42	2.34	0.17	408	39	807	64	69	7	-	-	-	-	-	14.3	0.8	-27.0	-4.87
7	4/02/21	TA308	0.758	0.022	6.42	0.38	2.17	0.18	315	33	686	60	62	7	-	-	-	-	-	16.8	1.0	-	-
8	26/03/21	TA314	0.027	0.016	5.21	0.31	1.86	0.16	201	24	420	41	52	7	-	-	-	-	-	-	-	-	-
9	9/03/21	TA321	0.177	0.018	0.47	0.06	0.16	0.03	171	21	28	4	3	3	-	-	-	-	-	-	-	-	-
10	7/04/22	TA353	0.699	0.023	8.15	0.34	3.04	0.22	456	54	1571	122	92	9	-	-	-	-	-	13.2	0.8	-26.5	-4.93
11	16/10/09	TA128	0.024	0.021	0.20	0.03	-	-	0	2	2	14	-	-	-	-	-	-	-	-	-	-	-
12	26/03/21	TA322	0.061	0.016	6.68	0.66	0.97	0.18	38	12	136	31	17	6	-	-	-	-	-	-	-	-	-
13	6/01/21	TA296	0.382	0.018	1.92	0.28	0.98	0.12	920	152	347	46	26	5	-	-	-	-	-	13.7	0.8	-30.2	-5.49
14	28/01/21	TA305	0.563	0.019	3.26	0.24	1.45	0.15	492	324	598	59	48	7	-	-	-	-	-	7.7	0.5	-28.3	-5.07
15	4/02/21	TA309	0.413	0.017	2.88	0.16	1.20	0.11	248	23	977	76	42	5	-	-	-	-	-	32.4	1.8	-31.1	-5.46
16	26/03/21	TA318	0.592	0.023	4.48	0.18	1.74	0.10	598	44	456	30	60	5	-	-	-	-	-	-	-	-	-
17	7/04/22	TA355	0.473	0.021	7.67	0.31	2.83	0.20	278	25	705	55	80	8	-	-	-	-	-	21.2	1.3	-29.0	-5.42
18	7/04/22	TA356	0.656	0.022	4.91	0.23	2.28	0.16	250	22	592	45	65	6	-	-	-	-	-	9.6	0.6	-28.1	-5.01
19	26/02/85	TM277	1.239	0.140	-	-	-	-	-	-	-	-	-	-	100	-	-25.0	-	-	-	-	-	-
20	9/03/21	TA313	0.478	0.021	0.63	0.09	0.37	0.04	8	4	83	7	2	3	41.3	0.2	-12.8	0.2	1745	-	-	-	-
21	26/02/85	TM281	0.147	0.100	-	-	-	-	-	-	-	-	-	-	1	-	-5.0	-	24800	-	-	-	-
22	26/02/85	TM280	2.881	0.230	-	-	-	-	-	-	-	-	-	-	10	-	-5.0	-	5730	-	-	-	-
23	28/08/17	TA231	0.010	0.013	0.14	0.13	0.09	0.08	2	3	5	2	0	5	-	-	-	-	-	-	-	-	-
24	26/02/15	-	-0.015	0.016	0.45	0.09	0.07	0.02	2	0	3	3	1	2	-	-	-	-	-	-	-	-	-
25	26/02/15	-	0.005	0.016	0.08	0.07	0.05	0.02	1	1	3	4	1	2	-	-	-	-	-	-	-	-	-
26	26/02/15	-	-0.008	0.016	0.05	0.07	0.04	0.01	1	0	5	6	1	5	-	-	-	-	-	-	-	-	-
27	11/03/21	TA315	0.306	0.019	8.39	0.37	2.19	0.13	201	20	520	36	66	6	89.6	0.3	-17.3	0.2	-	-	-	-	-
28	26/02/85	TM286	0.029	0.100	-	-	-	-	-	-	-	-	-	-	-	-	-	-	-	-	-	-	-
29	18/03/85	TM293	0.157	0.070	-	-	-	-	-	-	-	-	-	-	-	-	-	-	-	-	-	-	-
30	26/02/85	TM284	0.118	0.100	-	-	-	-	-	-	-	-	-	-	-	-	-	-	-	-	-	-	-
31	26/02/85	TM285	0.118	0.100	-	-	-	-	-	-	-	-	-	-	-	-	-	-	-	-	-	-	-
32	11/01/21	TA290	0.012	0.014	0.11	0.17	0.05	0.03	1	10	58	5	116	28	11.1	0.2	-17.1	0.2	15000	6.9	0.5	-27.3	-5.05
33	3/11/15	TA216	0.011	0.013	1.15	0.15	0.68	0.08	15	3	55	9	5	3	-	-	-	-	-	-	-	-	-
34	7/01/21	TA300	-0.004	0.014	1.31	0.20	0.12	0.03	0	1	4	3	1	4	-	-	-	-	-	27.5	1.5	-29.1	-5.09

No.	Date	T Code	TR	±	SF_6 (pptv)	±	Halon (pptv)	±	CFC-11 (pptv)	±	CFC-12 (pptv)	±	CFC-113 (pptv)	±	^{14}C (pmc)	±	$\delta^{13}C$ (‰)	±	^{14}C Age (y)	Rn (Bq/L)	±	$\delta^{2}H$	$\delta^{18}O$
35	11/01/21	TA289	-0.023	0.015	0.12	0.06	0.08	0.03	2	1	4	2	1	2	-	-	-	-	-	7.5	0.5	-29.3	-5.44
36	6/11/85	TM315	0.039	0.080	-	-	-	-	-	-	-	-	-	-	-	-	-	-	-	-	-	-	-
37	6/11/85	TM314	0.088	0.080	-	-	-	-	-	-	-	-	-	-	-	-	-	-	-	-	-	-	-
38	6/11/85	TM316	0.079	0.080	-	-	-	-	-	-	-	-	-	-	-	-	-	-	-	-	-	-	-
39	11/03/21	TA312	0.662	0.023	0.35	0.09	0.05	0.02	9	4	7	2	1	2	28.0	0.2	-21.0	0.2	9100	-	-	-	-
40	11/06/14	TA190	0.043	0.013	69000	7000	-	-	211	26	743	99	0	2	-	-	-	-	-	-	-	-	-
41	28/01/21	TA306	0.006	0.013	0.21	0.05	0.04	0.07	533	498	104	12	1	2	-	-	-	-	-	16.3	1.0	-30.4	-5.53
42	28/01/21	TA307	0.004	0.012	0.19	0.05	0.00	0.07	7	18	3	3	1	3	-	-	-	-	-	5.5	0.4	-30.5	-5.48
43	6/11/85	TM321	0.088	0.090	-	-	-	-	-	-	-	-	-	-	-	-	-	-	-	-	-	-	-
44	4/05/21	TA311	-	-	-	-	-	-	-	-	-	-	-	-	1.83	0.21	-13.6	0.2	28000	-	-	-	-
45	6/11/85	TM313	-0.010	0.080	-	-	-	-	-	-	-	-	-	-	-	-	-	-	-	-	-	-	-
46	7/01/21	TA299	0.016	0.012	0.90	0.19	0.30	0.04	0	2	49	5	1	2	-	-	-	-	-	6.6	0.4	-30.3	-5.35
47	7/01/21	TA298	-0.032	0.014	0.48	0.19	0.05	0.03	2	3	1	4	-1	-2	-	-	-	-	-	8.8	0.5	-29.7	-5.31
48	18/12/90	TM510	0.098	0.080	-	-	-	-	-	-	-	-	-	-	-	-	-	-	-	-	-	-	-
49	4/05/21	TA310	-	-	-	-	-	-	-	-	-	-	-	-	1.82	0.21	-13.6	0.2	28100	-	-	-	-

Table 4.3 Electric conductivity (EC), dissolved oxygen (DO), nitrate (NO_3-N), radon-222 (Rn), deuterium (δ^2H), oxygen-18 ($\delta^{18}O$), tritium ratios (TR) and mean transit times (MTT) for the streams sampled on 22 February 2022. Auckland Council (AC) ID code: G – gauging site at road bridge, and, from there, a few hundred metres U – upstream, D – downstream. 'T Code' is the Tritium laboratory code.

AC ID	Site Name	EC (µS/cm)	DO (mg/L)	NO_3-N (mg/L)	Rn (Bq/L)	±	δ_2H (‰)	$\delta^{18}O$ (‰)	T Code	TR	±	MTT (y)
1U	Hingaia at Cascades	-	-	-	0.6	0.09	-	-	-	-	-	-
1G	Hingaia at Cascades	198	9.4	4.3	0.49	0.08	-29.3	-5.15	TA325	0.648	0.020	21
1D	Hingaia at Cascades	-	-	-	0.46	0.08	-	-	-	-	-	-
2U	Hingaia at Stones Rd	-	-	-	0.11	0.04	-	-	-	-	-	-
2G	Hingaia at Stones Rd	213	9.7	3.5	0.11	0.04	-29.0	-5.29	TA326	0.626	0.020	24
2D	Hingaia at Stones Rd	-	-	-	0.99	0.12	-	-	-	-	-	-
3U	Hingaia at Ararimu Rd	-	-	-	0.18	0.05	-	-	-	-	-	-
3G	Hingaia at Ararimu Rd	182	9.1	8.6	0.18	0.05	-28.6	-5.21	TA327	0.545	0.022	30
3D	Hingaia at Ararimu Rd	-	-	-	0.22	0.05	-	-	-	-	-	-
4U	Hingaia at Maxted Rd	-	-	-	0.19	0.05	-	-	-	-	-	-
4G	Hingaia at Maxted Rd	253	9.6	8.8	0.19	0.05	-29.3	-5.28	TA328	0.548	0.022	30
4D	Hingaia at Maxted Rd	-	-	-	0.12	0.04	-	-	-	-	-	-
5U	Hingaia at Quarry Rd	-	-	-	0.26	0.06	-	-	-	-	-	-
5G	Hingaia at Quarry Rd	259	8.8	7.2	0.18	0.05	-28.8	-5.11	TA329	0.561	0.020	29
5D	Hingaia at Quarry Rd	-	-	-	0.27	0.06	-	-	-	-	-	-
13U	Maukua at Puni Aka Aka Rd	-	-	-	2.01	0.21	-	-	-	-	-	-
13G	Mauku at Puni Aka Aka Rd	285	7.9	15.0	1.95	0.2	-28.3	-4.91	TA330	0.672	0.021	20
13D	Mauku at Puni Aka Aka Rd	-	-	-	1.87	0.2	-	-	-	-	-	-
23U	Mauku at Fallows Wiley Rd	-	-	-	0.66	0.12	-	-	-	-	-	-
23G	Mauku at Fallows Wiley Rd	285	7.9	14.8	0.46	0.1	-26.5	-4.85	TA331	0.724	0.022	17

AC ID	Site Name	EC (µS/cm)	DO (mg/L)	NO_3-N (mg/L)	Rn (Bq/L)	±	δ_2H (‰)	$\delta^{18}O$ (‰)	T Code	TR	±	MTT (y)
23D	Mauku at Fallows Wiley Rd	-	-	-	0.41	0.09	-	-	-	-	-	-
16U	Mauku at Titi Rd	-	-	-	1.02	0.15	-	-	-	-	-	-
16G	Mauku at Titi Rd	296	6.8	9.1	0.75	0.12	-25.8	-4.55	TA332	0.818	0.023	13.5
16D	Mauku at Titi Rd	-	-	-	0.92	0.14	-	-	-	-	-	-
24U	Mauku at Wrights W Gardens	-	-	-	0.52	0.11	-	-	-	-	-	-
24G	Mauku at Wrights W Gardens	288	3.3	6.9	0.49	0.1	-26.3	-4.5	TA333	0.77	0.022	15
24D	Mauku at Wrights W Gardens	-	-	-	0.18	0.06	-	-	-	-	-	-
20U	Mauku at Swede Patullo Rd	-	-	-	0.53	0.1	-	-	-	-	-	-
20G	Mauku at Swede Patullo Rd	280	7.8	4.5	0.51	0.1	-26.5	-4.65	TA334	0.686	0.022	19
20D	Mauku at Swede Patullo Rd	-	-	-	0.46	0.09	-	-	-	-	-	-
15U	Ngakoroa at Mill Rd	211	n/a	-	0.58	0.09	-	-	-	-	-	-
15G	Ngakoroa at Mill Rd	211	n/a	2.9	0.65	0.1	-25.3	-4.33	TA335	0.908	0.026	11
15D	Ngakoroa at Mill Rd	209	n/a	-	0.24	0.06	-	-	-	-	-	-
7U	Ngakoroa at Ingrams	-	-	-	0.85	0.13	-	-	-	-	-	-
7G	Ngakoroa at Ingrams	242	6.4	4.6	1.21	0.16	-26.6	-4.7	TA336	0.779	0.024	15
7D	Ngakoroa at Ingrams	-	-	-	1.1	0.15	-	-	-	-	-	-
8U	Ngakaroa at Kern Rd	-	-	-	0.42	0.09	-	-	-	-	-	-
8G	Ngakaroa at Kern Rd	254	8.0	3.8	0.31	0.07	-26.8	-4.6	TA337	0.696	0.022	18
8D	Ngakaroa at Kern Rd	-	-	-	0.28	0.07	-	-	-	-	-	-
9U	Ngakaroa at Runciman	-	-	-	0.33	0.08	-	-	-	-	-	-
9G	Ngakaroa at Runciman	245	4.5	0.7	0.35	0.08	-27.1	-4.48	TA338	0.77	0.024	15
9D	Ngakaroa at Runciman	-	-	-	0.26	0.07	-	-	-	-	-	-

AC ID	Site Name	EC (µS/cm)	DO (mg/L)	NO_3-N (mg/L)	Rn (Bq/L)	±	δ_2H (‰)	$\delta^{18}O$ (‰)	T Code	TR	±	MTT (y)
10U	Oira at Tuhimata Rd	-	-	-	0.24	0.07	-	-	-	-	-	-
10G	Oira at Tuhimata Rd	246	2.7	0.0	0.33	0.08	-26.0	-4.57	TA339	0.551	0.021	30
10D	Oira at Tuhimata Rd	-	-	-	0.18	0.06	-	-	-	-	-	-
11U	Oira at Swing Bridge Woodlyn Dr	-	-	-	0.6	0.1	-	-	-	-	-	-
11G	Oira at Swing Bridge Woodlyn Dr	232	1.8	0.0	0.69	0.11	-28.2	-4.63	TA340	0.576	0.020	28
11D	Oira at Swing Bridge Woodlyn Dr	-	-	-	1.04	0.14	-	-	-	-	-	-
19U	Waitangi at Waiuku Rd	-	-	-	1.92	0.21	-	-	-	-	-	-
19G	Waitangi at Waiuku Rd	187	0.9	0.2	1.6	0.19	-27.2	-4.82	TA341	0.732	0.021	16.5
19D	Waitangi at Waiuku Rd	-	-	-	1.7	0.2	-	-	-	-	-	-
6U	Waitangi at SH Bridge	217	n/a	-	0.34	0.07	-	-	-	-	-	-
6G	Waitangi at SH Bridge	211	n/a	0.0	0.49	0.09	-25.6	-4.78	TA342	0.714	0.022	17
6D	Waitangi at SH Bridge	206	n/a	-	0.21	0.06	-	-	-	-	-	-
17U	Whangamaire at Railway Culv	-	-	-	0.56	0.1	-	-	-	-	-	-
17G	Whangamaire at Railway Culv	282	8.7	18.8	0.55	0.1	-26.4	-4.85	TA343	0.77	0.023	15
17D	Whangamaire at Railway Culv	-	-	-	0.56	0.1	-	-	-	-	-	-
18U	Whangamaire at D/S H Reserve	-	-	-	0.08	0.04	-	-	-	-	-	-
18G	Whangamaire at D/S H Reserve	281	9.6	18.6	0.03	0.02	-27.2	-4.88	TA344	0.784	0.023	15
18D	Whangamaire at D/S H Reserve	-	-	-	0.05	0.03	-	-	-	-	-	-
21U	Whangamaire at Ostrich Rd	-	-	-	0.13	0.05	-	-	-	-	-	-
21G	Whangamaire at Ostrich Rd	291	8.2	15.6	0.18	0.06	-26.7	-4.83	TA345	0.772	0.025	15.5
21D	Whangamaire at Ostrich Rd	-	-	-	0.27	0.07	-	-	-	-	-	-
26U	Whangamaire at Glenbrook Rd	-	-	-	0.41	0.08	-	-	-	-	-	-

AC ID	Site Name	EC (µS/cm)	DO (mg/L)	NO_3-N (mg/L)	Rn (Bq/L)	±	δ_2H (‰)	$\delta^{18}O$ (‰)	T Code	TR	±	MTT (y)
26G	Whangamaire at Glenbrook Rd	281	6.2	11.4	0.34	0.08	-25.4	-4.9	TA346	0.702	0.023	18
26D	Whangamaire at Glenbrook Rd	-	-	-	0.52	0.1	-	-	-	-	-	-
22U	Whangamaire at Fantail	282	-	-	0.16	0.05	-	-	-	-	-	-
22G	Whangamaire at Fantail	282	9.6	11.3	0.21	0.06	-26.4	-4.81	TA347	0.674	0.022	20
22D	Whangamaire at Fantail	274	-	-	0.13	0.05	-	-	-	-	-	-
25U	Whangapouri at Hickey Spr US	-	-	-	0.14	0.05	-	-	-	-	-	-
25G	Whangapouri at Hickey Spr US	273	7.0	4.6	0.07	0.03	-26.0	-4.73	TA348	0.767	0.022	15
25D	Whangapouri at Hickey Spr US	-	-	-	0.9	0.13	-	-	-	-	-	-
27U	Whangapouri at Paerata Falls	-	-	-	4.41	0.37	-	-	-	-	-	-
27G	Whangapouri at Paerata Falls	287	8.5	13.9	4.36	0.4	-27.2	-4.86	TA349	0.758	0.023	15.5
27D	Whangapouri at Paerata Falls	-	-	-	5.04	0.4	-	-	-	-	-	-
14U	Whangapouri at Glenbrook Rd	-	-	-	0.73	0.11	-	-	-	-	-	-
14G	Whangapouri at Glenbrook Rd	282	7.6	11.5	0.78	0.12	-27.1	-4.97	TA350	0.699	0.026	18
14D	Whangapouri at Glenbrook Rd	-	-	-	0.84	0.12	-	-	-	-	-	-
12U	Whangapouri at Pukekohe GC	-	-	-	0.98	0.14	-	-	-	-	-	-
12G	Whangapouri at Pukekohe GC	277	7.0	9.7	1.02	0.14	-26.8	-4.95	TA351	0.701	0.022	18
12D	Whangapouri at Pukekohe GC	-	-	-	0.85	0.13	-	-	-	-	-	-

5.0 DISCUSSION

In this section, results of the various methods are discussed. The meaning of the results regarding the groundwater flow processes is discussed in Section 6.

5.1 Water Dating and Age Distribution

No significant trends of increase or decline in groundwater levels (Kalbus et al. 2017) or stream flows (White et al. 2019) have been detected over recent decades in the Pukekohe–Bombay basalt aquifers; the groundwater systems are expected to be in reasonable steady-state flow conditions, meaning constant groundwater age over time. This is confirmed by generally good matches of time-series age-tracer data over the two sampling periods (2015 and 2022). However, several NGMP wells with long time-series of hydrochemistry and age-tracer concentrations indicate abrupt changes in water age and hydrochemistry (Section 5.6). Changes in groundwater age were also identified in a few isolated cases. In these cases, the latest age-distribution parameters are given.

MRTs are primarily based on the tritium concentrations in the groundwater, as the gas-tracer concentrations can be affected by contamination from local sources or during sampling and by degradation processes in the groundwater system. Where gas-tracer data was found consistent with other age-tracer data, it was used in a multi-tracer approach to derive the age distribution parameters. Usually, SF_6 behaves conservatively in groundwater, but several groundwater samples collected from the basalt aquifers were found to have extremely high SF_6 contamination levels (Section 5.8), and others may also have low levels of contamination. On the other hand, Halon-1301 behaved relatively conservatively in the oxic groundwaters from the basalt aquifers. So, between SF_6 and Halon-1301, there was generally one tracer that could be used together with tritium. Examples are shown in Figure 5.1.

The mixing model parameters were derived from best-fitting model output matches to the tracer time-series, or to multi-tracer concentrations. Where age-tracer data was insufficient to derive mixing parameters, a conservative estimate of 70% of exponential age distribution within the total flow volume with exponential piston flow age distribution was used. A summary of the model methodology is given in Appendix 1.

Several age-tracer datasets were found to be inconsistent and had to be discarded:

- **Tuhimata Road:** The relatively high tritium concentration is inconsistent with the SF_6 and ^{14}C concentrations and was therefore discarded. The ^{14}C age was used.
- **BJ Crowe:** All age-tracer time-series from the two sampling campaigns in 2014 and 2021 disagree (Figure 5.1). The 2021 data indicate significantly older water compared to 2014. The 2021 data were used.
- **Balance Agri:** The 2021 tritium concentration is inconsistent with the gas age-tracer time-series and 2014 tritium data. The 2021 tritium data was discarded.
- **Glen Hall:** The presence of a small amount of tritium is inconsistent with a relatively old ^{14}C age, probably indicating a mixture of younger into much older water within the well, which is likely to have a long screen. The ^{14}C age was used.

- **Kiwi Broilers:** No depth information was available for this well, therefore it had to be excluded from most of the interpretations. Despite relatively low tritium levels, the SF_6, CFCs and Halon-1301 data indicate young water. It is likely that this water had contact with air, either in the well or during sample collection. A strong meat smell was noticed in the lab when processing this water. Also, the carbon isotope data are indicative of exchange with atmospheric CO_2. The tritium age was used.

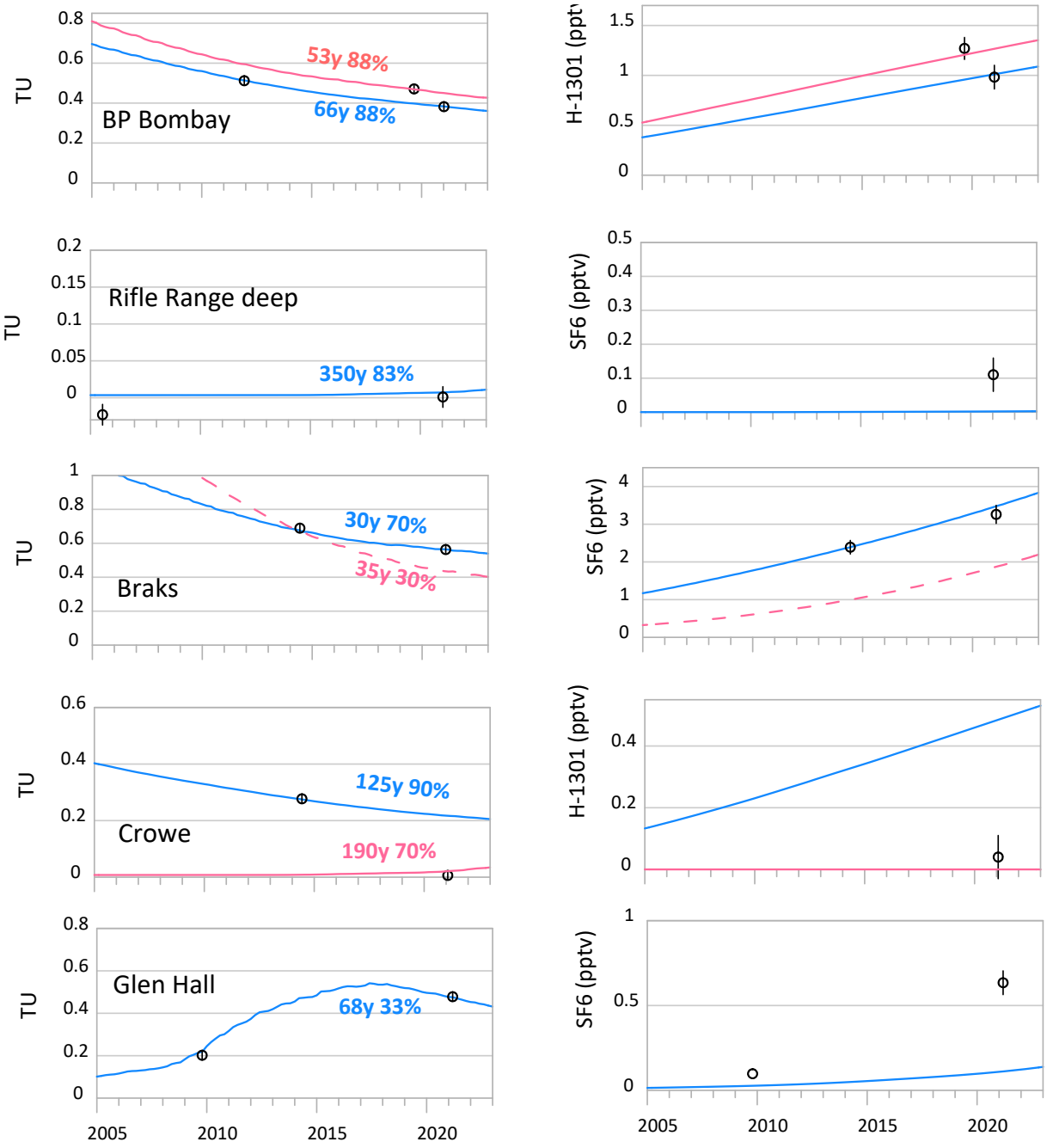

Figure 5.1 Tritium, SF_6 and H-1301 time-series (error bars one-standard deviation) with matched exponential piston flow model outputs for various wells. Blue and red curves show different model outputs (bullet points in text below). Labels show sample name and matching age-distribution parameters. The first parameter is MRT in years and the second parameter is *f*, the fraction of the exponential (mixed) flow volume within the total flow volume.

Five examples of groundwater age modelling are shown in Figure 5.1, with:

- **BP Bombay:** showing consistent results between tritium and Halon-1301. The 2011 and 2021 tritium data (summer samples) match the same age-distribution parameters, indicating steady-state flow condition (blue line). However, both the tritium and Halon-1301 data indicate seasonal variability. The water at the end of August 2019 was younger, likely due to enhanced recharge during winter (red line).
- **Rifle Range Deep:** showing consistently zero or near-zero concentrations for tritium and SF_6. The low tritium concentration indicates that the water is older than MRT 350 years.
- **Braks:** being an example where the age-tracer time-series, available due to the re-sampling in 2021, shows that the model assumption of high piston flow fraction in van der Raaij (2015) is not realistic. Both tritium and SF_6 together and their time-series cannot be fitted to a model with a high piston flow component (red dashed line). Only with a 70% exponential (mixed) flow component can all the data be fitted (blue line).
- **Crowe:** showing a well now drawing significantly older water (red line) compared to previously younger water (blue line). This is a single case and not characteristic of the area.
- **Glenn Hall:** being an example where historic data (from 2009) was able to constrain an unusually high piston flow fraction. Again, this is only one of a few cases and not typical for the area. The high piston flow fraction is likely related to fracture flow (Section 6.5).

In the previous study, in absence of time-series data, van der Raaij (2015) proposed high piston flow fractions in the groundwater to explain high nitrate concentrations observed in relatively old water. The tracer time-series data from the current study were able to constrain the mixing parameters, proving the absence of high piston flow in most of the wells. An example is shown in Figure 5.1 (Braks).

MRT as derived from tritium, SF_6 and Halon-1301 data using the RPM are listed in Table 5.1. All of the groundwaters included in this study are relatively old, with MRT >15 years. Some historic data could not be interpreted into MRT because, at earlier sampling times, there was still some interference from remaining bomb-tritium from the atmospheric thermonuclear weapons testing in the early 1960s.

Table 5.1 Groundwater mean residence times (MRT) in years. E%PM is the fraction (%) of exponential flow within the total flow volume of an exponential piston flow model. Values of 70% (in red) are estimated, and all others are derived from data.

No.	ID 2015	Site ID	Name	E%PM	MRT (y)
1	P5	7428105	Rifle Range Shallow NEW	20	*40*
2	-	7428103	Rifle Range Deep	83	*>350*
3	-	7419127	Hickey Spring	70	*18*
4	-	-	Crisp Ave. Spring	70	*18*
5	PA	3506	Agrisystems	95	*23*
6	P4	7428031	Wilcox Gun Club	93	*19*
7	P2	3573	Plant Food Res	70	*16*
8	P1	3598	Balance Agri	70	*23*
9	P3	3623	Nicholls	40	*90*
10	-	43915	Patumahoe Spring	70	*17*
11	-	-	Douglas	70	>160

No.	ID 2015	Site ID	Name	E%PM	MRT (y)
12	PW	3610	AS Wilcox	96	*>500*
13	BP	7419121	BP Bombay	88	*66*
14	B2	4315	Braks	70	*30*
15	B1	21950	Thich Phuoc An	67	*45*
16	BW	4352	Wallath	99	*55*
17	-	7419126	Hillview Spring	70	*36*
18	-	-	Pilgrim Rd Spring	70	*21*
19	-	-	Coster	70	58
20	-	7417001	Glen Hall	33	*68*
21	-	-	McKenzie Well B	70	>100
22	-	-	McKenzie Well A	-	Ambiguous
23	-	-	Cornwall Rd Well	70	>180
24	-	8592	STCWR	70	>180
25	-	92189	STVIC	70	>180
26	-	174235	STWKU	70	>180
27	-	28320	Kiwi Broilers	70	*6/75*
28	-	-	Noort Well	70	>130
29	-	-	Falcon Orchards	70	82
30	-	-	Tucker	70	>130
31	-	-	Brundell	70	>130
32	-	7417021	Seagrove	83	*>320*
33	-	-	Kingseat Well	70	>180
34	-	7418023	Ostrich Shallow	70	*>200*
35	-	7418027	Ostrich Deep	83	*>340*
36	-	-	NZ Dairy Co #12	70	>130
37	-	-	NZ Dairy Co #9	70	>100
38	-	-	Pukekohe Borough Council	70	>130
39	-	-	Tuhimata	-	Ambiguous
40	B5	4185	Taylor	70	*>300*
41	B3	4162	Crowe	70	*>190*
42	B4	4133	Martyn	50	*>130*
43	-	-	Rainbow Park Nurseries	70	>130
44	-	20424	Underglass	-	Not analysed
45	-	-	Harnett Orchards	70	>130
46	-	7419009	Fielding Volcanic	70	*195*
47	-	7419007	Fielding Sand	70	*200*
48	-	-	Oostdam	70	>130
49	-	30129	Brink	-	Not analysed

Deeper groundwaters in the Pukekohe–Bombay area were often found to have tritium and gas age-tracer concentrations close to zero (e.g. van der Raaij 2015). These groundwaters could potentially be significantly older than a MRT of several hundred years, the dating limit for the tritium method. They could be up to thousands of years old. To estimate the age range of such old groundwater, ^{14}C samples were collected from selected sites (Table 4.2). To account for dilution of ^{14}C by dead carbon from minerals, the isotope dilution method after Mook (2001) was used (Figure 5.2).

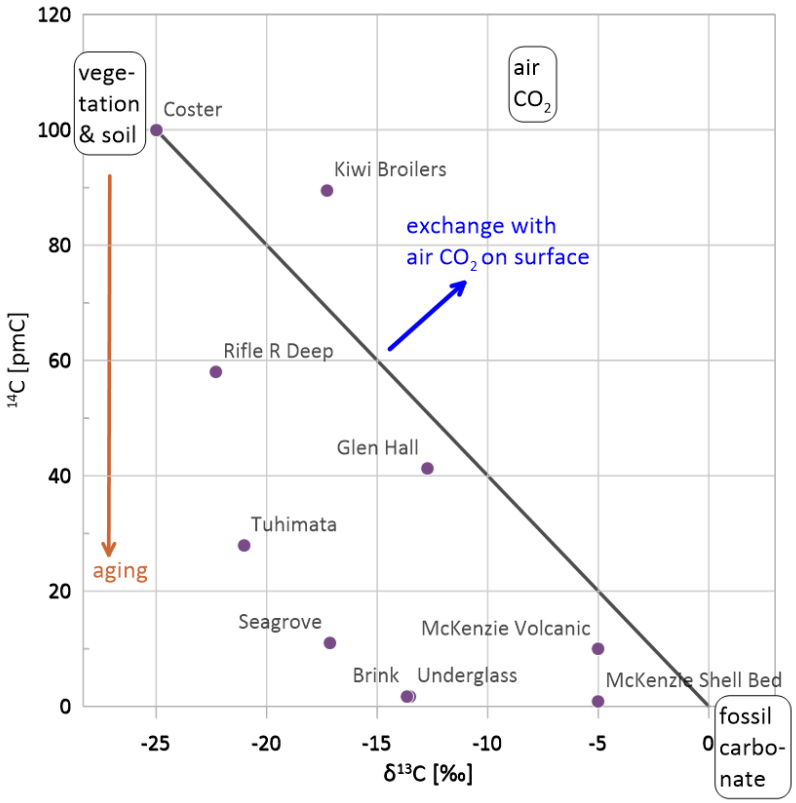

Figure 5.2 ^{14}C versus $\delta^{13}C$ for dissolved inorganic carbon in groundwater. Data for McKenzie well from historic database. Carbon isotope dilution after Mook (2001).

The groundwater at Kiwi Broilers is likely to have been in exchange with air CO_2, and the water is likely to be young. The carbon isotope data for the groundwater from the Glenn Hall and Coster wells are close to the isotope dilution line; these groundwaters are relatively young, as indicated by tritium. The carbon isotope data in the groundwater of the Tuhimata well are inconsistent with tritium, indicating mixing of young and very old water. This is likely to be occurring within the well due to a long well screen. The groundwaters in the wells at Underglass, Brink, Seagrove and Rifle Range Deep are likely to be relatively old, on the ^{14}C scale. ^{14}C ages are listed in Table 4.2.

For the 27 sampled stream sites, the MTT were inferred from the measured tritium concentrations, consistently using an EPM with 70% of exponential flow distribution within the total flow volume. Results are listed in Table 5.1.

Figure 5.3 shows groundwater MRT for all sites with available data in the area of the Pukekohe–Bombay basalt lava, including data collected for this project (Table 5.1, circle symbols) and data from previous projects (shown as square symbols). To provide a more complete picture of groundwater flow processes, data from historic projects available from the Waikato part of the Pukekohe–Bombay basalt lava has also been included. All historic age-tracer data was interpreted consistently together with the new 2021/22 data.

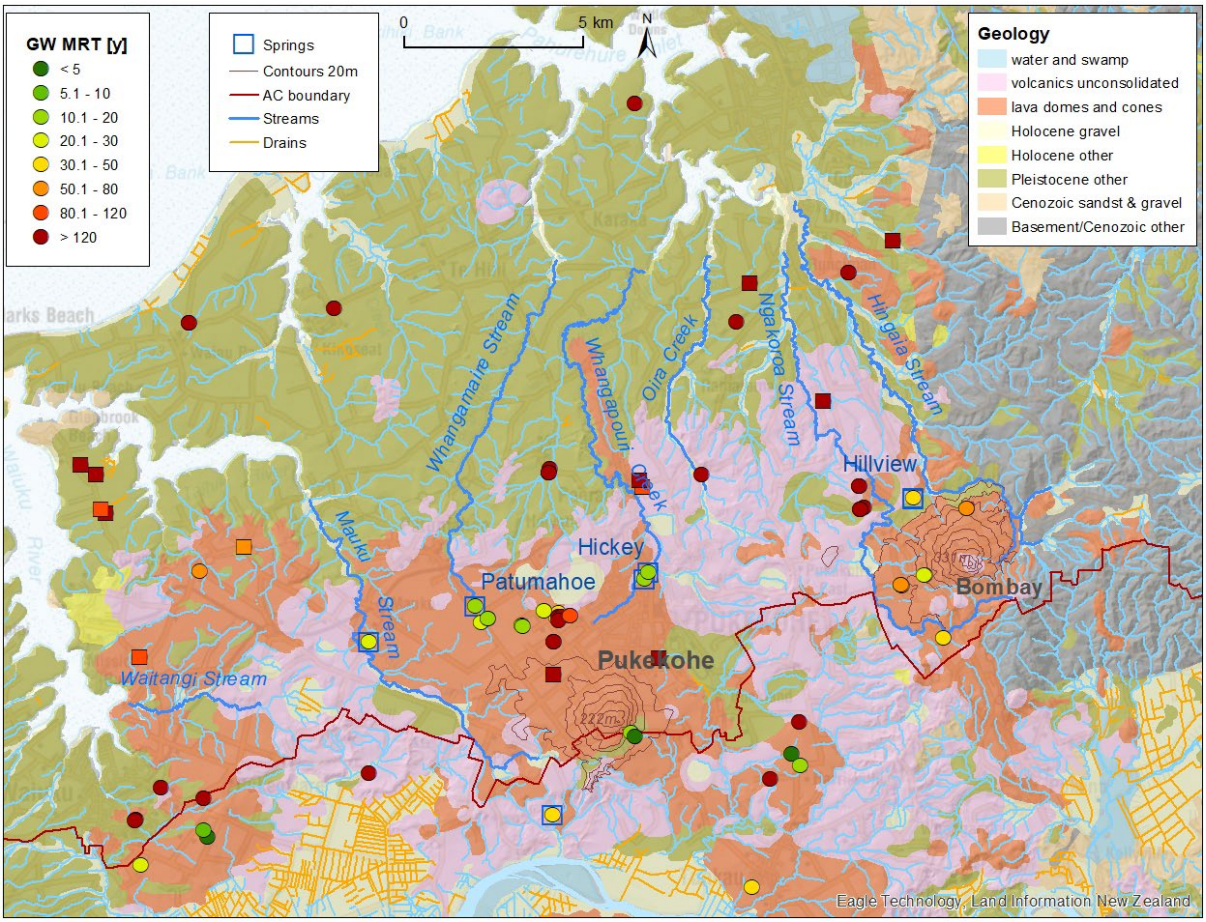

Figure 5.3 Groundwater mean residence times (MRT) in years shown for the area of the Pukekohe–Bombay volcanoes. Square symbols are derived from historic data for the Auckland region. Data south of the Auckland Council boundary are from the Waikato database.

All wells in the Pleistocene deposits and underlying Kaawa shell aquifer and Waitemata Group, and unconsolidated volcanic deposits between the basalt lava and Manukau Harbour, contain old water, as indicated by the dark red symbols in Figure 5.3. The MRT of most of these groundwaters is older than 120 years, close to or beyond the dating range of the tritium method. These groundwaters are likely to be thousands of years old. Table 5.1 shows that ^{14}C indicated an age of 28,000 years in two of the wells in the Pleistocene deposits (Brink and Underglass) and an age of 9100 years in one well in the Kaawa shell aquifer (Tuhimata). All of these wells are deep (Figure 2.4), indicating limited groundwater availability and recharge in this area due to low hydraulic conductivity. These wells tap into groundwater systems that are not part of the active drainage; therefore, there is little recharge to these groundwater systems (Section 6.4).

Young groundwaters (<80 years) indicative of active recharge systems were observed only within the shallow groundwater systems of the basalt lava and in their spring discharges. The sampled groundwaters were youngest at the Pukekohe basalt lava. The main springs discharge water with MTT = 18 years, and the youngest sampled groundwater has MRT = 16 years. At the Bombay basalt lava, the water of the main spring discharge and the youngest groundwater in wells was approximately twice as old, compared to the Pukekohe lava, with Hillview Spring discharging water with MTT = 36 years and the youngest groundwater having MRT = 30 years.

In the less extensive basalt lava to the west, near Waitangi Stream, the groundwater is significantly older but still contains tritium, with MRTs in the range of 60–100 years. This indicates a less active recharge and groundwater flow system due to the shallower nature of the basalt formation.

The groundwater in the deep Pukekohe basalt lava is also significantly older, as indicated by the dark red symbols in the centre of the Pukekohe basalt lava. This implies that the deeper lava formation is not part of the very active groundwater flow system observed in the shallower system. This agrees with observations of delayed response to rainfall and different water tables, indicating hydraulically distinct groundwater systems.

On Waikato's southern flanks of the basalt lava, younger groundwaters (MRT ca. 5 years) were encountered. However, there is limited information available about the wells. These may be very shallow. In general, this area is not expected to be representative of the Auckland part of the basalt lavas due to the northward dip of the geologic formation. A spring in this area (Liefting Spring) discharges water from the basalt lava with MTT = 41 years, similar to Hillview Spring (springs are indicated in figures by blue square symbols).

Figure 5.4 shows the MTT of the water through the groundwater system, as measured in the springs and streams, together with MRTs of the shallow groundwaters with ages in the same range. Groundwater MRTs and stream MTTs are shown at the same time scale. The older/deeper groundwater ages are not shown.

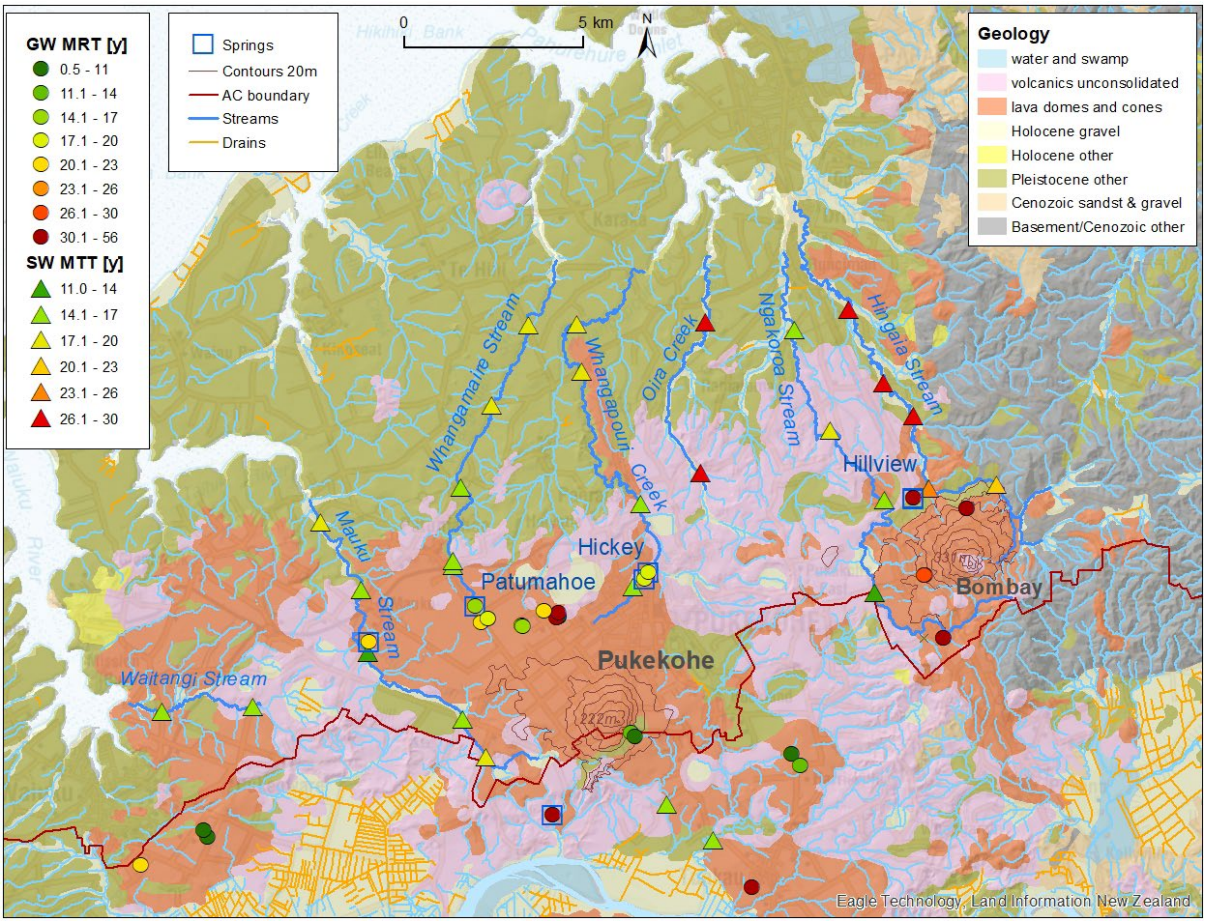

Figure 5.4 Groundwater mean residence time (MRT) in wells (circles) and water mean transit time (MTT) in streams (triangles), shown at the same scale for the younger waters.

Groundwater MRTs in the basalt lavas are consistent with those of their spring discharges through Hillview, Hickey and Patumahoe springs and the MTTs of the water in the respective streams (Hingaia, Whangapouri and Whangamaire). The basalt groundwaters are the source of the main springs and of these streams.

In contrast, Ngakoroa Stream and Oira Creek mainly discharge water with MTTs that do not match the MRTs of the nearby basalt lavas. Ngakoroa Stream discharges significantly younger water compared to Bombay basalt groundwater, which discharges via Hingaia Stream, and Oira Creek discharges significantly older water compared to Pukekohe basalt groundwater, which discharges via Whangapouri Creek. Ngakoroa Stream and Oira Creek appear to be sourced by separate, more localised groundwater systems.

Mauku and Waitangi streams discharge water of similar MTT compared to that discharging from the Pukekohe basalt lava via Whangapouri Creek and Whangamaire Stream.

In summary, except for the basalt lavas, there is no active groundwater recharge in this area. Only the basalt lava contain young water, indicating active recharge. Whangamaire Stream and Whangapouri Creek mainly drain the actively recharging groundwater from the Pukekohe basalt lava, and Hingaia Stream drains the groundwater from the Bombay basalt lava. The remaining streams drain small local groundwater systems.

5.2 Hydrochemistry

5.2.1 Groundwater Quality National Context

Table 5.2 compares the hydrochemical composition of the Pukekohe–Bombay groundwaters with average New Zealand groundwater. Overall, the Pukekohe–Bombay groundwaters have slightly higher solute concentrations for chloride, bicarbonate, sodium, potassium and silica and significantly higher solute concentrations for magnesium, nitrate and dissolved reactive phosphorous (more than double for the New Zealand 50th percentiles).

Table 5.2 Hydrochemistry statistics, showing number of wells; minimum and maximum concentrations; and the 25th, 50th and 75th percentiles for all hydrochemistry data from wells with groundwater age-tracer data. The New Zealand percentiles, shown for comparison, are for groundwater quality data obtained from over 1000 sites collected as part of the SOE monitoring programmes run by regional authorities and compiled by the New Zealand Ministry for the Environment (Daughney and Wall 2007).

Parameter	Units	Pukekohe–Bombay Data						New Zealand Percentiles		
		No.	Min.	25%	50%	75%	Max.	25%	50%	75%
Ca	mg/L	16	1.5	13.0	15.3	17.3	163	9.6	15.5	30.0
Cl	mg/L	16	4.7	19.7	21.5	25.8	159	7.3	15.3	30.1
HCO_3	mg/L	16	16	50.5	67.8	152	245	40.0	62.7	144.6
K	mg/L	16	0.090	1.7	2.1	4.0	9.2	1.0	1.6	3.7
Mg	mg/L	16	0.0100	9.5	12.0	14.2	20.4	2.6	4.6	8.5
Na	mg/L	16	12.0	18.7	22.5	25.5	112	9.4	15.0	29.6
NO_3-N	mg/L	16	0.0010	0.0053	9.3	19	36.1	0.00	1.3	4.4
SiO_2	mg/L	16	3.2	34	40	47	74	13.5	17.0	29.5
SO_4	mg/L	11	0.020	0.98	2.2	3.2	26	3.0	6.5	13.0
DRP	mg/L	11	0.0040	0.039	0.052	0.17	0.56	0.01	0.02	0.07
Fe	mg/L	9	0.0031	0.0083	0.020	0.035	0.34	0.01	0.03	0.23
Mn	mg/L	16	0.0005	0.0005	0.0007	0.023	0.274	0.00	0.01	0.24
NH_3-N	mg/L	16	0.0025	0.0049	0.0088	0.14	1.00	0.00	0.01	0.06
Cond.	µS/cm	16	0.18	264	306	357	800	145	210.0	371
pH	pH unit	13	4.8	6.2	6.7	7.9	10.1	6.4	6.8	7.2

5.2.2 Redox Conditions

Dissolved oxygen (DO) and methane, both indicators of the redox state of the groundwater, are shown in Figure 5.5. Only the shallow groundwater in the basalt lavas is oxic (green inner circles), with DO concentration in this water typically >5 mg/L. Due to its oxic status, this water is free of methane (green outer circles). In contrast, all wells north of the basalt lava into the formations below the Pleistocene deposits and into the deep volcanics contain water depleted in DO and high in methane (red inner and outer circles), indicating highly anoxic environments up to the stage of methane fermentation. These groundwaters are from stagnant groundwater systems.

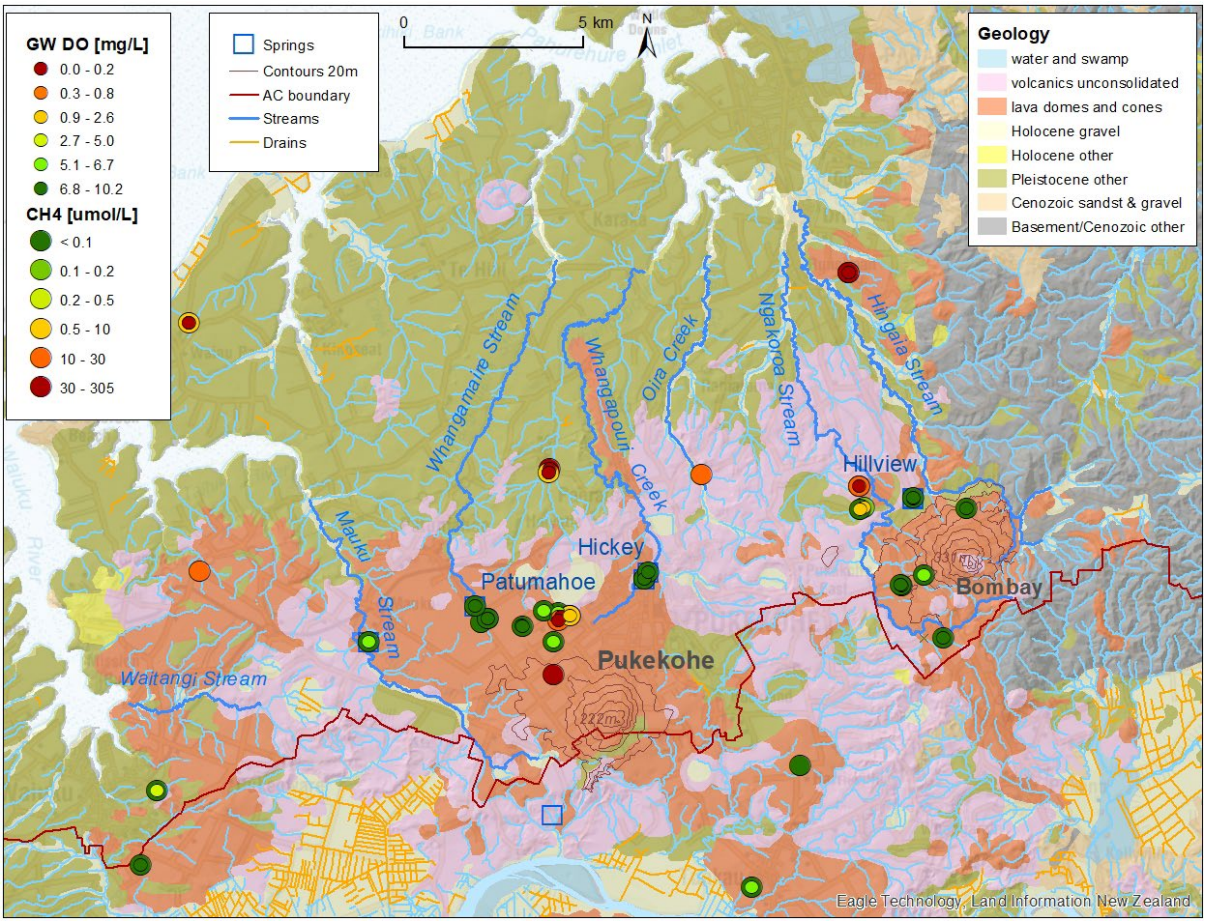

Figure 5.5 Map of dissolved oxygen (DO; inner circle) and methane (CH_4; outer circle) concentrations in groundwater.

Figure 5.6 shows the distribution of DO concentrations in the stream waters measured at the time of stream sampling. The largest discharges from the basalt lavas – Hingaia Stream, Whangapouri Creek and Whangamaire Stream – contain DO concentrations close to equilibrium saturation with air (c. 10.5 mg/L) at most of the sampled sites.

However, the smaller streams contain water that is partially depleted in DO. This is likely to indicate at least partial discharge of anoxic groundwater into these streams. Mismatching MTTs between these stream waters and the groundwater discharges from the basalt lava indicate that these streams are not sourced from the basalt lava. In particular, Oira Creek and Waitangi Stream contain water that is highly depleted in DO, with concentrations <2 mg/L. This may indicate that these streams are sourced from anoxic groundwater systems, with potential for denitrification processes in the groundwater systems, as also indicated by low nitrate concentrations observed in these streams (Section 5.7). These findings are consistent with the long-term (2005–2021) DO records at the Waitangi Stream reported in Casanovas et al. (2022).

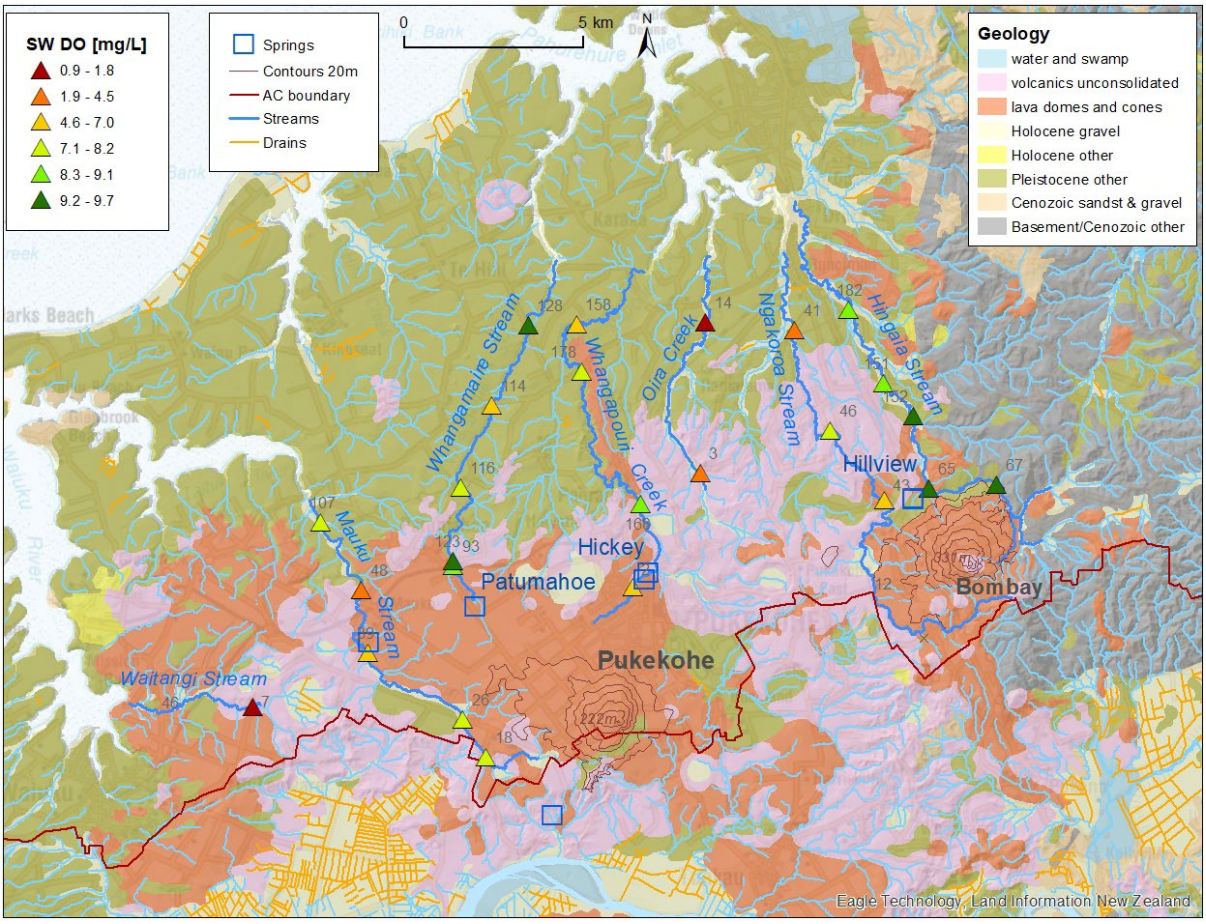

Figure 5.6 Map of dissolved oxygen (DO) of stream water.

5.2.3 Hierarchical Cluster Analysis

Hierarchical cluster analysis (HCA) categorises hydrochemistry data based on similarities in selected characteristics. Similarities in hydrochemistry may be able to link groundwater to sources in specific geological formations and help distinguish between different groundwater recharge sources (river water versus local rain). However in the Pukekohe–Bombay area, sufficient hydrochemistry data for performing HCA was available only for groundwater, not for stream water (as a limited number of streams have long-term monitoring). Therefore, identification of connections between surface water and groundwater is based only on MRT and the stable isotope composition of the water, radon and nitrate, as these were measured in the stream water (Sections 5.4, 5.5 and 5.7).

HCA results are displayed as a dendrogram (Figure 5.7). Each vertical line ends at a single sample site. Horizontal lines join hydrochemical groups. The similarity between sites and groups of sites is indicated by the height up the y-axis (distance) of the respective connecting horizontal line. Low horizontal lines join sites with the most similar chemistry. Selection of appropriate threshold lines divides the sites into clusters with similar chemistry.

At the highest threshold, the data is divided into three clusters: A, B and C (Figure 5.7). Cluster A consists of a single site (Seagrove), which exhibits a distinct sodium chloride dominant hydrochemical signature in contrast to clusters B and C. The main difference between clusters B and C is the oxygenation state, with Cluster B exhibiting reduced and Cluster C oxic conditions. At the second threshold, Cluster C is divided into two clusters, C1 and C2, with C1 showing a lower solute loading.

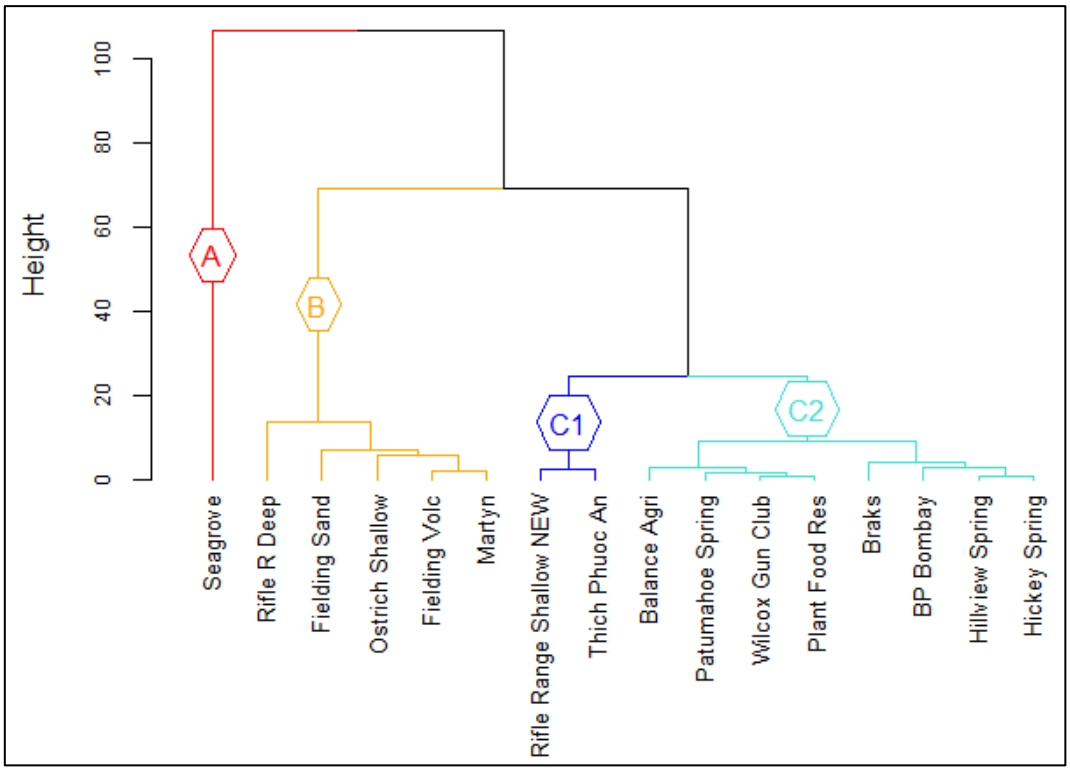

Figure 5.7 Dendrogram produced by hierarchical cluster analysis.

Groundwater sampled from the basalt aquifers was predominantly of type Mg-Na-Ca-HCO_3-NO_3-Cl or Mg-Na-Ca-NO_3-HCO_3-Cl (Figure 5.8; van der Raaij 2015). The dominance of magnesium observed in Cluster C reflects the basalt mineralogy [i.e. the presence of magnesium-rich olivine (Mg2+, Fe2+)2SiO4 and pyroxenes such as augite (Ca,Na)(Mg,Fe,Al,Ti)(Si,Al)2O6].

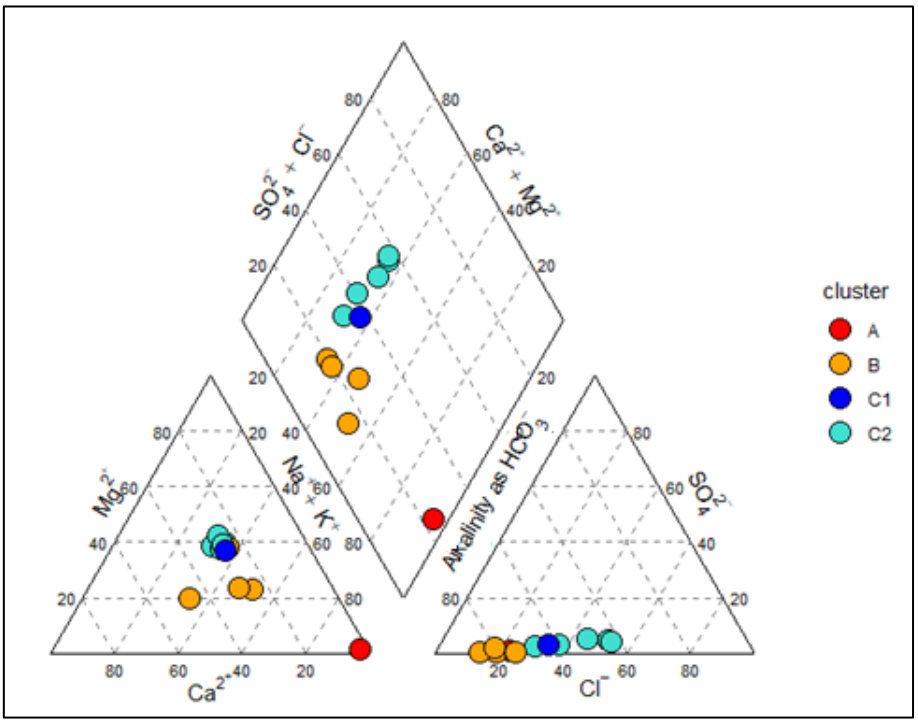

Figure 5.8 Piper diagram showing the variation of major ion groundwater chemistry by cluster. The left and right triangles show the major cation and anion ratios on an equivalence basis, respectively, and the centre diamond plots projections based on the two triangular plots. Sites are grouped into clusters assigned by hierarchical cluster analysis (Figure 5.7).

The three clusters can be described as follows (Figure 5.9; Table 5.3):

- Cluster A (n = 1) has the highest conductivity (median of 411 µS/cm) and high sodium, chloride and bicarbonate concentrations. DO concentration is low (median of 0.1 mg/L), and nitrogen occurs in the form of ammonia (median of 0.0.22 mg/L as N). MRT is over 300 years. The well depth is 201 m below ground level, and the screen intersects the Waitemata Formation.
- Cluster B (n = 5) exhibits lower conductivity (centroid median of 315 µS/cm); calcium and bicarbonate are dominant species, indicating that calcium may be derived from altered basalts, which have approximately 10 wt% of CaO (Cook et al. 2004), and DO concentration is low (centroid median of 0.14 mg/L). Nitrogen occurs in the form of ammonia (centroid median of 0.15 mg/L as N). Groundwater MRTs range from 195 to over 300 years. Well depths range from 48 to 90 m below ground level, and screens are sourced from multiple aquifers with a range of confinement status (Holocene sedimentary deposits, South Auckland volcanics and the Kaawa shell aquifer). Cluster B encompasses mixed aquifer sources and therefore exhibits a larger variability in chemical composition.
- Cluster C1 (n = 2) has the lowest conductivity (centroid median of 214 µS/cm). Concentrations of calcium, magnesium, sodium, chloride and sulphate are lowest within clusters B and C. Nitrate concentrations are moderate (median c. 8 mg/L as N at both wells), suggesting lower land-use impact. DO concentration is high (centroid median of 7.3 mg/L), indicating oxygenated conditions. Groundwater MRTs range from 40 to 45 years. Well depths range from 26 to 42 m below ground level, and screens are sourced from the basalt aquifers.
- Cluster C2 (n = 8) consists of Ca-Mg HCO_{3}-type waters with a similar solute loading to Cluster B (median conductivity of 307 µS/cm). Concentrations of calcium, potassium, bicarbonate, nitrate and sulphate are higher than the other cluster DO concentrations, indicating intermediate to oxygenated aquifer conditions (centroid median of 8.0 mg/L). Groundwater MRTs range from 16 to 66 years. Well depths range from 26 to 42 m below ground level, and screens are in the basalt aquifers (where information is available, unconfined). Clusters C1 and C2 are characterised by lower pH, silica, bicarbonate and potassium concentrations, reflecting the mineral composition of the main rock type. Cluster C2 exhibit high concentrations of nitrate (>15 mg/L as N), chloride and sulphate, indicators that, in conjunction, have been reported to indicate excess leaching from fertilisers (Morgenstern and Daughney 2012). Fertilisers have reportedly been used in Franklin (White et al. 2019), and associated leaching to groundwater recently tested and demonstrated in the area (Rogers and Buckthought 2022). The impact on groundwater quality is high within cluster C2 and moderate in C1.

Table 5.3 Hierarchical cluster analysis clusters showing water type and a general description of notable hydrochemistry and well depths from each cluster.

Cluster	Sites	Water Type	Description
A (n = 1)	Seagrove	Water types: Na-Cl	Reducing conditions, Waitemata Group – highest concentrations for Na, Cl and HCO_3. Old groundwater.
B (n = 5)	Ostrich Shallow, Fielding Sand, Fielding Volc, Rifle Range Deep, Martyn	Mixed water types: Ca-Mg-HCO_3-SO_4 to Na-Ca-HCO_3-Cl	Reducing conditions, impacted mixed sources – higher concentrations for SiO_2 and DRP. Old groundwater.
C1 (n = 2)	Rifle Range Shallow NEW, Thich Phuoc An	Mixed water types: Ca-Mg-HCO_3-SO_4 to Na-Ca-HCO_3-Cl	Moderately impacted volcanics – oxygenated conditions, low total dissolved solids, moderate nitrate concentrations. Young groundwater with MRT 40–45 years.
C2 (n = 8)	Hillview Spring, Hickey Spring, Patumaohe Spring, BP Bombay, Wilcox Gun Club, Plant Food Res, Balance Agri, Braks	Mixed water types: Ca-Mg-HCO_3-SO_4 to Na-Ca-HCO_3-Cl	Severely impacted volcanics – oxygenated conditions, widespread, high total dissolved content, high nitrate concentrations. Young-to-moderate groundwater with MRT 16–66 years.

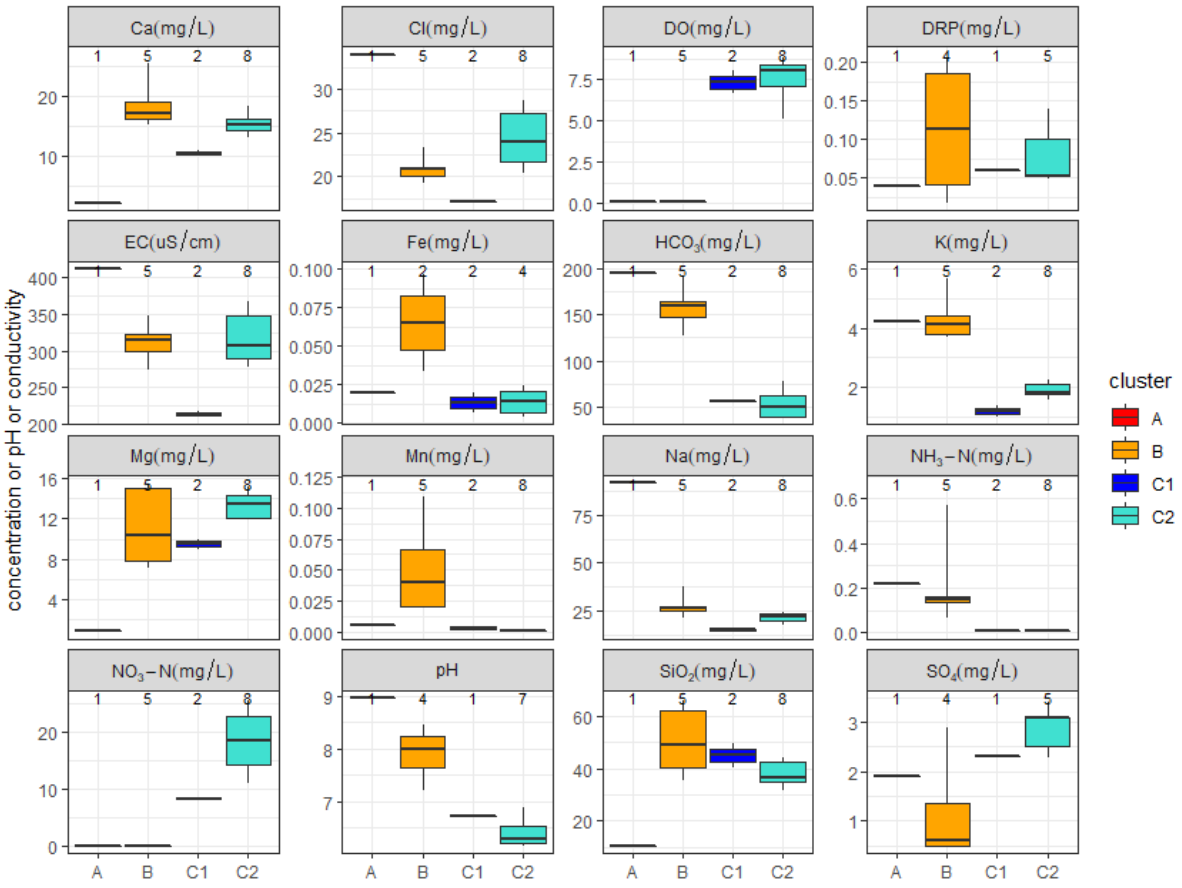

Figure 5.9 Box plots of hydrochemistry parameters organised by second threshold cluster. The numbers displayed above each box indicate the number of samples for each cluster.

The spatial distribution of the clusters is shown in Figure 5.10. Cluster A is located on a Pleistocene outcrop by the coast. Cluster B occurs both in the basalt lavas and the Pleistocene deposits. Clusters C1 and C2 occur in the unconsolidated volcanics in the recharge area of the Pukekohe and Bombay volcanoes.

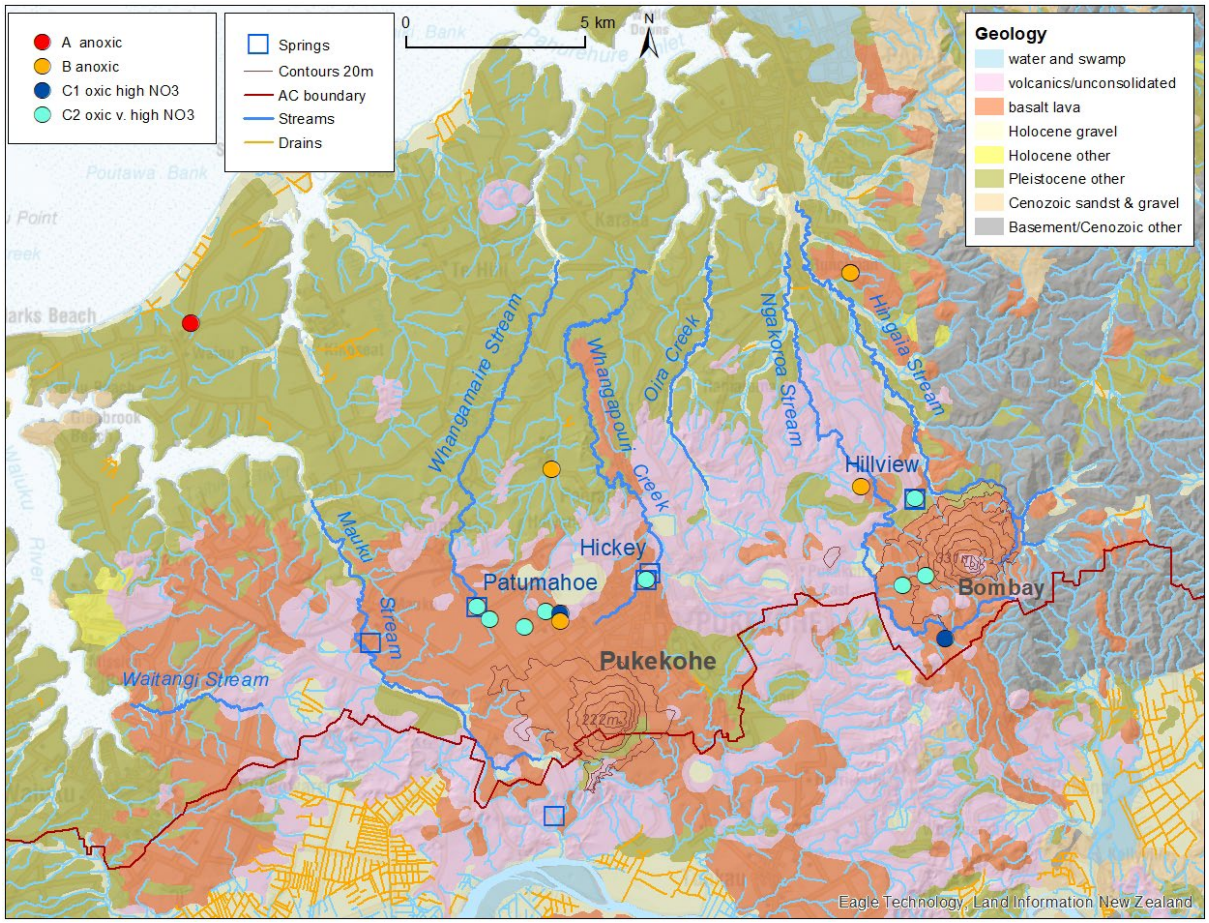

Figure 5.10 Spatial distribution of hydrochemistry clusters as determined by hierarchical cluster analysis.

5.2.4 Water-Rock Interaction

Previous studies have found that groundwater of the basalt aquifers can be separated into two distinct types (Murphy 1991): Type 1 is characterised by low alkalinity and high nitrate concentrations and Type 2 is characterised by high alkalinity and low nitrate concentrations. These types can also be distinguished by MRT, with Type 1 having less than 70 years and Type 2 including older groundwater (van der Raaij 2015). Figure 5.11 shows the bicarbonate and nitrate concentrations from wells in this study, which are consistent with previous findings about basalt aquifer groundwater types. Clusters A and B contain Type 1 characteristic groundwater, and Cluster C sites (basalts) contain Type 2 characteristic groundwater. In the 2015 study, Type 1 was generally linked with shallower basalt aquifer systems and Type 2 with deeper basalt aquifers. This was not observed in this study, as all sites from Cluster C are classed as Type 2 and located in the recharge areas, including the springs.

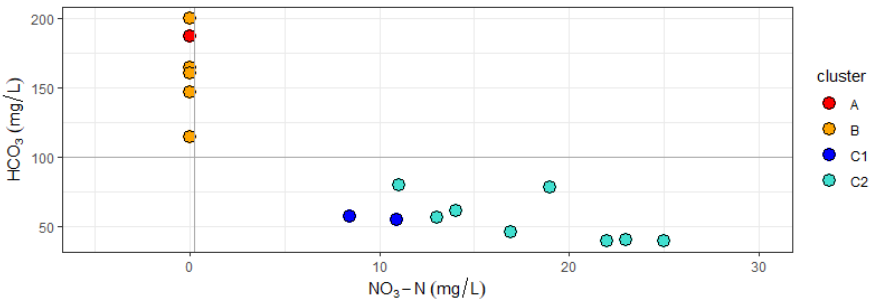

Figure 5.11 Plot of bicarbonate against nitrate-nitrogen for samples collected in this study. The vertical line depicts the nitrate-nitrogen concentration natural baseline (0.25 mg/L) defined by Morgenstern and Daughney (2012) for absence of human impact. The horizontal line represents the HCO_3 concentration threshold between Type 1 and Type 2 groundwaters from previous studies (Murphy 1991; van der Raaij 2015).

Bicarbonate alkalinity arises from dissolution of rock minerals by carbonic acid. Alternatively, calcium in the groundwater is derived primarily from weathering of plagioclase (e.g. anorthite) and other minerals, as well as from surface inputs such as fertilisers (Murphy 1991). Overall, samples from Clusters A and B do not exhibit a linear relationship between calcium and bicarbonate, suggesting a mixture of sources, whereas Cluster C samples demonstrate more water-rock interaction influence (Figure 5.12; Murphy 1991).

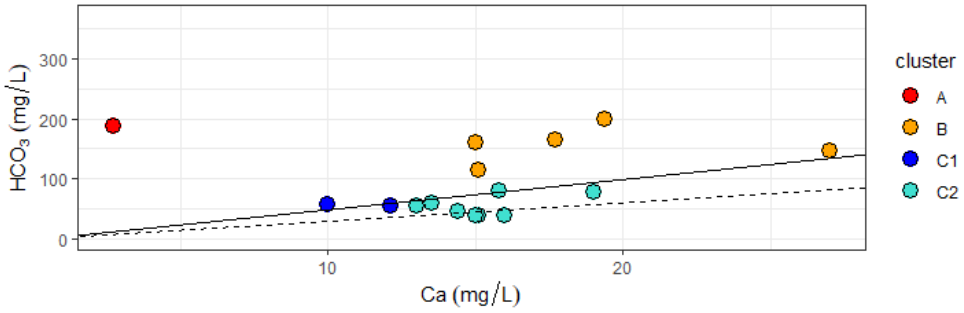

Figure 5.12 Plot of calcium against bicarbonate. The dashed line depicts ratios of bicarbonate and calcium expected for dissolution of plagioclase anorthite or calcite (dashed) and pyroxene (solid), respectively.

Magnesium may be derived from the dissolution of rock minerals by carbonic acid, from weathering of ferromagnesium minerals (e.g. augite, olivine) and other minerals or from surface inputs such as fertilisers (Murphy 1991). Magnesium from Cluster C (basalts) is likely to be derived from dissolution of ferromagnesium minerals, whereas, for the remaining samples, a mixture of sources is more likely (Figure 5.13).

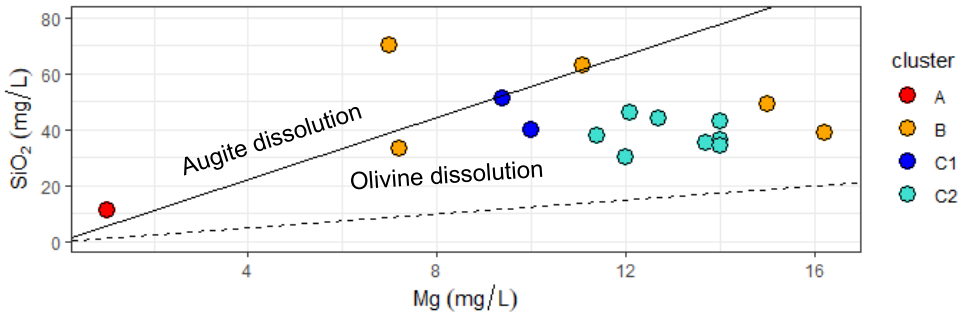

Figure 5.13 Plot of silica against magnesium. The lines depict ratios of silica and magnesium that would be expected for the dissolution of augite (solid) and olivine (dashed), respectively.

Comparison of chloride to sodium concentrations shows that roughly 15–50% of sodium is not derived from marine-origin sodium chloride (Figure 5.14), which is consistent with but has a wider range than previously reported (30–50% in van der Raaij [2015]). This 'excess' sodium may be derived from dissolution of sodium feldspars (Figure 5.15) and/or ion exchange processes within the aquifer, which result in sodium replacing calcium in the presence of clays, particularly for Clusters A and B. Inputs from fertiliser use may also be possible. The oldest groundwaters exhibit strong 'excess' sodium, which reflect advanced water-rock interaction through long residence time.

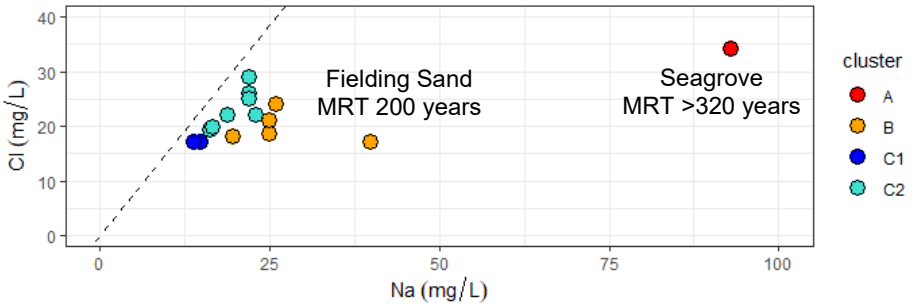

Figure 5.14 Plot of chloride against sodium. The dashed line is the seawater concentration dilution line.

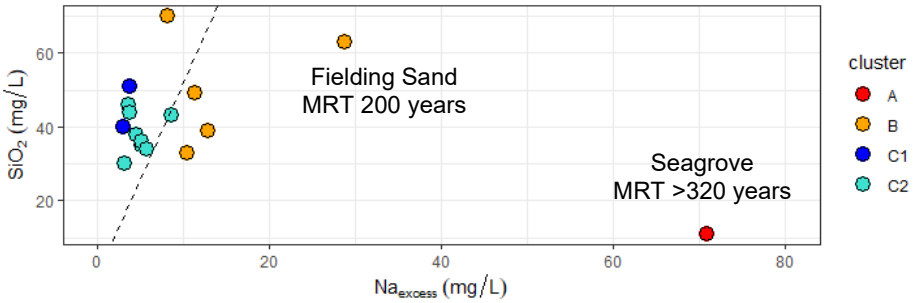

Figure 5.15 Plot of silica against sodium concentrations, corrected for sodium derived from marine sources. The dashed line depicts ratios of silica and sodium that would be expected for dissolution of the sodium plagioclase albite.

5.2.5 Time Trends Hydrochemistry

Twelve wells from this study are part of the Auckland Council SOE monitoring network and/or the NGMP. Long-term monotonic trends over time are identified using the non-parametric, seasonally adjusted Mann-Kendall test (Helsel et al. 2020). This test indicates whether a change in parameter generally follows the same direction over time (either increasing or decreasing trend) or whether there is no statistically significant change over time. Once a trend is identified, the magnitude is calculated using Sen's slope estimator. Trend testing was undertaken via the R software (version 3.6.2) using the LWP-Trends (version 2101) and NADA (version 1.6-1.1) libraries (Lee 2022; Snelder and Fraser 2021). The results of these tests are presented in Table 5.4.

In this section, trend magnitudes (Sen's slope) are reported without consideration for the p-value, consistent with recent changes in reporting (McBride 2019). However, to account for the natural variability for a parameter at a given site, trends were classed as 'perceptible' if the change in concentration (calculated over the time period) fell within four times the MAD – the criterion commonly used to detect extreme outliers – and 'imperceptible' outside the 4 × MAD range. This classification is somewhat indicative of confidence in the ability to detect a trend measured through the MAD (Moreau and Daughney 2021) over the natural range of variability in measured concentrations.

Most sites do not exhibit perceptible trends in major ion concentrations (Table 5.4), although some variability exists over time (Figures 5.16–5.19). Perceptible bicarbonate increases were observed within the basalt aquifers at Patumahoe and Hickey springs. Perceptible chloride and sulphate increases were only observed within the Waitemata aquifer (Seagrove). Perceptible trends for nitrate concentrations were only observed at three wells sourced from the basalt lavas, increasing at well BP Bombay and Rifle Range Shallow NEW (up to 2010) and decreasing at the Wilcox Gun Club well, as previously reported (Foster and Johnson 2021). At the BP Bombay and Rifle Range Shallow NEW wells, the increases were accompanied either by a calcium or a magnesium increase.

Table 5.4 Chemistry trend analysis results for sampled wells over the full sampling period. Period varies, with a maximum range from 1996 to 2021. Listed are calculated Sen slopes, with perceptible trends indicated by grey cells. Superscripts: H – Holocene sediments, K – Kaawa shell aquifer, B – basalts, W – Waitemata Group sediments. N/A – not applicable.

Site	Ca (mg/L)	Cl (mg/L)	HCO_3 (mg/L)	Mg (mg/L)	Na (mg/L)	NH_3N (mg/L)	NO_3N (mg/L)	SiO_2 (mg/L)	SO_4 (mg/L)
Fielding Sand [H]	0.04	<0.01	<0.01	0.049	-0.02	0.002	<0.01	0.11	N/A
Ostrich Shallow [K]	0.02	-0.03	0.08	0.022	<0.01	-0.006	<0.01	0.17	-0.007
Ostrich Deep [K]	<0.01	NA	<0.01	0.008	-0.08	<0.001	<0.01	0.14	-0.002
Patumahoe Spring [B]	<0.01	-0.19	0.60	0.062	0.00	<0.001	-0.05	<0.01	-0.018
Fielding Volc. [B]	<0.01	<0.01	-0.16	0.019	0.03	-0.002	<0.01	0.11	-0.007
BP Bombay [B]	0.09	<0.01	0.00	0.053	0.06	N/A	0.17	0.14	-0.001
Hillview Spring [B]	0.16	<0.01	0.60	0.101	0.13	N/A	<0.01	0.19	-0.057
Hickey Spring [B]	0.03	<0.01	0.57	0.028	0.13	<0.001	-0.06	0.27	-0.067
Wilcox Gun Club [B]	<0.01	-0.16	0.34	<0.001	<0.01	N/A	-0.24	<0.01	-0.031
Rifle Range Deep [B]	-0.10	<0.01	-0.61	-0.019	<0.01	<0.001	0.00	0.05	0.011
Rifle Range Shallow NEW [B *]	0.20	-0.06	-0.20	0.17	0.01	N/A	0.50	<0.01	-0.06
Rifle Range Shallow NEW [B **]	0.03	0.06	0.25	<0.01	-0.04	N/A	0.30	<0.01	<0.01
Seagrove [W]	0.01	0.13	-1.81	-0.001	-0.27	-0.002	<0.01	0.01	0.093

* Trend magnitude calculated up to 2010.

** Trend magnitude calculated between 2014 and 2021.

Examination of time-series (Figures 5.16–5.19) yielded the following observations:

- Cluster A time-series confirm the aforementioned perceptible trends, as well as a sudden change in chemistry occurring in 2015, when calcium, iron and manganese rose significantly before settling back to background level (Figure 5.16). This could be linked to a change in water level and flow.
- Cluster B time-series exhibit some variations with time but overall remain consistent, except for the Ostrich Shallow well source by Kaawa Formation, which exhibited a slight decrease in manganese over time (Figure 5.17).
- Cluster C1 time-series are only available for the Rifle Range Shallow NEW well, which confirmed the perceptible increases. The chemical record, perturbed between 2010 and 2014, had returned to background levels (Figure 5.18).

- Within Cluster C2, the BP Bombay site holds the longest record. Although other sites were added later, there is consistency in the time-series for this cluster (Figure 5.19).

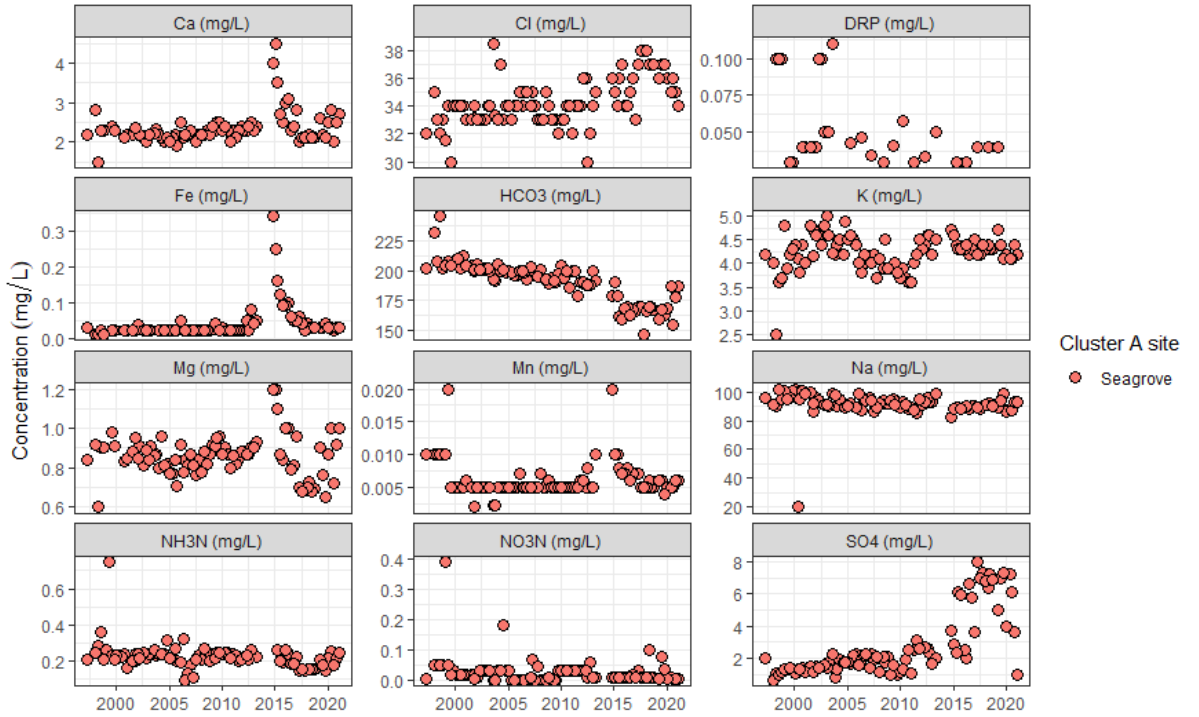

Figure 5.16 Changes in chemistry for selected parameters over time in the Pukekohe and Bombay aquifers for Cluster A.

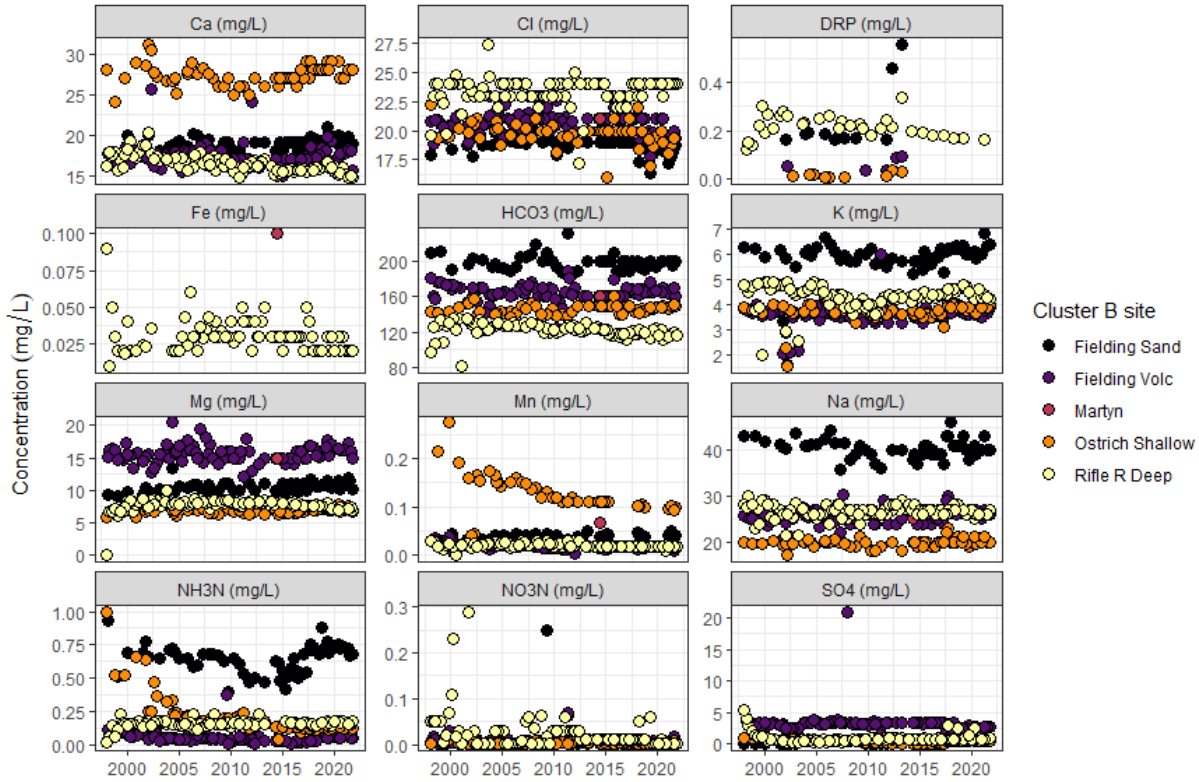

Figure 5.17 Changes in chemistry for selected parameters over time in the Pukekohe and Bombay aquifers for Cluster B.

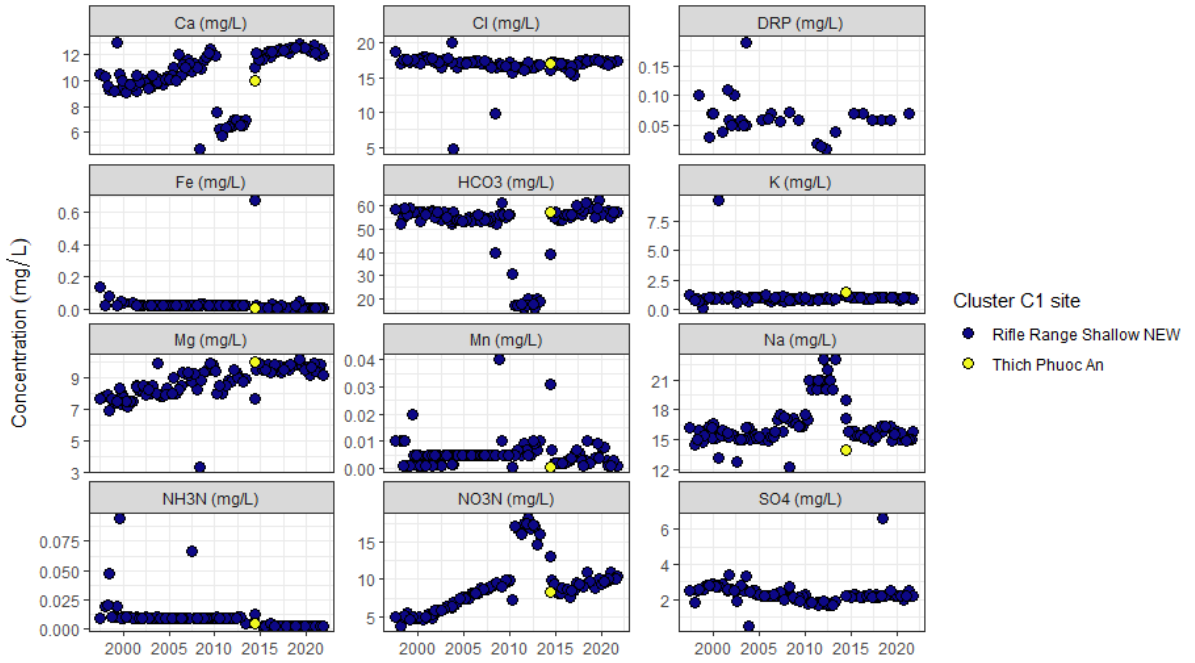

Figure 5.18 Changes in chemistry for selected parameters over time in the Pukekohe and Bombay aquifers for Cluster C1. The abrupt changes in the Rifle Range Shallow NEW time-series are discussed in Section 5.6.

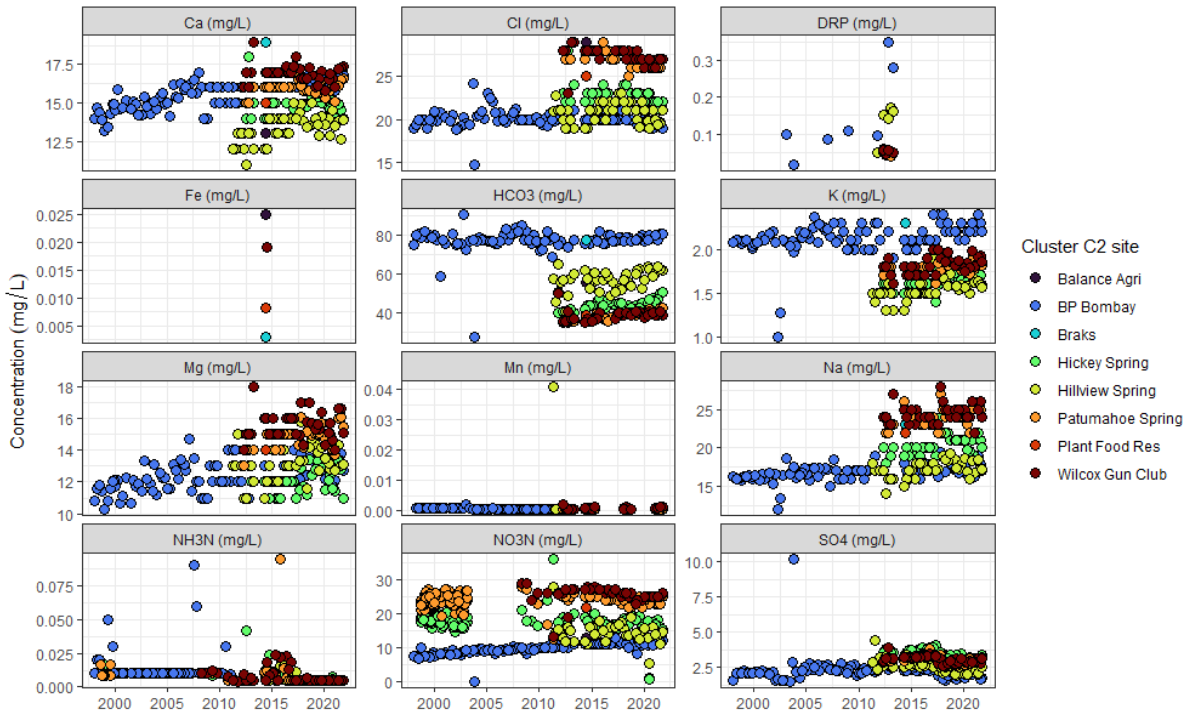

Figure 5.19 Changes in chemistry for selected parameters over time in the Pukekohe and Bombay aquifers for Cluster C2.

5.2.6 Variation in Chemistry with Groundwater Age

In the following section, the relationship of hydrochemistry to groundwater MRT is examined. Note that, for wells with insufficient or inconsistent data to derive the mixing parameters, mixing parameters were estimated. For older groundwaters, the hydrochemistry data are plotted at minimum MRT, as defined by the detection limit of the tritium dating method. These groundwater ages could be much older, up to several thousand years. Thus, the

relationships may not necessarily be as linear as depicted. R^2 values, which are presented in the following graphs as an indication of statistical significance, should therefore be treated as illustrative only.

The pH of groundwater generally increases with MRT (Figure 5.20). The pH of young groundwater is about 6 and gradually increases to around 9 for old groundwater. Dissolved oxygen decreases with MRT, with very old water becoming anoxic. There is a narrow conductivity range for groundwater sourced by the Waitemata aquifer, due to the increased time for water-rock interaction and subsequent dissolution of minerals in the aquifer matrix. In contrast, the basalt aquifer samples with young MRT (<50 years) have a wide range of conductivities. This result is probably due to the higher solute loading in younger groundwater due to land-use intensification.

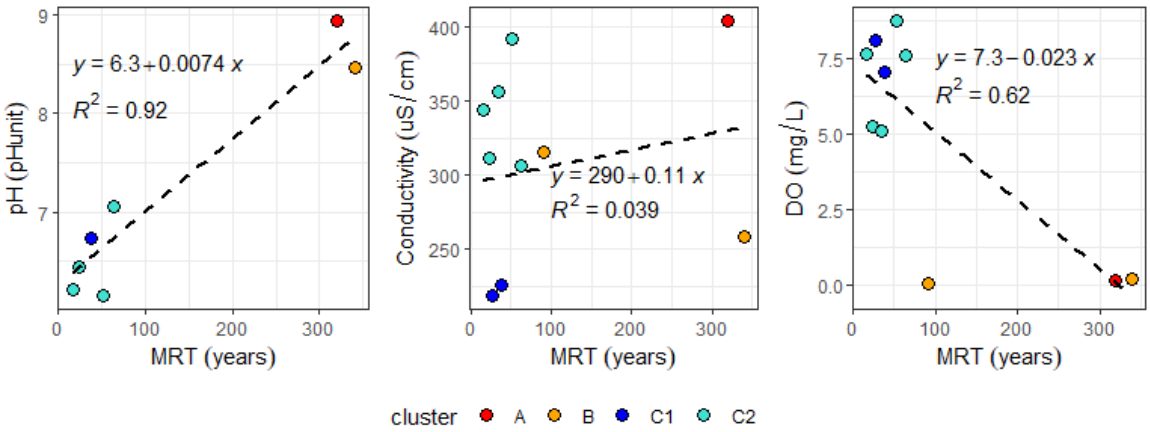

Figure 5.20 Plots of the relationship between field pH, electrical conductivity and dissolved oxygen chemistry and mean residence time (MRT).

Dissolved silica, bicarbonate and potassium concentrations increase with MRT for most samples (Figure 5.21). Bicarbonate shows a positive relationship with MRT (Figure 5.21), which may indicate that the chemistry changes are driven by water interaction with fine sediment layers between the basalt aquifer systems. Potassium also shows a positive relationship with MRT, likely to increase as mineral dissolution increases.

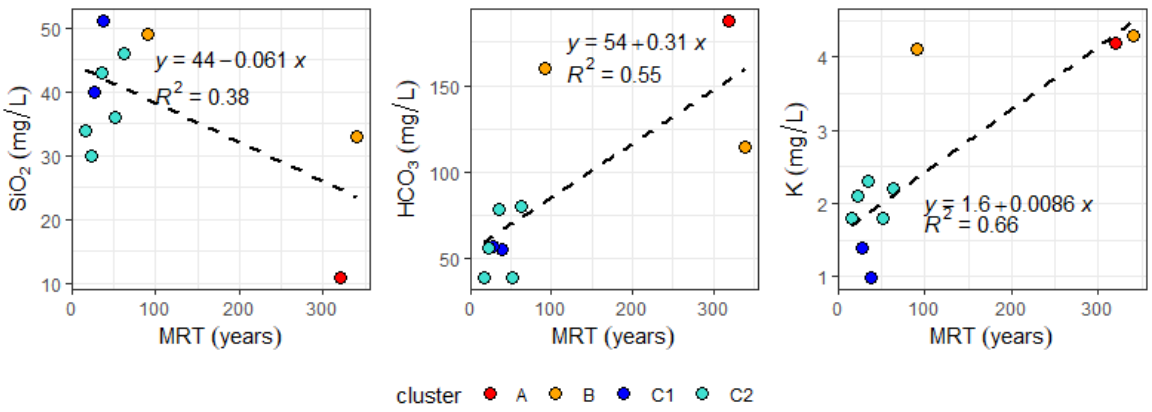

Figure 5.21 Plots of the relationships between chemistry and mean residence time (MRT), including (a) silica (SiO_2), (b) bicarbonate (HCO_3) and (c) potassium (K).

Magnesium and calcium concentrations show no relationship to MRT (Figure 5.22). This could mean either that equilibrium concentrations of these analytes with respect to mineral dissolution are reached quickly with little change thereafter or that these analytes may also be derived from surface inputs resulting from land-use activities. The former explanation

is unlikely, as in the younger groundwater both calcium and magnesium are under-saturated with respect to bicarbonate. Alternatively, these cations may be replaced in solution over time by ion-exchange processes releasing sodium ions. However, sodium concentrations do not increase over time, and therefore surface inputs resulting from land-use activities seems the most likely explanation for the lack of relationship between magnesium and calcium concentrations and MRT. Chloride concentrations vary within Cluster C2 without any relationship with groundwater. Chloride does not come from mineral dissolution but can be sourced either by marine deposits, sea-spray deposition or fertilisers (Figure 5.22). The groundwater age of the samples makes it unlikely that the high chloride concentrations observed in Clusters A and B are due to agricultural contamination; therefore, they are more likely to be linked to marine deposits and/or saline connate water. An examination of Cl:Br ratios may further delineate these sources (Rosen 2001).

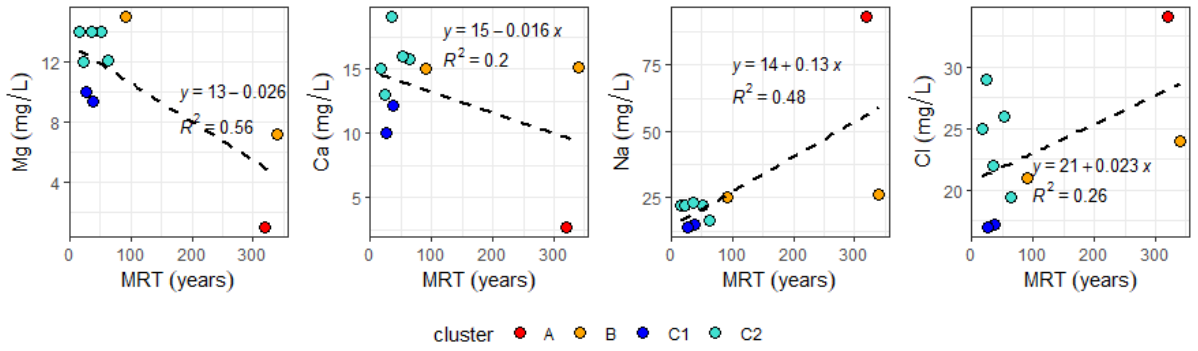

Figure 5.22 Magnesium (Mg), calcium (Ca), sodium (Na) and chloride (Cl) concentrations' relationships with mean residence time (MRT).

Younger groundwaters exhibit a wide range of nitrate concentrations. In contrast, older groundwaters have negligible nitrate but measurable ammonia concentrations. This reflects the reducing conditions measured in these groundwaters whereby, through natural, bacteria-mediated processes, nitrogen can only be present in ammonia form (Figure 5.23). The variability and high nitrate concentrations of younger waters reflect the impacts of recent land use (Figure 5.23).

Iron and manganese have negligible concentrations in young groundwater and higher concentrations in older groundwater (Figure 5.23). This reflects the increased availability of these analytes due to prolonged water-rock interaction and mineral dissolution in the older groundwater and the enhanced mobility of these analytes due to the groundwater changing towards an anoxic redox state (Figure 5.24).

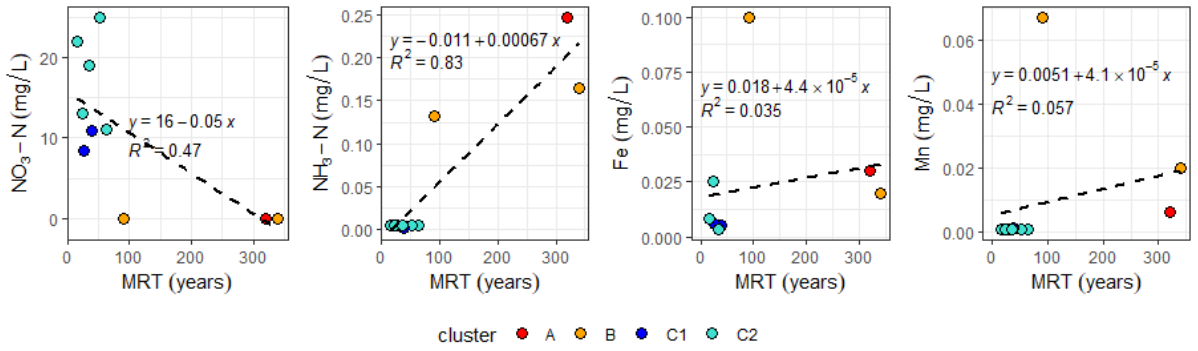

Figure 5.23 Nitrate-nitrogen (NO_3-N), ammonia-nitrogen (NH_3-N), dissolved iron (Fe) and dissolved manganese (Mn) concentrations' relationships with mean residence time (MRT).

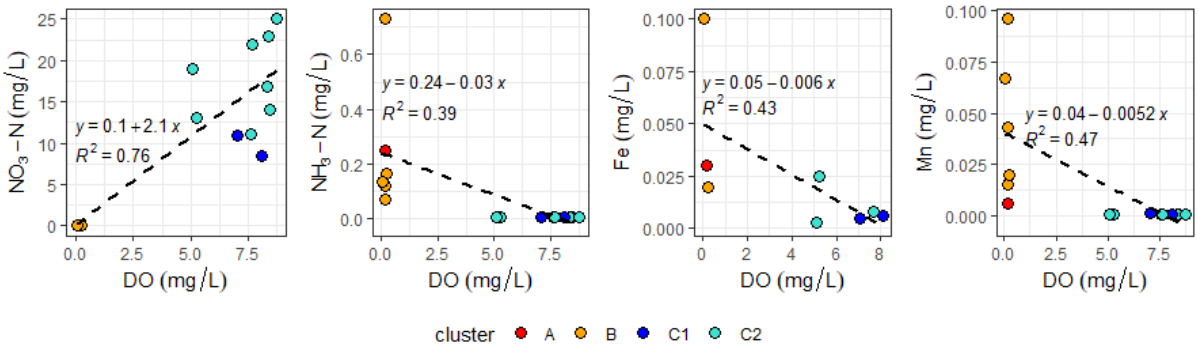

Figure 5.24 Nitrate-nitrogen (NO_3-N), ammonia-nitrogen (NH_3-N), dissolved iron (Fe) and dissolved manganese (Mn) concentrations' relationships with dissolved oxygen.

5.3 Recharge Temperature and Excess Air

The measured argon and nitrogen concentrations (Table 4.1) allow calculation of recharge temperatures and excess air, assuming equilibrium conditions for the oxic groundwaters (van der Raaij 2015; Section 5.2). Calculated recharge temperatures (Table 4.1, Figure 5.25) for the major springs lie around the mean annual air temperature of 14.5°C, although most of the wells in the volcanic formation contain groundwater with recharge temperature biased toward winter recharge temperatures. Bias of the groundwaters toward winter recharge temperature was also observed in the earlier study (van der Raaij 2015). The data for the wells in the Pleistocene deposits are not shown because their gas concentrations are likely to be impacted by highly anoxic processes – they all contain methane, indicating redox status up to methane fermentation with potential for degassing. Arrows in Figure 5.25 indicate expected shifts in argon and nitrogen compositions for several competing processes.

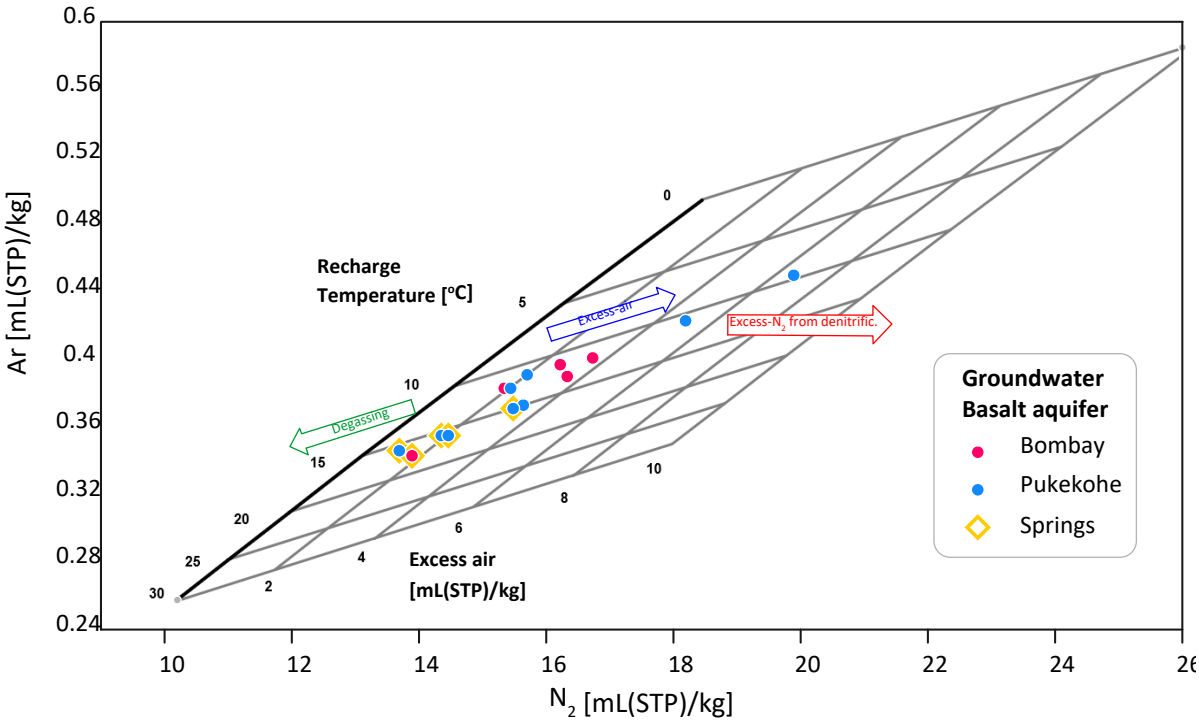

Figure 5.25 Plot of dissolved nitrogen (N_2) versus argon (Ar) concentrations, normalised to sea level. The positions of the samples within the grid indicate recharge temperatures and excess air concentrations (Heaton and Vogel 1981). The bold line on the left of the grid indicates gas concentrations in water in equilibrium with the atmosphere. Dissolved Ar, N_2 and excess air concentrations are expressed in millilitres of the respective gas at standard temperature and pressure (STP = 273.15 K, 101.325 kPa) per kilogram of water. Arrows indicate competing processes that can alter gas concentrations. Data for the wells in the Pleistocene deposits are not shown.

In the basalt lava with deep water tables (>5 m), recharging groundwater is expected to be in equilibrium with air at mean annual air temperature when transitioning into the closed system below the water table. Figure 5.26 shows that groundwater recharge temperatures at around the local mean annual air temperature of 14.5°C were observed only at or near the spring discharges. The groundwaters in the basalt lava have gas concentrations that are consistent with significantly lower recharge temperatures.

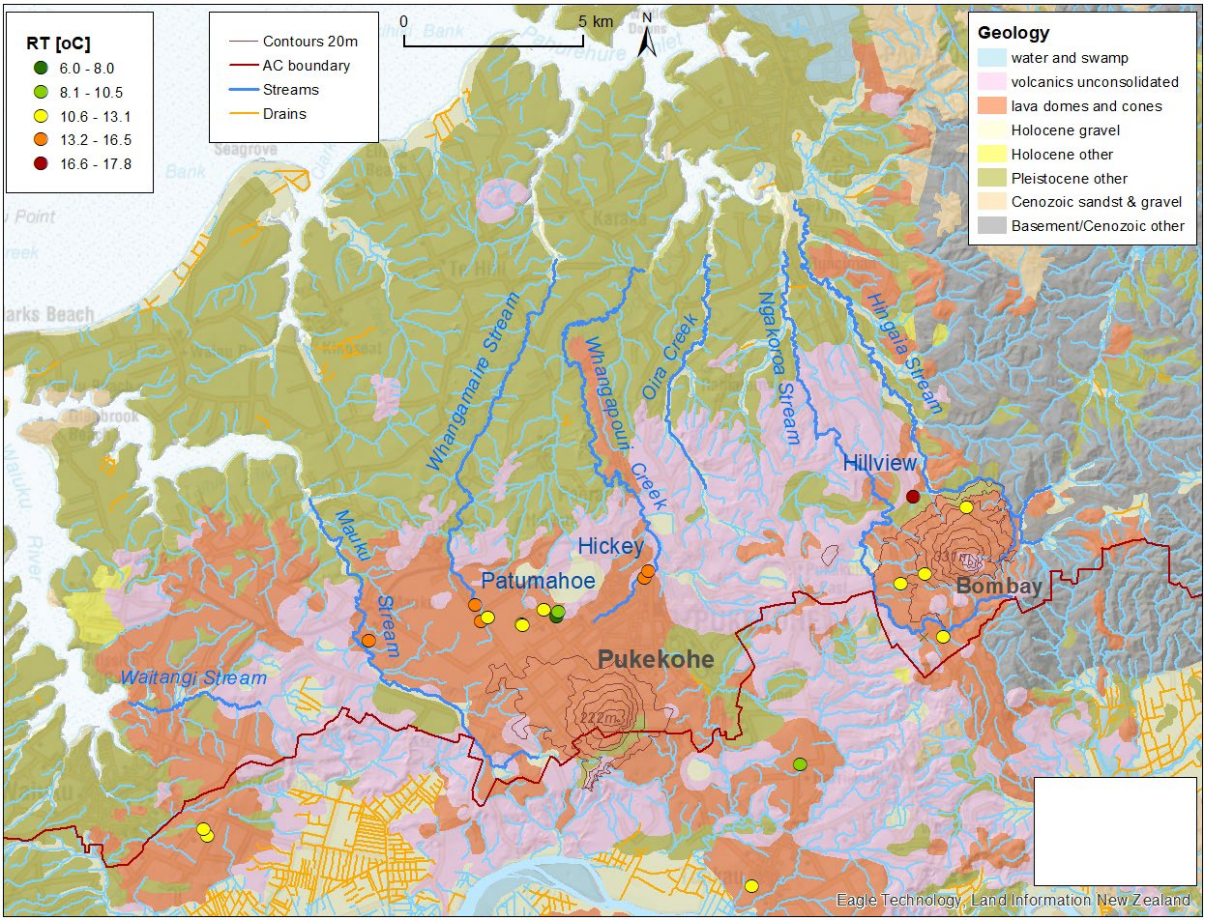

Figure 5.26 Spatial distribution of groundwater recharge temperature (RT).

5.4 Water-Stable Isotopes

Isotopic ratios in westerly rainfall and river water in New Zealand are expected to plot on the meteoric line for $\delta^{2}H$ and $\delta^{18}O$ of $\delta^{2}H = 8 \times \delta^{18}O + 13$ (Stewart and Morgenstern 2001). The groundwater-stable isotope ratios from the Pukekohe–Bombay area plot on this local meteoric water line (Figure 5.27), indicating that these stable isotope compositions reflect the prevailing weather patterns of westerly rainfall.

The isotopic ratios of the water within the groundwater system up to the discharge point (springs) plot close to the expected meteoric line, confirming that evaporation within the groundwater system is insignificant. However, in the streams, the isotopic ratios of the water tend to be biased by evaporation toward a line with a slope of 5. It is expected that evaporation occurs in the streams during summer.

Oira Creek and Ngakoroa Stream, having some of the lowest flows (Figure 2.5), show the largest impact from evaporation (Figure 5.27). Across all streams, Hingaia Stream water has the most negative isotopic ratios, reflecting its higher altitude recharge in the Bombay Hill area.

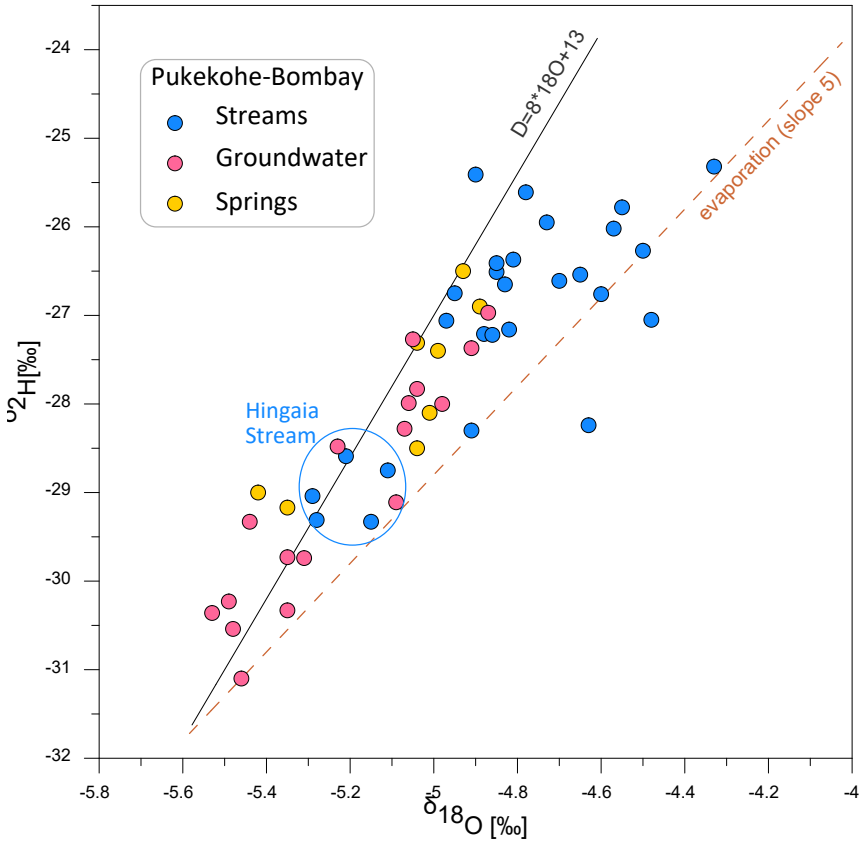

Figure 5.27 Plot of $\delta^{18}O$ versus $\delta^{2}H$ in surface water and groundwater of the Pukekohe–Bombay area. Hingaia Stream data circled to indicate the most negative stable isotope ratios compared to other streams.

Figure 5.28 shows the spatial distribution of $\delta^{18}O$ in groundwater and surface water. $\delta^{18}O$ and $\delta^{2}H$ are related to each other (Figure 5.27), so $\delta^{2}H$ would show a similar distribution to $\delta^{18}O$. Therefore, only $\delta^{18}O$ is shown.

Matching stable isotope compositions between surface water (triangles) and groundwater (circles) enables identification of water sources and connections between groundwater and surface water. Because no major ion chemistry data is available for all the streams in the Pukekohe–Bombay area, connections between surface water and groundwater are established based mainly on $\delta^{18}O$, supported by water age, DO, radon and nitrate.

In Waitangi Stream and Oira Creek, low DO concentrations were observed (Figure 5.28). In addition to low DO groundwater influx, this oxygen depletion may have been caused partially by in-stream processes promoted by the lower flow of these streams (Table 2.2) and related slow water turnover in pools. It is unlikely that such in-stream processes, if present, have modified the stable isotope compositions of these stream waters significantly, as they do not show more impact from evaporation than others in Figure 5.27. It is therefore reasonable to consistently interpret the stable isotope ratios of all streams to provide recharge sources.

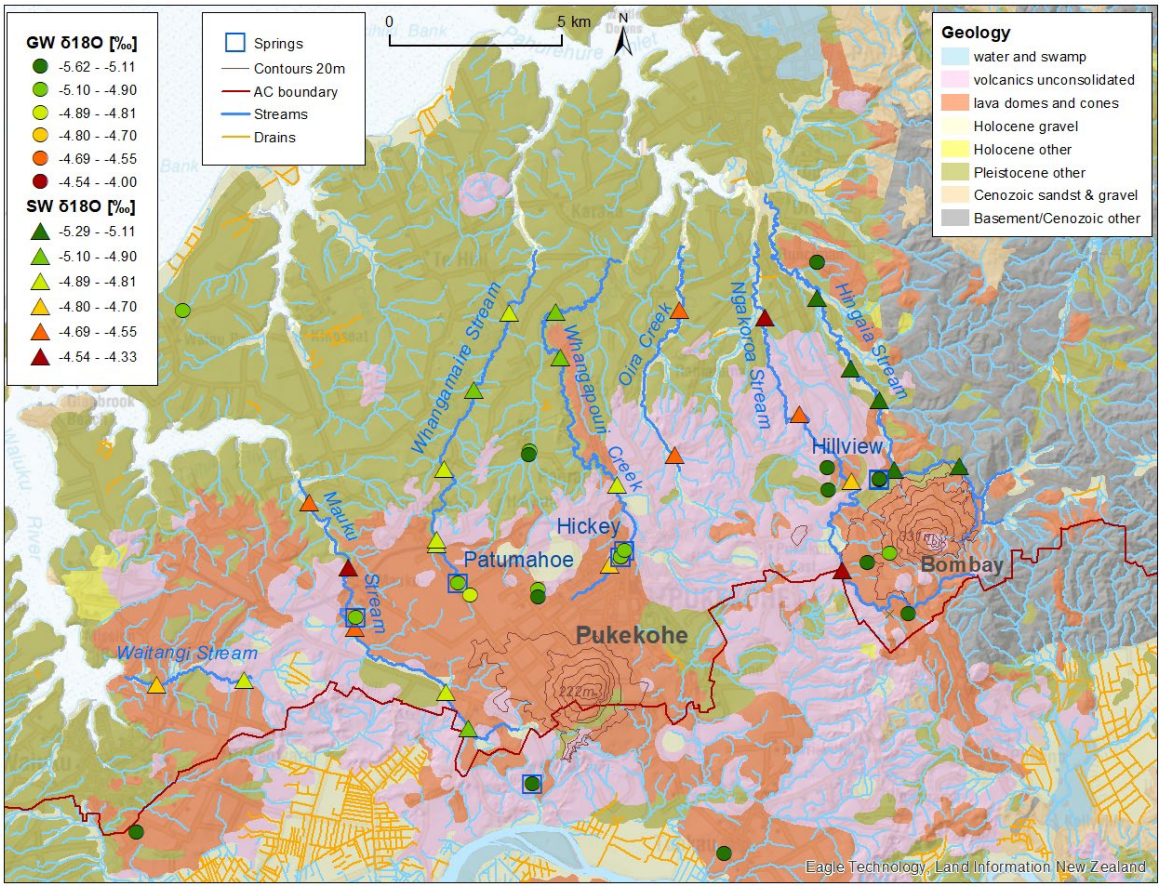

Figure 5.28 Spatial distribution of oxygen-18 ($\delta^{18}O$), at consistent scales, in groundwater (circles) and surface water (triangles).

The waters of Hingaia Stream, Whangapouri Creek and Whangamaire Stream (the main discharges from the basalt lavas) have $\delta^{18}O$ ratios matching those of their respective basalt lavas, confirming that these streams drain these basalt lavas. The $\delta^{18}O$ ratios of the waters of Ngakoroa Stream, Oira Creek and Mauku Stream do not match those of the basalt lava groundwater, indicating that they are not sourced from the basalt lava. Waitangi Stream also cannot be sourced from the basalt lavas due to its location. No groundwater data from the Waitangi Stream area are available to help establish the source of this stream.

The $\delta^{18}O$ ratios of the water of Hingaia Stream match those found in the groundwater of the Bombay basalt lava. These waters have the most negative $\delta^{18}O$ ratios, according to their highest elevation recharge area at the Bombay basalt lava. The $\delta^{18}O$ ratios of the water of Whangapouri Creek and Whangamaire Stream match those found in the groundwater of the Pukekohe basalt lava. Their $\delta^{18}O$ ratios are slightly less negative than those of the Bombay basalt lava, according to their lower altitude recharge area.

The waters of Ngakoroa Stream, Oira Creek and Mauku Stream have significantly less negative $\delta^{18}O$ ratios than those of the main basalt lavas, indicating lower altitude catchments. These catchments capture the least depleted early-rain signature of the north-westerly weather systems. Due to their different stable isotope composition, water ages (Section 5.1) and nitrate concentrations (Section 5.6), it is clear that these streams are not sourced from the main basalt lavas. They drain local catchments on the north-western flanks of the basalt lavas. These non-basalt groundwater systems are likely to contribute anoxic water (Section 5.3). Note that this is the situation during summer baseflow and that during wet seasons, when episodically to seasonally shallow pathways are active, these anoxic, low-nitrate, old-water discharges are likely to be overwhelmed by younger, oxic, high-nitrate water.

The few $\delta^{18}O$ ratios available for the southern part of the Pukekohe basalt lava (Waikato), with ratios more negative than those observed in the central and northern part of the basalt lavas, are likely to indicate local catchment recharge. These areas are in the rain shadow of the north-westerly weather systems and therefore likely to receive rain with more negative isotope ratios.

5.5 Radon in Groundwater and Stream Water

Radon-222 (^{222}Rn) gas is a radioactive intermediate decay product of uranium, which is ubiquitous in almost all rocks and soils. In a closed system in contact with these rocks, groundwaters accumulate ^{222}Rn released from the minerals, resulting in elevated ^{222}Rn concentrations in the groundwater. These concentrations are a result of equilibrium between ^{222}Rn delivery and radioactive decay (half-life 3.8 days) and can vary considerably depending on the uranium content and ^{222}Rn emanation potential of the aquifer material. In surface waters, ^{222}Rn concentrations are low because of limited contact with its source and because of decay and degassing into the air. Radon-222 can also indicate the presence of young (up to weeks) groundwater that has not yet reached equilibrium with ^{222}Rn delivery from the minerals.

The contrast between high ^{222}Rn concentrations in groundwater and low concentrations in surface water allows the identification of groundwater seepage into surface water, as indicated by elevated ^{222}Rn concentrations in streams. Conversely, recent river water recharge into groundwater systems is indicated by low ^{222}Rn concentrations in groundwater, as it takes approximately three weeks (5–6 half-lives) for the ^{222}Rn to build up and equilibrate to the ambient concentration of the groundwater.

All sampled groundwaters are sufficiently old (Section 4.2) to have reached ^{222}Rn equilibrium concentration with the aquifer material. The ^{222}Rn concentrations in the large spring systems (Hickey, Patumahoe, Hillview) were similar to those usually observed in New Zealand groundwaters, around 30 mBq/L (Table 4.3). However, most of the groundwaters from the wells in the basalt lava had significantly lower ^{222}Rn concentrations of around 10–15 mBq/L. This indicates reduced contact of the water with the rock matrix, causing lower radon supply into the water. Most deep wells containing highly anoxic water have very low ^{222}Rn concentrations (<10 mBq/L), indicating radon absorption on organic matter (Morgenstern et al. 2012).

The spatial distribution of the Radon-222 (^{222}Rn) concentrations in groundwater and stream water is shown in Figure 5.29. In the basalt lava, high ^{222}Rn concentrations, as expected for groundwater older than a few weeks, were measured only in the large spring systems (Hickey, Patumahoe, Hillview) and in one groundwater location in the southern part of the Bombay basalt lava. Radon concentrations in the remaining groundwaters are significantly lower, which may indicate reduced contact of the water with the aquifer matrix and/or absorption.

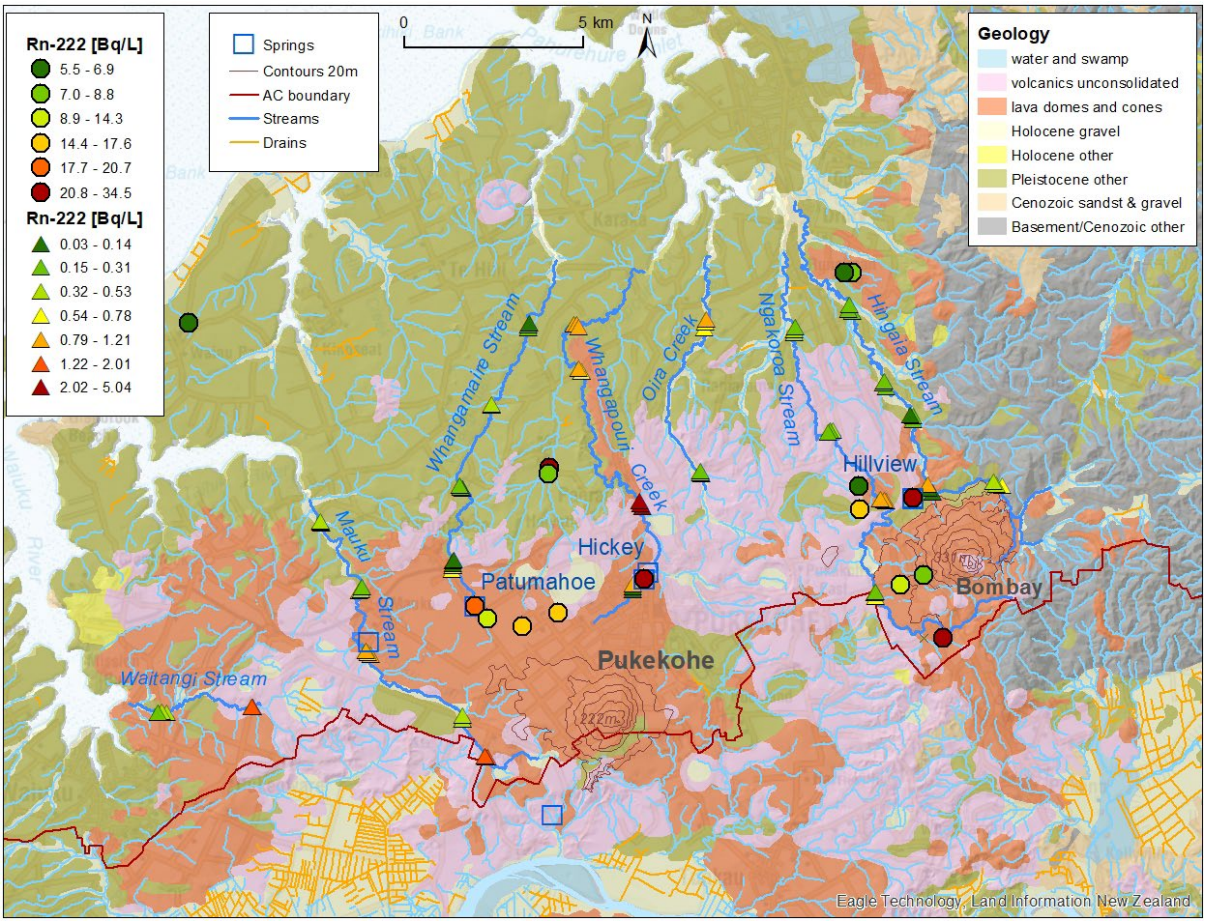

Figure 5.29 Spatial distribution of Radon-222 (^{222}Rn) concentrations in groundwater (circles) and stream water (triangles). Note the different scales.

All streams have reaches with elevated radon concentrations at the sampled sites, indicating groundwater seepage into the stream at these sites. Whangapouri Creek showed elevated radon at all sampled sites, especially around Hickey Spring, where the stream gains most of its flow. High radon at Paerata Falls (Table 4.3) indicates that this stream also receives significant groundwater discharge downstream from Hickey Spring.

5.6 Basalt Aquifer Changing Flow

The NGMP dataset showed a sudden, drastic change of the water age in the Rifle Range Shallow (RRS) well, accompanied by drastic changes of hydrochemistry, in early 2010 (e.g. van der Raaij 2015). Unrelatedly, a well in the basalt in the southern part of the Pukekohe basalt lava (Waikato Region) showed similar changes in in mid-2017.

After ruling out potential damage to these wells and the possibility of changes of sampling procedures, including accidental swapping of samples from nearby wells, as cause for these changes, we investigated all other NGMP wells in the basalt aquifer around Pukekohe with long-term consistent hydrochemistry data (Figure 5.30), including Rifle Range Deep, Graham and Handcock wells. Surprisingly, all shallow wells in the basalt displayed sudden changes in hydrochemistry at various times (Figure 5.31).

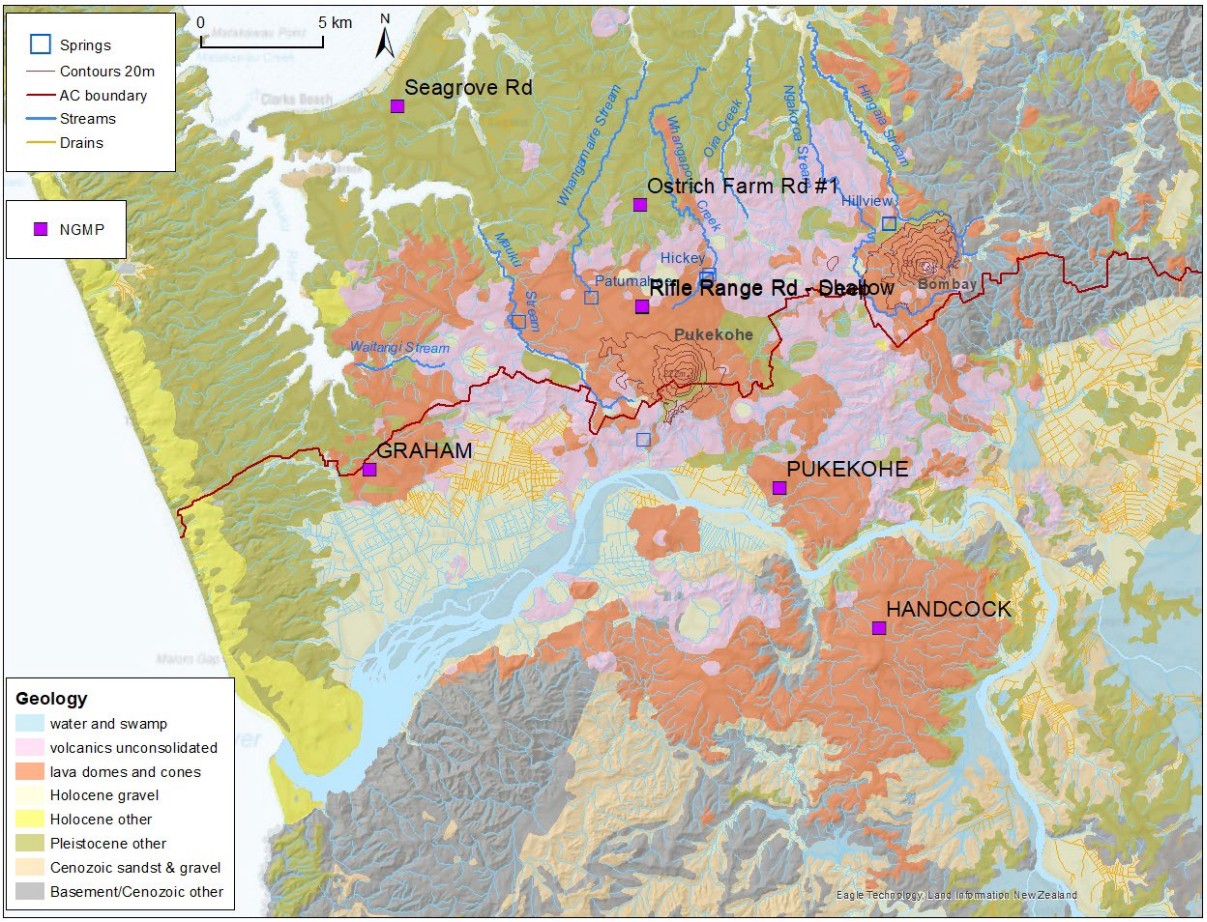

Figure 5.30 National Groundwater Monitoring Programme (NGMP) wells in the basalt lava around Pukekohe.

Note that the RRS well was replaced by a new well in 2014, drilled within 3 m distance of the previous well and screened at the same level, because, at the time, Auckland Council assumed that the old well had become leaky. The old RRS well was abandoned. Sampling of the NGMP wells in Waikato occurred consistently at the same wells over time.

The two wells in the Pukekohe basalt lava, only about 10 km apart and both with relatively shallow screens (Auckland Council RRS 30–42 m; Waikato Regional Council (WRC) Pukekohe 25–35 m), exhibited similar changes: at some stage, the hydrochemistry of the water changed drastically, accompanied by a change from old to much younger water.

These two wells, RRS and Pukekohe, are part of two different regions' independent monitoring networks. Other wells of the NGMP monitoring network outside the shallow basalt lavas do not exhibit such changes. Therefore, the observed changes in the shallow basalt wells are unlikely to be related to sampling, analytical or database errors. No damage to the wells was observed. In addition, the remaining two shallow wells in this basalt lava (WRC Graham and Handcock, Figure 5.30) also exhibited similar (but less drastic) changes in hydrochemistry. This suggests that, although the underlying cause is still unknown, these changes are systematic to the geologic formation.

The changes occurred with sudden onset, were permanent and occurred mostly at different times for the different wells. For the four shallow wells in the basalt aquifer, the data resolution allows for identification of three events that caused significant changes in the water source. The change in the RRS well occurred early 2010, in the Environment Waikato (EW) Pukekohe well late in 2017 and in the EW Graham well in mid-2007 (Figure 5.31). The change at EW's Handcock well also occurred around 2007 and therefore may be related to the same mid-2007

event. However, access to the well was denied by landowners over this period, so no higher-resolution data are available. The time of the three events is marked by vertical dashed lines in Figure 5.31, with black indicating the change in the respective well and grey lines indicating the time of the change in the other wells.

5.6.1 Wells with Drastic Changes (Rifle Range Shallow and Pukekohe)

Despite two obviously different events causing the changes at these wells, and the wells being 10 km apart, the overall changes are very similar (Figure 5.31, left two panes):

- The water has become younger. The tritium concentrations and modelled tritium output for the age-distribution parameters are shown in the bottom panes for each well in Figure 5.31. The tritium concentrations before the change are shown in blue and after the change in red. The changes in age distributions for both wells are shown in Figure 5.32. For the RRS well, the green data come from the replacement well, which yielded a very different age distribution, with high piston flow fraction (80%). It is likely that a different fracture has been intercepted by this well screen.
- Nitrate concentrations increased in step changes. At RRS, nitrate concentrations before the change define a nearly linear increasing trend, then stepped from 10 to 17 mg/L NO_3-N after the change. The replacement well contains water with lower nitrate concentration and does not follow the trend of the water in the old well before the change. In the Pukekohe well, nitrate levels before the change were relatively low but rising. It is likely that the low and rising nitrate levels were due to the old age of the water, causing a lagged response to nitrate loading. Then, about mid-2017, the nitrate concentration tripled, from about 3 to 10 mg/L NO_3-N.
- Chloride concentrations are slightly higher at Pukekohe compared to RRS, likely due to higher impact by coastal rain. In contrast to most other parameters, chloride concentrations did not significantly vary after the events that changed the source of the water in the wells. Also, the RRS replacement well had similar chloride concentrations compared to the old well. This indicates that chloride concentrations are homogeneously distributed, originating from coastal rain, without local sources and sinks. In contrast, sodium step-increased in the wells, indicating local sodium sources that cause different sodium concentrations in water recharged from different surface land uses.
- Calcium concentrations dropped significantly in both wells after the events that changed the water sources. The magnesium concentration at Pukekohe dropped slightly after this event. At the RRS replacement well, magnesium and calcium concentrations continued the trend of the water from the old well before the change.
- Bicarbonate concentrations decreased significantly at both wells after the event. Silica also decreased, but to a lesser extent. In the RRS replacement well, bicarbonate and silica concentrations continued the trend from before the change in the old well.
- Sulphate concentrations have slightly decreased at both sites over time but did not change significantly after the events.
- DRP decreased significantly at both wells after the events.
- The pH of the water decreased after events at both sites.
- The water at both wells was slightly more oxic after the events, with dissolved oxygen increasing from ~7 to 8.5 mg/L.
- The water levels in both wells rose after the events, at RRS by ~4 m and at the Pukekohe well by ~2 m.

Sudden changes after the events occurred not only for hydrochemistry parameters related to fertilisers (e.g. nitrate, calcium, magnesium), which would just indicate changing capture zone of the well, but also for parameters related to geology (e.g. bicarbonate, silica, phosphorus). This indicates that different water sources were captured by the wells after the events. The changes of hydrochemistry are consistent with the age tracers, indicating that water became younger after the events. Also, rising water levels indicate input of shallower, and therefore likely younger, water into the wells after the events.

5.6.2 Wells with Moderate Changes (Graham and Handcock)

In the Graham well, moderate changes occurred after mid-2007, with decreases in magnesium, calcium, bicarbonate and silica concentrations of the water indicating a change in the source of the water and different land use in the new capture zone. The nitrate concentration of the water continued its slight upward trend after the event, indicating similar land use in the new capture zone of the well. The age tracers did not indicate a significant change in groundwater age after the event, a finding supported by the fact that nitrate did not show a step-change after the event, indicating similar nitrate lag time.

In the Handcock well, increasing bicarbonate concentrations at around the same time, during 2007 or early 2008, indicate a change of the water source. Decreasing concentrations of parameters related to agrochemicals (e.g. calcium, magnesium, chloride and nitrate) indicated a decrease in agrichemical loading within the capture zone of the well before the change. After the event, calcium, magnesium and chloride continued their downward trend, while nitrate decreased suddenly from about 30 to 24 mg/L NO_3-N.

5.6.3 Well without Significant Changes (Rifle Range Deep)

No significant changes in hydrochemistry occurred at the Rifle Range Deep well after all three events that caused changes in the shallow wells. This indicates that these events have impacted only on the shallow basalt lava, above 80 m depth.

All indications suggest that the events that changed the water source in the wells are related to the geology of the shallow basalt lava. One plausible cause may be sudden changes (e.g. collapses) of basalt fractures, possibly due to settling of the basalt. Earthquakes are a less likely explanation, as these changes are very localised, occurring only at one well at a time.

This page left intentionally blank.

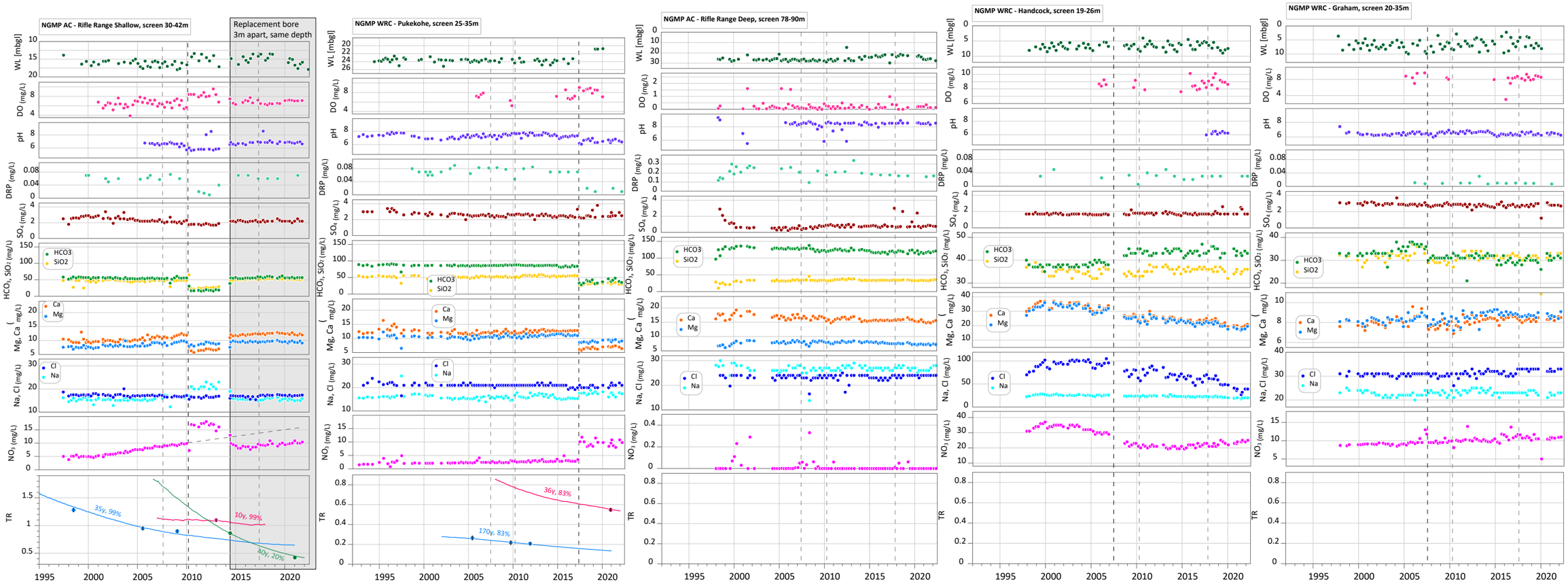

Figure 5.31 Hydrochemistry over time in five wells from the basalt lava around Pukekohe. Dashed vertical lines mark the time of three events that changed the hydrochemistry of the water, with darker black lines indicating the change in the respective well and grey indicating the time of the change in the other wells. The bottom panes show the tritium data and modelled outputs with labelled age-distribution parameters for the two nearby NGMP wells Rifle Range Shallow (Auckland Council) and Pukekohe (WRC).

This page left intentionally blank.

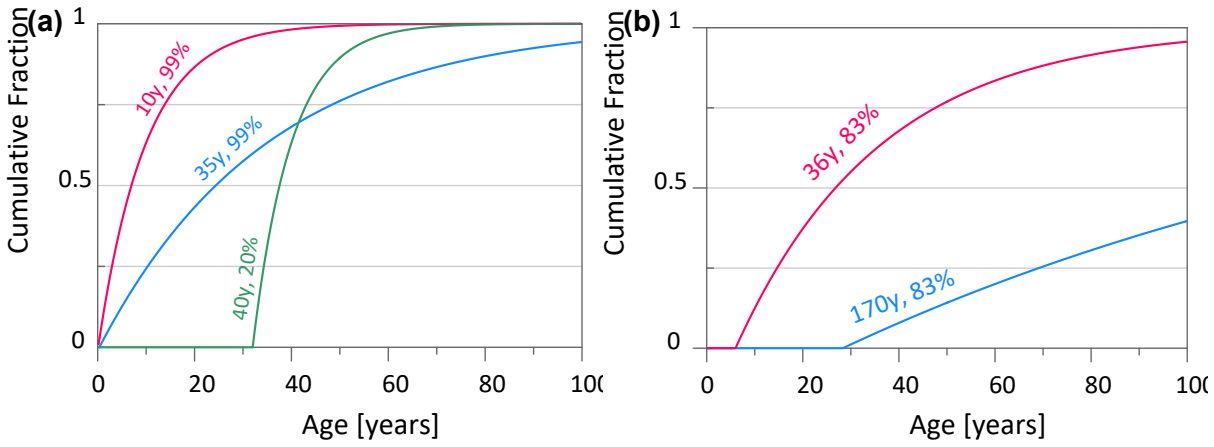

Figure 5.32 Changing age distributions and their parameters for the (a) Rifle Range Shallow (Auckland Council) and (b) Pukekohe wells (Environment Waikato). The red, blue and green age-distribution curves refer to the matched tritium outputs in Figure 5.31.

5.7 Nitrate Distribution

Figure 5.33 shows the spatial distribution of nitrate (NO_3-N) in groundwater and surface water. To illustrate connections between groundwaters and surface waters, their concentrations are shown with consistent concentration colour scales. Also shown are the areas of crop production (market gardening) and dairy farming, land uses that cause major nitrate leaching (Snelder et al. 2018). The Pukekohe and Bombay basalt lavas are dominated by market gardening, which is subject to high nitrate leaching into oxic groundwater systems, resulting in high nitrate concentrations in the groundwater and its discharges. At the Pukekohe basalt lava, groundwater NO_3-N concentrations in the basalt lavas are typically 20–30 mg/L and in their spring discharges 18–25 mg/L. At the Bombay basalt lava, groundwater NO_3-N concentrations in the basalt lava are typically 10–20 mg/L and in their spring discharge 15 mg/L.

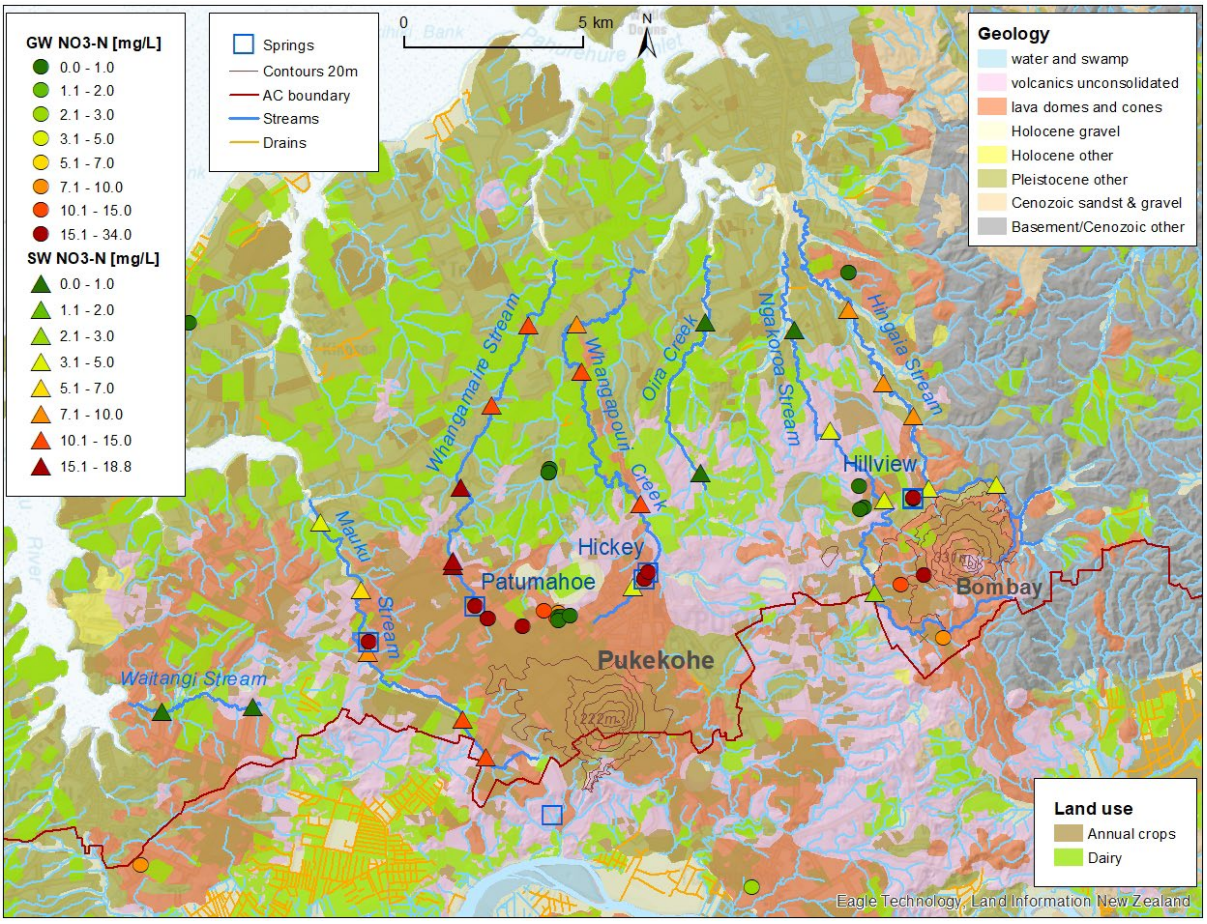

Figure 5.33 Spatial distribution of nitrate (NO_3-N) in groundwater (circles) and surface water (triangles), with consistent concentration scale for groundwater and surface water. Springs are denoted by blue square outlines. Also shown are the areas of land use that cause major nitrate leaching: crop production and dairy farming (MfE Data Service 2012).

The large springs (Patumahoe, Hickey, Hillview) discharging the groundwater at the perimeter of the basalt plateau and cone have nitrate concentrations that match those of the groundwater in their basalt lavas. Matching nitrate concentrations, together with matching water ages (Section 5.1) and stable isotope compositions (Section 5.5), consistently demonstrate that these springs discharge from the basalt lava. The high nitrate loads through these springs then dominate the nitrate concentrations in the receiving streams, Hingaia Stream, Whangapouri Creek and Whangamaire Stream.

At Hingaia Stream, upstream of the Hillview Spring discharge, nitrate leaching from crop production results in NO_3-N concentrations of c. 4 mg/L (already above the National Policy Statement for Freshwater Management 2020 nitrate national bottom line [NBL] [Ministry for the Environment 2020]). Excessive nitrate loads via the contribution of Hillview Spring cause the NO_3-N concentrations in the stream to more than double, to about 9 mg/L. Only at the furthest downstream site, the NO_3-N concentration slightly decreased again, likely due to dilution. The stream flow there increases by 20% from catchments of volcanic formations with less nitrate leaching land use.

At Whangapouri Creek and Whangamaire Stream, the situation is similar, except the nitrate loads are higher, causing NO_3-N concentrations in the streams of 10–19 mg/L (nearly eight times the nitrate NBL).

Ngakoroa Stream appears to receive groundwater and nitrate load discharges only in its upper reaches. Nitrate concentrations decrease downstream, probably due to attenuation processes in the stream. NO_3-N concentrations upstream are 3–5 mg/L and at the furthest downstream site 0.7 mg/L.

Mauku Stream receives little groundwater in its upper reaches, but this water is likely from the Pukekohe basalt lava. Its high nitrate concentration, water age and stable isotope composition are consistent with those of the water from the basalt lava. While receiving further flow downstream, the NO_3-N concentrations in the stream decrease, from 15 mg/L upstream to 4.5 mg/L at the furthest downstream site. This decreasing nitrate concentration is likely due to dilution with water that has undergone denitrification within the groundwater system. Two facts point toward this: (1) due to the decreasing nitrate concentration downstream, the stream must receive low-nitrate groundwater, despite large crop cover in the area; and (2) the groundwater discharges are likely to be anoxic.

At Waitangi Stream, the NO_3-N concentrations are very low during baseflow conditions, <0.2 mg/L. The catchment is covered with a significant fraction of dairy land, but, at baseflow conditions, the shallow flow paths from the surrounding dairy land are not active; the stream receives only a small amount of old water, likely from an anoxic groundwater system. The nitrate load from dairy farming is flushed into the stream during the wet seasons when the shallow flow paths are active. NO_3-N concentrations in Waitangi Stream are significantly higher during the wet seasons, up to c. 3.5 mg/L (https://www.lawa.org.nz).

Oira Creek discharges very little (in comparison to other streams in the area) and old water during baseflow conditions. It also had NO_3-N concentrations of <0.02 mg/L, despite a significant fraction of the catchment being covered with dairy land. The situation at this stream is likely to be like that at Waitangi Stream, with inactive nitrate flow paths during baseflow conditions and flushing of nitrate load out of the catchment during the wet seasons.

In areas of the Pleistocene deposits and deeper basalt aquifers, the nitrate load from dairy (or crop) farming is unlikely to arrive in the deeper groundwater systems. This is due to the old age of the water (large lag time) and the highly anoxic conditions in these groundwater systems. Instead, the nitrate loads in these areas are likely to take shallow flow paths (which are not active during baseflow conditions) directly into streams and the harbour or to undergo partial attenuation at the boundary of the redox zone. The nitrate loads from these areas are likely to be flushed from the land during the wet seasons at high flow, when the shallow flow paths are active.

5.8 SF_6 and CFC-11 Contamination

Three wells in the area contain water with extremely high SF_6 concentrations, one of them in Waikato (Table 4.2, Figure 5.34). Two of these wells contain young groundwater, which indicates artificial contamination sources. However, one of these wells (Taylor) contains old water. This rules out artificial contamination and indicates that volcanic SF_6 sources are present in the area.

Three wells also show CFC-11 contamination, with all three of them containing water with MRT <70 years, indicating contamination from artificial sources. One of these wells, Agrisystems, is also contaminated with SF_6, which suggests artificial sources for both CFC-11 and SF_6.

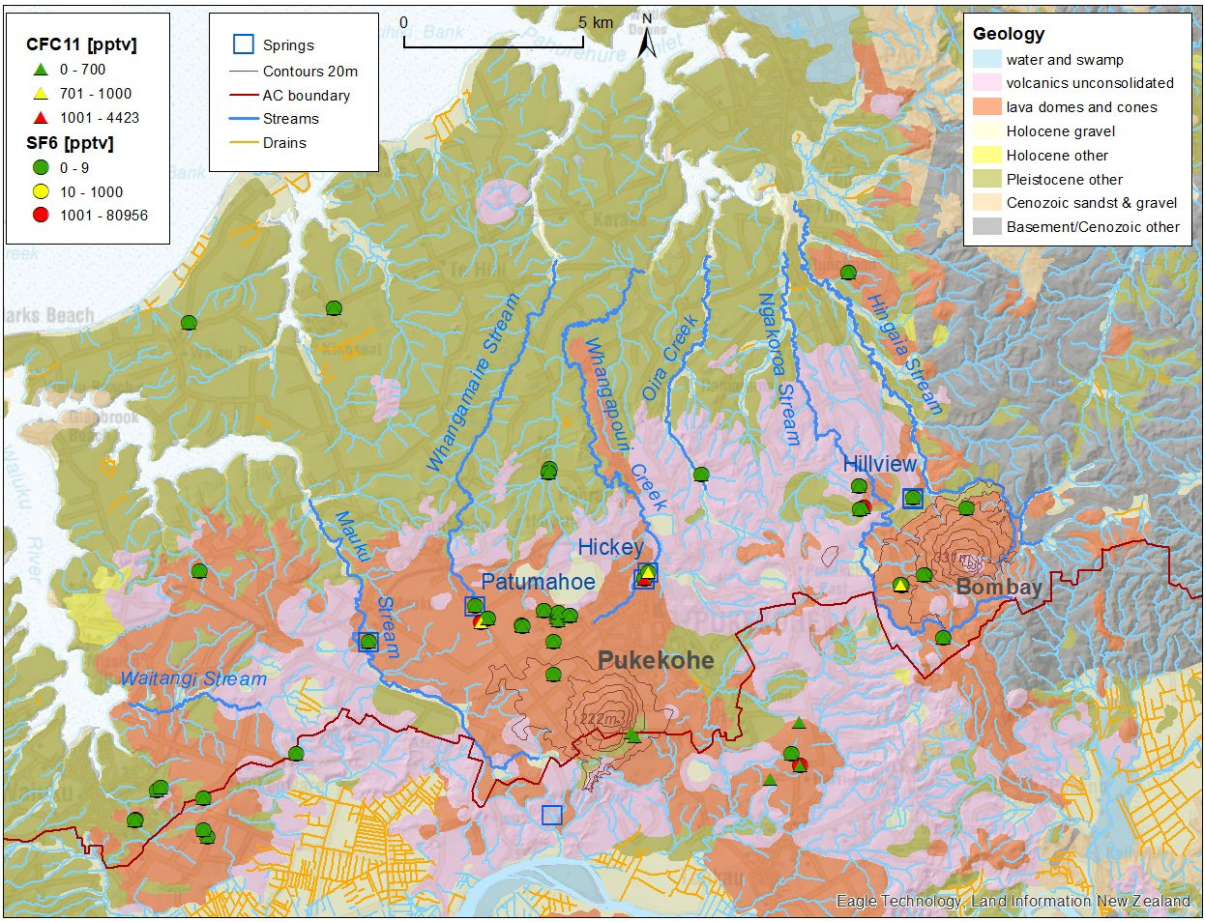

Figure 5.34 Spatial distribution of CFC-11 and SF_6 concentrations. Green symbols indicate concentrations in equilibrium with the atmosphere, yellow symbols indicate slightly higher concentrations and red symbols indicate high artificial contamination levels.

6.0 CONCEPTUAL UNDERSTANDING OF GROUNDWATER FLOW

6.1 Baseflow Drainage

During baseflow conditions, the area between the basalt lavas and Manukau Harbour is dominated by discharge from the Pukekohe and Bombay basalt lava. Discharge occurs mainly through three large spring systems: Hickey, Patumahoe (at the Pukekohe basalt lava) and Hillview (at the Bombay basalt lava). The streams gain insignificant flow north of the basalt lavas, indicating only little baseflow contribution from the Pleistocene deposits. This is consistent with the fact that only old groundwater was observed in the Pleistocene deposits, indicating stagnant flow conditions in its deeper groundwater system. This implies that the main discharge from this area is through episodically to seasonally active shallow pathways during the wet seasons. The storage of this shallow system is too small to maintain significant discharge throughout seasonal dry periods.

Surface water predominantly drains northward (Figure 2.5). The groundwater flow path through the basalt lavas also drains mainly northward, discharging at the northern perimeters of the basalt plateau and cone. This reflects the northward dip of the basalt lavas. Northward-dipping has been described by White et al. (2019) for the Pukekohe basalt lava. The situation is likely to be similar for the Bombay basalt lava, with its main discharge through Hillview Spring also located at the northern perimeter of the basalt lava.

Groundwater recharge mainly occurs through the basalt lavas and, to a small degree, through the unconsolidated volcanic deposits. The basalt lavas allow for efficient water infiltration from the surface into deeper groundwater systems. Effective subsurface drainage is indicated by a low stream density toward the centre of the basalt lavas (Figure 2.5) combined with baseflow-dominated springs at their perimeters. The old age of the spring water discharging from the basalt lavas implies drainage through a large groundwater reservoir (Section 6.5). The emergence of the springs mainly at the perimeter of the basalt plateau and cone confirms that the groundwater flow is restricted in the Pleistocene and unconsolidated volcanic deposits due to lower hydraulic conductivity.

The Whangamaire, Whangapouri and Hingaia streams drain the basalt lava mainly through three large spring systems. The groundwater ages, stable isotope composition and hydrochemistry in the basalt lava match those of the spring discharges. The mean transit time of the water through the Pukekohe basalt lava is 18 years and through the Bombay basalt lava 36 years.

In contrast, Mauku Stream, Oira Creek and Ngakoroa Stream have less negative stable isotope compositions compared to the higher-altitude basalt recharge areas. This indicates that these small streams discharge localised, lower-altitude groundwater mainly from the unconsolidated volcanic deposits. Oira Creek discharges relatively old water, with a similar transit time to that draining the Bombay basalt lava via Hillview Spring, but with different stable isotope and nitrate composition, indicating that it is not sourced from the Bombay basalt lava. Mauku and Ngakoroa streams discharge younger water, with a similar transit time to that draining the Pukekohe basalt lava. While Waitangi Stream discharges water with a similar transit time and stable isotope composition to discharges from Pukekohe basalt lava, there is insufficient groundwater data from this area to draw conclusions about flow connections. Note that this discharge pattern is the situation during summer baseflow and that, during winter, when episodically to seasonally shallow pathways are active, these anoxic, low-nitrate, old-water discharges are likely to be overwhelmed by younger, oxic, high-nitrate water.

The drainage on the northern slopes of the Pukekohe basalt lava is not necessarily related to the drainage southward (into Waikato) because of the northwards dip of the geologic formations. However, a similar discharge pattern was observed on the southern slopes. Transit time of the stream and spring discharges were similar. Residence time of the groundwater at shallow depths of the basalt lavas and old water in deeper formations was also similar.

6.2 Recharge Mechanism

In the area between the Pukekohe/Bombay basalt lavas and the Manukau Harbour, active groundwater recharge and flow is limited to the highly permeable basalt lava. Calculated groundwater temperatures, derived from argon and nitrogen concentrations, can inform understanding of recharge processes.

Calculated recharge temperatures for the groundwater recharge in the basalt lavas are significantly below the mean annual air temperature of 14.5°C (Figures 5.25 and 5.26). This indicates preferential recharge during winter. However, the depths and water levels of the sampled wells in the basalt lava areas are typically greater than 30 m below ground level at Pukekohe and greater than 50 m below ground level at Bombay (Kalbus et al. 2017). This is significantly deeper than the depth to which the seasonal ground surface temperature variation usually penetrates (approximately 4 m). Therefore, the gas concentrations of the groundwater, even if recharged during winter, would be expected to be equilibrated to mean annual air temperature.

Recharge temperatures to the deep groundwater system well below mean annual air temperature (derived from the dissolved gas concentrations) may indicate recharge through preferential flow paths (fractures) during winter. Only bulk flow through preferential flow paths would be able to sustain the low winter temperature signal through the unsaturated zone to below 4 m depth without equilibration of the gas concentrations to those at mean air temperature. This suggests that fracture flow dominates groundwater recharge to the deeper basalt lava. This may be considered independent confirmation of fracture flow in the basalt lava, which is generally understood from hydrogeological findings but now also shows that fracture flow applies to the shallow unsaturated zone (top 4 m).

The atmospheric gas concentrations of the springs, in contrast to those of the groundwaters, are in equilibrium with those at mean annual air temperature of 14.5°C. This suggests recharge through the bulk formation (matrix flow) of the unsaturated zone for the spring recharge, in contrast to recharge through shallow fractures to the deeper groundwater.

This may indicate that spring water and groundwater from the wells are being recharged through two different mechanisms: preferential flow through fractures to the deeper basalt aquifer and matrix flow through the surface formation supplying the shallow flow near the water table to the springs. Despite limited available data, the measured atmospheric gas-tracer data suggests different recharge mechanisms for well water and spring water. Only the tracer signatures of the water can reveal such details of groundwater flow.

The measured radon concentrations also support the hypothesis of fracture flow domination in the deeper basalt aquifer. Radon concentrations in the main spring discharges are significantly higher than those in the deeper groundwaters, indicating the deeper groundwaters are fracture-flow-dominated. Water from fracture flow is expected to come from a flow system with a smaller ratio of water volume to effective contact area with the basalt, resulting in lower radon concentrations, as less radon is supplied into the water.

6.3 Recharge Rates

Unconfined recharge situations result in stratified groundwater ages, and vertical recharge rates can be estimated from the age-depth relationships of the groundwater (Cartwright and Morgenstern 2012; Morgenstern et al. 2009). Figure 6.1 shows groundwater MRT versus mid-screen depth for the wells in the basalt aquifers.

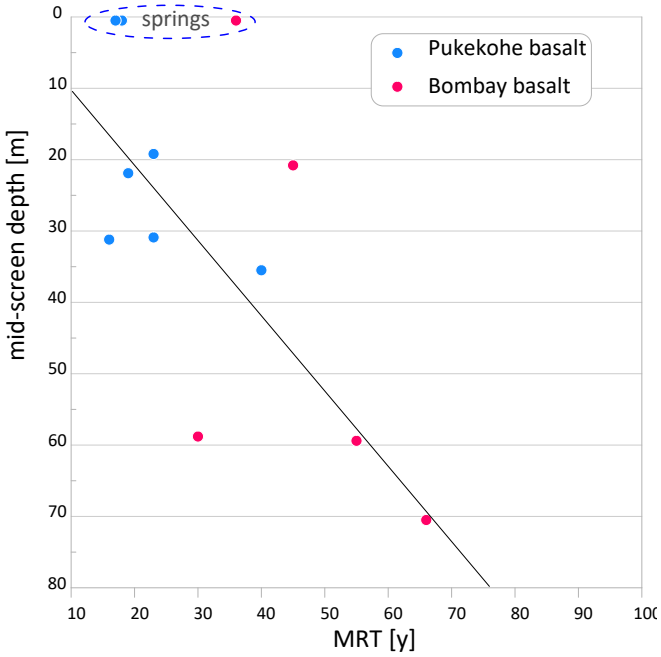

Figure 6.1 Groundwater mean residence time (MRT) versus mid-screen depth for wells in the Pukekohe and Bombay basalt aquifers. Age versus depth trend of 0.92 m/y for vertical recharge rate of 280 mm/y (assuming porosity of approximately 0.3).

There is no unique trend overall between groundwater age and depth. A close correlation between age and depth is not expected considering the fracture-dominated flow situation. Despite high variability in the age-depth relationship, this method allows an estimate of recharge into the deep basalt aquifer.

From the depth-age gradient of 0.92 m/y and an assumed porosity of approx. 0.3, a vertical recharge rate of 280 mm/y into the deeper basalt lava aquifers can be deduced, to a depth of 35 m at the Pukekohe basalt lava and a depth of 71 m at the Bombay basalt lava. Similar flow rate through the shallow and deep basalt lava systems indicates that the (uniform) hydraulic transmissivity restricts the flow. This is expected, because otherwise there would be no shallow lateral flow supplying the springs.

The overall recharge estimate using groundwater age data provides an average throughout the area and recharge depth covered by the monitoring wells and is based on data covering an age range of 65 years. Therefore, this estimate is more robust than those from surface observations recorded at single points and covering only a few years.

At both basalt lava formations, the springs discharge some of the youngest water (Figure 6.1) despite being at the end of the natural subsurface drainage flow paths. Hickey and Patumahoe springs (Pukekohe) have a MRT of c. 18 years versus a MRT of 6–40 years in the groundwater. Hillview Spring (Bombay) has a MRT of 36 years versus a MRT of 30–67 years in the groundwater. The wells are likely to draw water from well below the water table. This indicates that most groundwater drainage flow feeding the springs occurs close to the surface of the saturated zone (water table).

The recharge estimate of 280 mm/y into the deeper basalt aquifer does not account for the additional recharge into the shallow basalt that feeds the spring flows. The sum of deep and shallow system recharge is the total recharge into the basalt aquifer.

A summary of vertical recharge estimates using various methods (commonly water budgets) is provided in White et al. (2019). Estimates cover a considerable range: for the Pukekohe area, 500–680 mm/y; for the the Bombay area, 500 mm/y; and, for the area outside the Pukekohe basalt, 17 mm/y. Recharge into the deeper, non-basalt aquifers (deep Kaawa shell aquifer and Waitemata Group) is estimated to be <4 mm/y. These estimates are based on ^{14}C ages and well depths (Tables 2.1 and 4.2) for the Tuhimata and Underglass wells.

The total estimated recharge of 500–680 mm/y into the basalt formation found in this study implies that about half of the total recharge is into the deep basalt system, while the other half provides for the spring flow via the shallow basalt aquifer. This is in agreement with spring flow estimates from the basalt of 254 mm/y by White et al. (2019).

6.4 Flow Rates, Shallow Groundwater and Lag Time

Groundwater flow rates can be estimated from travel distance per time. Within the fractured basalt lavas, horizontal groundwater age gradients are insufficient for estimating groundwater flow rates. However, total travel time through the groundwater systems is known (Table 5.1), and the average distance between the recharge area and the main discharges can be estimated. This enables estimates of flow rates through the basalt lavas.

For the Pukekohe basalt, the average travel distance for Hickey Spring is estimated to be 3.5 km from the recharge area and for Patumahoe Spring is 2.8 km. Using the mean residence times for these spring systems, the estimated groundwater flow rate through the Hickey Spring system is 190 m/y and for the Patumahoe spring system is 160 m/y. At the Bombay basalt, the Hillview Spring system has an estimated travel distance of 2.3 km, resulting in an estimated average groundwater flow rate of 65 m/y. The lower flow rate through the Bombay basalt lava may be due to it travelling through a deeper saturated groundwater system as a result of the larger gradient between the recharge and discharge areas, compared to the shallow drainage flow and flatter gradient through the Pukekohe basalt, mainly near the water table. For the remaining streams, there is insufficient data on distances between recharge and discharge areas to enable flow-rate estimates.

6.5 Fracture Flow and Sudden Changes

Fracture flow in the basalt lava, as identified by Auckland Regional Water Board (1989), is confirmed by the fact that, at Rifle Range Shallow, the old and new shallow wells, drilled within 3 m distance and screened to the same depth, intercepted water with very different age distributions and hydrochemistry. After the changes in hydrochemistry and water age occurred, the old well drew water from a different flow conduit compared to the new well.

This fracture flow in the basalt lava appears to be undergoing change. Over the last 20 years, all four shallow wells throughout the area of basalt lava showed sudden changes of the water source in Section 4.7. Each well had a change, all at different times. These changes have drastically changed the age and hydrochemistry composition of the water in the wells.

6.6 Connection of Shallow and Deep Aquifers

From hydrogeologic observations, Viljevac et al. (2002) concluded that the deep volcanic and Kaawa shell aquifers are recharged by vertical (downward) leakage from the upper basalt aquifers. The limited groundwater tracer data currently available appears to confirm this model in general.

In the deeper volcanic and Kaawa shell groundwater, ^{18}O matches the signature of recharge from higher elevation on the Pukekohe and Bombay hills (Figure 5.26). The recharge from higher elevation has greater hydraulic head (pressure). Therefore, it is likely to be pushed into the deeper volcanic and from there into the Kaawa shell aquifer. Recharge into the deeper Pukekohe basalt aquifer (Section 6.4) is estimated to be approximately 8 mm/y from the ^{14}C age and well depth (Tables 2.1 and 4.2) at the Rifle Range Deep well. Matching ^{18}O ratios of the groundwater in the Kaawa shell aquifer with those of high-elevation recharge from Bombay and Pukekohe hills indicates that vertical recharge through the overlaying sediments of the Kaawa shell aquifer may be insignificant.

The small number of ^{14}C ages available (Table 4.2) agree with outward flow from the basalt lava into and through the Kaawa shell aquifer. The water in the deep aquifer near Bombay Hill is 3500 years old. With increasing distance from the high-elevation recharge areas of the Pukekohe and Bombay hills, the water in the Kaawa shell aquifer becomes older, increasing to 9100, 15,000 and 28,000 years.

6.7 Groundwater Storage

The age of the water in stream and river discharges is linked to the age of the water in the groundwater reservoir that feeds those rivers and streams (e.g. Berghuijs and Kirchner 2017). Most groundwater is exchanged only slowly with surface water and is therefore relatively old. Tritium concentrations of the water in rivers and streams can be used to estimate the groundwater volume (storage) that actively feeds these rivers and streams.

The active groundwater storage (S), defined here as the water stored in the subsurface that is mobile and flowing toward a stream or river, is related to groundwater flow (Q) and groundwater MTT via the fundamental equation $S = Q \times MTT$ (e.g. Małoszewski and Zuber 1982; Morgenstern et al. 2010). Flow rate and MTT at a given sampling point provide the storage of groundwater that is actively contributing to the flow of the rivers and streams at that discharge point, at the sampled and measure flow conditions.

Seven streams draining the Pukekohe and Bombay basalt lavas were gauged and sampled during baseflow conditions on 22 February 2022 at 27 sites (Figure 2.5). Flows and MTTs of these streams at sites representative for the discharges from the basalt lava are listed in Table 6.1, together with the estimated groundwater storage that actively feeds these streams at these gauging sites (Auckland Council [AC] ID shown in Figure 2.5). The relatively old age of the stream waters draining the Pukekohe and Bombay basalt lavas indicates large groundwater reservoirs feeding these streams.

Table 6.1 Measured water flow, mean transit time (MTT) and estimated groundwater storage actively feeding these streams during baseflow conditions (as sampled on 22 February 2022).

Stream	Auckland Council ID	MTT (y)	Flow (L/s)	Storage (Mm^3)
Hingaia at Quarry Rd.	5	29	182	166
Mauku at Swede (Patullo Rd Bridge)	20	19	107	64
Mauku at Titi Rd Bridge	16	13.5	39	17
Ngakoroa at Kern Rd.	8	18	46	26
Ngakoroa at Ingrams	7	15	43	20
Oira at Swing Bridge (Woodlyn Dr)	11	28	14	12
Waitangi at SH Bridge	6	17	46	25
Whangamaire at Fantail	22	20	128	81
Whangapouri at Glenbrook Rd Bridge	14	18	178	101

Whangamaire Stream and Whangapouri Creek together drain the Pukekohe basalt lava at its northern perimeter, with groundwater storage at Whangamaire at Fantail of 81 Mm^3 and at Whangapouri at Glenbrook of 101 Mm^3. The upper reaches of Mauku Stream also drain part of this basalt lava at its south-western perimeter, with groundwater storage from the basalt lava into Mauku Stream at Mauku at Titi Rd Bridge of 17 Mm^3.

Hingaia Stream mainly drains the Bombay basalt lava at its northern perimeter and also receives water from the Bombay basalt lava at its north-eastern perimeter, with groundwater storage at Hingaia at Quarry Rd of 166 Mm^3. The upper reaches of Ngakoroa Stream also drain locally recharged water from the Bombay basalt lava at its south-western perimeter, with groundwater storage from this part of the basalt lava into Ngakoroa Stream at Ngakoroa at Ingrams of approximately 20 Mm^3.

The combined groundwater storage for the Pukekohe basalt lava is approximately 199 Mm^3 and for the Bombay basalt lava is approximately 186 Mm^3. Both formations have similar groundwater storage that feeds the streams they drain into, despite the Pukekohe basalt lava having a larger spatial extent than Bombay. This implies that the active groundwater flow reservoir at Bombay is significantly deeper, likely a result of the steeper gradient of Bombay Hill.

Mauku Stream also receives flow from a sizable groundwater storage in its lower reaches, draining from the north-western flanks of the basalt lava. This groundwater storage volume is approximately 47 Mm^3, the difference of the calculated storage at Mauku at Swede and Mauku at Titi Rd Bridge. Ngakoroa Stream receives very little additional flow in its lower reaches. Oira Creek and Waitangi Stream are also fed by relatively small groundwater reservoirs during summer baseflow, with water volumes of 12 and 25 Mm^3, respectively. These groundwater discharges have different tracer signatures compared to the groundwater in the main basalt lava, implying different groundwater sources.

6.8 Nitrate Lags and Denitrification

Groundwaters in the **Pleistocene** deposits, Kaawa shell aquifer and Waitemata Group are all old and highly anoxic, and therefore free of nitrate. The presence of only old water in these formations implies that nitrate loads from land-use activities in these areas (mainly dairy) discharge via shallow flow paths, without significant lag time of years, which would impact on

nutrient-management decisions. The storage in these shallow flow-path reservoirs is too small to maintain flow for a few months during the dry season. For these mainly shallow flow paths, there may be potential for partial nitrate attenuation at the interface between the oxic and the reduced zones (Woodward et al. 2013). Nitrate leached from these overlaying soils and not attenuated in the shallow groundwater system or through in-stream processes is likely to discharge through episodically to seasonally active shallow near-surface pathways into the Manukau Harbour, mainly during winter.

The main spring discharges from the basalt lava all contain oxic water, indicating absence of organic material and inorganic electron donors, which is required to facilitate microbial denitrification reactions. Denitrification in the basalt lava is therefore unlikely. Initial results from argon-neon-nitrogen analyses (Phase 2 of this project) in five spring samples indicate that the water from these springs does not contain excess-N_2 (i.e. N_2 in excess to that of intrinsic N_2 from equilibrium with air or contributions from excess air). This also indicates absence of denitrification within the basalt lava – excess-N_2 would have accumulated in the water of these springs if denitrification had occurred anywhere along the flow path. The larger argon-nitrogen dataset of the samples from the groundwater wells also shows no evidence of excess-N_2 in these groundwaters (Figure 5.23). van der Raaij (2015) also found absence of excess-N_2 in the previous argon-nitrogen dataset.

The existing data suggests that denitrification does not occur in the groundwater systems of the basalt lava. These groundwaters, despite carrying high nitrate loads from farming activities (mainly cropping), do not flow through sufficiently anoxic zones to enable microbial denitrification reactions. This implies that nitrate loads from land-use activities around the basalt lavas entering the groundwater system will eventually discharge from the groundwater system back to the surface (streams) without nitrate attenuation, but with a lag time.

Short and longer water and nitrate flow paths combine at springs, causing the groundwater from the springs to have a mixture of ages. The age-distribution parameters for the Hillview, Hickey and Patumahoe springs are listed in Table 5.1. MTTs of 18 years in the discharges from the Pukekohe basalt lava via Hickey and Patumahoe springs, and 36 years from the Bombay basalt lava via Hillview Spring, indicate that significant lag times are expected in the nitrate load response of the springs to land-use / good management changes. The contribution of water younger than the MTT will cause earlier responses. The contribution of water older than the MTT will cause later responses compared to the mean transit time. Using the age distribution of the spring discharges, future nitrate loads from current and historic land-use activities can be forecasted (Morgenstern et al. 2015).

Figure 6.2 shows the modelled nitrate response for the main springs draining the basalt lavas, assuming constant nitrate leaching starting from 1955 (although this assumption may not be correct). The mid-1950s are commonly regarded as the onset of industrial agriculture associated with high nitrate leaching (Morgenstern and Daughney 2012), including in the Pukekohe–Bombay area (Murphy 1991). Under the assumption of constant nitrate loading since 1955, Patumahoe and Hickey springs, with MTT = 18 years, would already be fully adjusted to these land-use practises, while Hillview Spring, with MTT = 36 years, may have reached about 90% of its nitrate load. The dashed lines show the potential decrease in nitrate concentrations in these springs if nitrate leaching were able to be completely discontinued in 2024 (an unlikely management scenario). This is only a theoretical scenario to show the response of the springs to decreased catchment-derived nitrate loading. Hillview Spring shows a more significant lag response due to its water being twice as old compared to Patumahoe and Hickey Spring.

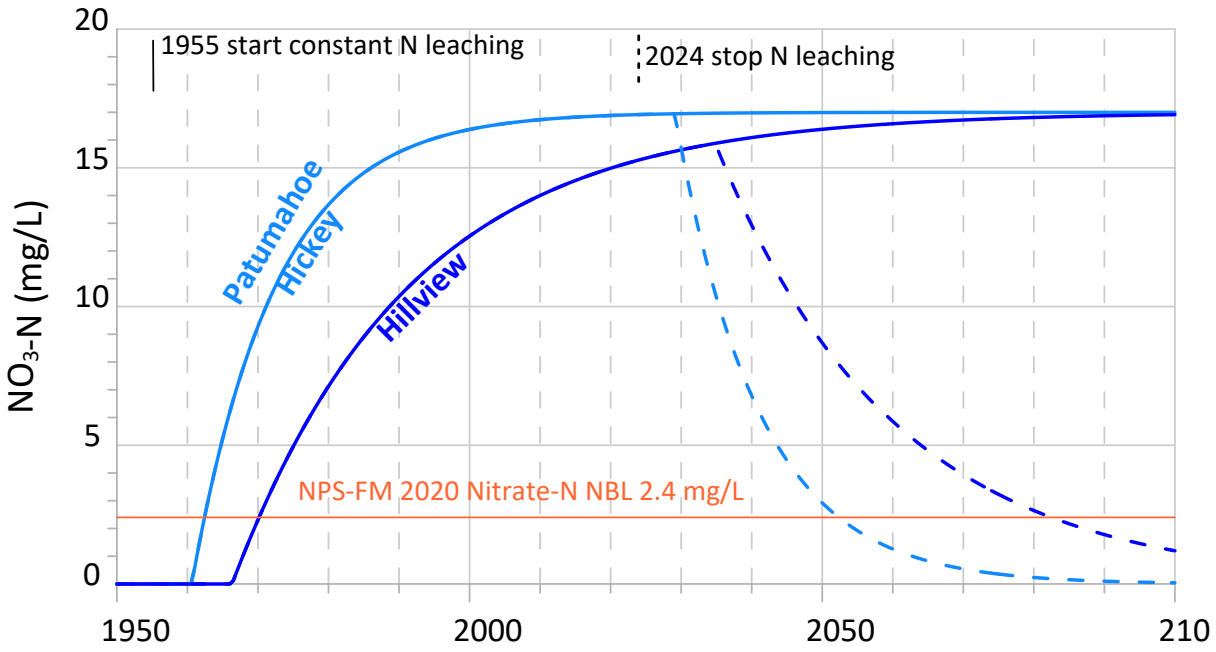

Figure 6.2 Response of nitrate concentrations for the main spring discharges from the Pukekohe and Bombay basalt lavas to the land-use scenario of start of constant nitrate loading at 1955 (full lines), followed by a theoretical discontinuation of nitrate loading in 2024 (dashed lines). Patumahoe and Hickey springs (MTT = 18 years) drain the Pukekohe basalt lava, and Hillview Spring (MTT = 36 years) drains the Bombay basalt lava.

If nitrate loading were stopped in 2024, an improvement to below NBL would be seen by 2050 for Pukekohe and by 2080 for Bombay. However, the times for approaching NBL are likely to be longer, as nitrate loads were probably not constant over recent decades but have increased. This means that the springs have not yet adjusted to historic loads, with larger loads to come than shown in Figure 6.2.

In contrast to the streams discharging from the basalt lavas, nitrate concentrations in Ngakoroa Stream, Oira Creek and Waitangi Stream are low during baseflow conditions. The nitrate loads will be flushed from these catchments by episodically to seasonally active shallow pathways, mainly in winter (Section 5.7).

Potential for nitrate attenuation along the eastern flanks of the basalt lavas (ellipses 1, 2 and 4 in Figure 8.1) is still unknown. No data from groundwater or springs/seeps in these areas are available yet. The stable isotope compositions indicate that discharges into Mauku and Ngakoroa streams are not sourced from the main basalt lava. Despite similar land use compared to the recharge area of the main basalt lava, these discharges are likely to carry lower nitrate loads because these discharges appear to dilute nitrate concentrations in the streams in these areas (at baseflow conditions). It is likely that denitrification is occurring in these groundwater systems. This will be addressed in Phase 2 of this project by sampling and measuring age tracers and excess-N_2 in such discharges.

6.9 Conceptual Groundwater Flow from Tracer Signatures

The interpretation of the age, chemistry and isotope data (presented in the previous sections) enables new conceptual understandings of groundwater sources and flows in the Pukekohe–Bombay area south of Auckland (see overview in Figure 6.3).

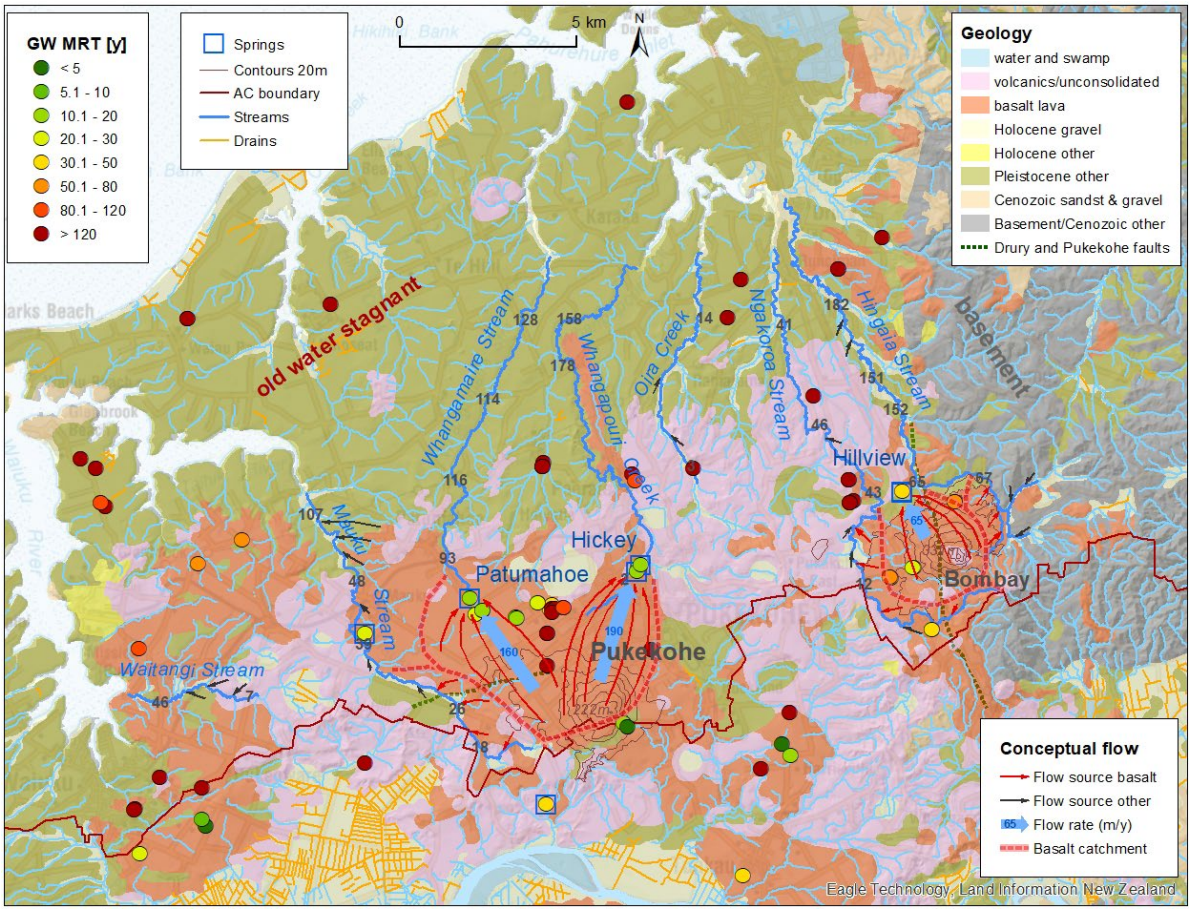

Figure 6.3 Groundwater dynamics and conceptual flow in the Pukekohe–Bombay area inferred from groundwater ages (MRT, circles) in conjunction with stable isotope and nitrate data (not shown). Deeper groundwater recharge and flow in areas outside of basalt lavas is negligible, with the water being stagnant. Major water drainage through large groundwater systems occurs only through the basalt lavas (red arrows), with flow rates indicated by blue arrows (blue numbers indicate flow rates in m/y, length of arrow proportional to flow rate). Dashed red lines indicate approximate catchment boundaries. Black arrows indicate baseflow water contribution to streams from sources other than basalt lavas. Numbers superimposed on streams are measured baseflow rates in L/s.

Active subsurface drainage through large groundwater reservoirs only occurs through the Pukekohe and Bombay basalt lavas. The groundwater drainage system from the basalt lavas via the three main springs (Patumahoe, Hickey and Hillview) is indicated in Figure 6.3 by the longer red arrows. Average groundwater flow rates to these springs are indicated by blue arrows, with the blue numbers indicating groundwater flow rates in m/y and the length of the arrows being proportional to the flow rate. Dashed red lines indicate recharge catchment boundaries for the basalt lavas. Black arrows indicate water contribution to streams from sources other than the basalt lavas. Numbers in streams are measured flow rates in L/s.

Whangamaire Stream and Whangapouri Creek drain the Pukekohe basalt at the northern perimeter of the volcanic plateau, where they receive most of their flow. Groundwater age, isotopes and hydrochemistry (including high nitrate) match those of the water in these streams. There is no significant flow gain within the Pleistocene deposits north of the basalt lavas, indicating the absence or insignificance of deep groundwater flux to the streams. This implies that these areas drain only via shallow flow paths that are depleted during summer baseflow conditions.

Hingaia Stream receives water in its upper reaches partially from greywacke basement rock catchments and partially from the north-eastern perimeter of the basalt lava (Figure 6.3). The mixture of water from the essentially pristine greywacke recharge catchment with water

recharged in areas of high nitrate-leaching activities (Bombay basalt lava) results in medium nitrate concentrations instream. At the northern perimeter of the Bombay basalt lava, where Hillview Spring discharges into the stream, flow and nitrate concentration more than double. Groundwater ages, isotopes and hydrochemistry (including high nitrate) match those of the water discharging from Hillview Spring.

For the upper reaches of Ngakoroa Stream, the isotopes and nitrate concentrations indicate flow contribution from the south-western low-altitude flanks of the basalt cone. North of the basalt cone, the stream does not gain any significant flow. However, the nitrate concentration decreases significantly, likely due to in-stream attenuation processes.

Mauku Stream gains flow from the south-western perimeter of the Pukekohe basalt lava. Groundwater ages, isotopes and hydrochemistry match those of the water in the upper reaches of the stream. From the north-western flanks of the Pukekohe basalt lava, the stream receives groundwater recharged at lower altitudes, which is likely to be anoxic. The stream flow here more than doubles with this input, while nitrate concentrations become diluted.

Oira Creek has a very low flow relative to other streams in the area. It discharges locally recharged, relatively old water with low nitrate concentration. Similarly, Waitangi Stream discharges locally recharged groundwater with low nitrate concentration. Both streams are likely to drain anoxic groundwater systems.

Figure 6.3 shows two faults that could affect groundwater flow in the basalt lava of the Pukekohe–Bombay volcanoes. For the upper reaches of Mauku Stream, the Pukekohe Fault may be partly responsible for the deflection of the groundwater flow to the west of the volcano (red arrows). The Pukekohe Fault has a ~30-m-high scarp cutting the lava flows in this area and also a small scarp displacing probable late Pleistocene deposits (Bland et al. 2023). Such an offset could disrupt groundwater flow paths.

For the Bombay volcano, which had mostly built up and draped over the existing Drury Fault scarp, the majority of displacement on the fault had occurred before the volcano formed (Bland et al. 2023). The overall offset (e.g. on the top of basement rocks) is >200 m, but the surface scarp crossing Bombay volcano is only ~5–8 m high. This suggests that the fault has not significantly displaced the shallow subsurface materials to deflect groundwater flows. However, the Drury Fault may act as a major conduit through the Bombay basalt lava to Hillview Spring. The spring emerges in close proximity to the fault.

The eastern edge of Bombay volcano seems to be a lava flow that has come from the summit area and flowed in a curved path around the edge of the main cone. This flow now forms a distinct ridge with streams on either side the western stream captures flow from the basalt lava (three red arrows), and the eastern stream captures flow from the greywacke hills to the east (three black arrows). It is possible that a similar ridge beneath the western flank of the main Bombay volcano diverts the groundwater flow either to the east or the west, as shown by the drainage divide (dashed line).

The active groundwater flow systems in the basalt lavas have sufficient storage to maintain significant stream baseflow over the course of years. The three main streams draining the basalt lavas on their northern perimeters, Whangamaire Stream, Whangapouri Creek and Hingaia Stream, have a combined groundwater storage of approximately 350 Mm^3. On the south-western flanks of the basalt lavas, the upper reaches of the Mauku and Ngakoroa streams also receive discharge from the basalt lavas (shorter red arrows, Figure 6.3). These secondary basalt catchments have a combined groundwater storage of approximately 37 Mm^3.

The most active groundwater drainage flow (containing the youngest water) feeding the springs occurs near the surface of the saturated zone (water table). Slightly deeper groundwater is older than expected for the upstream position in the active flow path towards the springs. Recharge to the deeper groundwater system is estimated to be 280 mm/y. As indicated by calculated water temperatures, recharge to the deeper groundwater system appears to be preferential flow through fractures allowing fast flow to below the water table. This contrasts with the groundwater providing the spring discharges, which is recharged via matrix flow through the unsaturated zone.

Fracture flow in the shallow basalt lava appears to be unstable. In all four basalt lava wells with long-term monitoring data, hydrochemistry parameters (indicative of land use and geologic sources) have changed drastically over the last 20 years. These changes were permanent, usually from older to younger water, with raising water tables. This indicates changing capture zones for the wells, with each well changing at a different time.

The weathered basalts form rich horticultural soils that are considered elite (Land-Use Capability [LUC] class 1) and prime (LUC classes 2 and 3) and are therefore highly versatile for growing a wide range of crops. High-intensity market gardening on these soils since the 1950s, associated with high nitrate leaching, has resulted in high nitrate loads into the transmissive basalt lava. These basalt lavas discharge oxic groundwater. This indicates the absence of organic matter and inorganic electron donors in the aquifer that would be required for facilitation of microbial reactions, including denitrification. Without denitrification occurring, the nitrate load into the basalt lava is expected to discharge without any nitrate attenuation, with a lag time – the travel time (age) of the water – through the aquifer.

The average lag time of the nitrate load at the Pukekohe basalt lava is 18 years. At the Bombay basalt lava, it is 36 years. Assuming a constant nitrate load for the last 65 years (since the onset of industrial agriculture at around 1955), groundwater discharges from the basalt lavas have essentially adjusted to the high nitrate loads in the recharge areas. However, in the deeper groundwater (for example, at approximately 40 m depth at the Rifle Range Road Shallow well), nitrate concentrations in the groundwater are still increasing and adjusting to the high nitrate loads in their recharge areas. Due to the relatively large lag times, reductions in nitrate loads will take many decades to manifest in the baseflow spring discharges from the basalt lavas. Note that the response will be faster in the non-basalt lava areas where nitrate is flushed out mainly through episodically to seasonally active shallow pathways.

In contrast to the oxic water discharging from the basalt lavas, significant amounts of water (approximately 60 L/s) discharge from the north-western flanks of the Pukekohe basalt lava that appear to be anoxic. This water is low in nitrate despite discharging from areas with land use associated with high nitrate leaching. There is potential for significant nitrate attenuation in this groundwater system. Denitrification may also be possible in the shallow drainage system of the Pleistocene deposits, near the redox zone.

Groundwaters in the Pleistocene deposits and in the formations underlying these, in the unconsolidated volcanic deposits, and in the deep basalt aquifers are all old, indicating very little active circulation through these systems. This implies that rain in these areas drains, mainly during the wet season, through episodically to seasonally active shallow pathways. This shallow drainage system has insufficient storage reservoir to sustain significant stream baseflow through the dry season but contributes to the flow during the wet seasons.

7.0 CONCLUSIONS

Combining and interpreting tracer data and studies from various GNS, Auckland Council and Environment Waikato projects and monitoring programmes led to new understandings of groundwater processes and of the flow system in the Pukekohe–Bombay area from recharge through aquifers and discharge into streams. Historic and new tracer data, water isotopes, hydrochemistry and gas concentrations all contributed to a better understanding of this 'wicked' puzzle.

Tracer signatures in groundwater accumulate over the entire flow system. They provide information about groundwater processes, including: source, recharge catchment boundaries, recharge mechanism, flow rates, storage, nitrate pathways and lag time and potential for denitrification. Tracer signatures are particularly useful in the Pukekohe and Bombay basalt systems. In these systems, groundwater source, flow and recharge catchment boundaries from hydrogeologic data are limited due to fracture-dominated flow and existence of various perched aquifers.

The various techniques used in this study contributed to an improved understanding of the groundwater baseflow system:

- Groundwater ages enabled identification of drainage through active groundwater systems in the basalt aquifers versus nearly stagnant groundwater flow conditions outside the basalt aquifers. The groundwater ages allowed for estimation of recharge rates, flow rates through the shallow part of the aquifer that provides for the spring baseflow, groundwater storage, lag time for nitrate loads and forecasting of the lagged response of the spring systems to land-use/management changes.
- At the boundary of the volcanic formations, hierarchical cluster analysis allowed for identification of water sourced from the underlying marine deposits.
- Most sites do not exhibit perceptible trends in major ion concentrations over time. Most hydrochemistry parameters show a trend with groundwater age.
- The water-stable isotopes enabled differentiation between two different baseflow water sources for the seven streams draining the basalt lavas: active drainage through the basalt aquifers and separate locally recharged groundwater systems.
- Recharge temperatures derived from atmospheric gas concentrations and groundwater ages suggest a dual groundwater recharge flow path system. There is both matrix flow recharge through the unsaturated zone into the shallow groundwater system that feeds the springs and fast preferential flow recharge through fractures into the underlying groundwater system.
- Radon identified areas of groundwater discharge into streams, which is useful for identification of diffuse groundwater seepage through stream beds.
- Redox parameters, together with groundwater age, show that denitrification is unlikely in the basalt aquifers but possible in other groundwater systems.

Groundwater flow processes are complex, and hence a multi-faceted approach as undertaken in this study is required for detailed understanding of conceptual groundwater flow.

8.0 RECOMMENDATIONS

8.1 Cover Remaining Knowledge Gaps About Groundwater Flow

1. Perform a similar study at winter baseflow conditions to quantify (i) baseflow and nitrate loads from the basalt aquifers during winter; and (ii) surface drainage from the Pleistocene deposits and unconsolidated volcanic deposits, as well as related nitrate loads into the streams and harbour (high dairy cover). Note that the nitrate flow pathways from the Pleistocene deposits and unconsolidated volcanic deposits are likely to be active only during the wet season.
2. Collect more age-tracer and hydrochemistry samples from critical areas at the Pukekohe basalt lava, as the existing age-tracer data covers only a small area. A critical knowledge gap area is the western perimeter of the basalt lava to Mauku Stream, where anoxic groundwater processes may support nitrate attenuation – the only area with potential for significant groundwater nitrate attenuation.
3. Install a monitoring well and collect one-off samples from 2 to 3 wells in the Waitangi Stream catchment, as there is insufficient groundwater data to enable understanding of groundwater flow connections to this stream.
4. Sample and analyse more wells for ^{14}C to enable better understanding of recharge into and flow processes through the deep volcanic and Pleistocene aquifers. Choosing wells that already have tritium and SF_6 data would yield relatively large spatial coverage at minimum additional cost. Include modelling of the ^{14}C dilution by organic matter (net-path modelling).
5. Enable use of historic age-tracer data that was subject to various issues and therefore can only be used in a limited way by re-sampling sites, including: Kiwi Broilers, Tuhimata, Crowe, Watson Ave and Balance.
6. If more wells within basalt lavas are available with hydrochemistry time-series, investigate for further evidence of sudden changes in capture zones of wells, likely caused by collapses of fractures.

8.2 Understanding Denitrification Potential: Sampling Phase 2

Naturally occurring nitrate attenuation processes could form an important part of improved nutrient-management regimes. This naturally occurring environmental denitrification service may allow for crop production with minimum environmental impact. We therefore suggest making areas with potential for nitrate attenuation the focus of Phase 2 of this project, with the aim of understanding denitrification processes in the groundwater systems.

Mauku Stream gains significant flow before the last gauging site (#20, Table 2.2), increasing from 48 to 107 L/s (flow labels outlined in Figure 8.1). These gains come from contributories that Viljevac (1996) identified as springs V24–28, which drain the volcanic formation. This water is relatively old, as it causes the water in Mauku Stream to become considerably older at site #20 (Figure 5.2). This seepage / spring water must also have low nitrate concentrations, as it dilutes the higher nitrate concentrations of Mauku Stream observed further upstream (Section 5.6). This seepage water is also likely to be anoxic (Section 5.3). A combination of these factors, and further considering that this area has high crop farming cover and therefore similar nitrate loading as in the central Pukekohe basalt lava, point toward significant nitrate attenuation occurring in this groundwater system. Further sampling would help elucidate the processes occurring at a more localised scale and to quantify denitrification occurring in the groundwater system.

The following areas with high potential for nitrate attenuation in the groundwater systems should be investigated in Phase 2 and be sampled for age tracers; excess-N_2 (via neon); and hydrochemistry, including nitrate:

- Areas 1 and 2 marked by red ellipses in Figures 8.1 and 8.2 would target the discharges into the lower Mauku Stream. It is not known if potential sites listed in Viljevac (1996) exist as discrete springs or, if so, how significant they are. However, there is considerable stream flow gain in this area, and it should therefore be possible to find springs along the streams or seepage into the streams that are suitable for sampling. Most of these sites are close to public roads and should be reasonably easily accessible.
- Area 3 would target discharges from the southern Pukekohe basalt lava into Whangamaire Stream. If such discharges exist at baseflow, it could be expected that denitrification occurs in this groundwater system.
- Areas 4 and 5 would target locations with similar potential for nitrate attenuation on the western and northern flanks of the Bombay basalt lava. Less is known about potential spring seepages around the Bombay basalt lava.

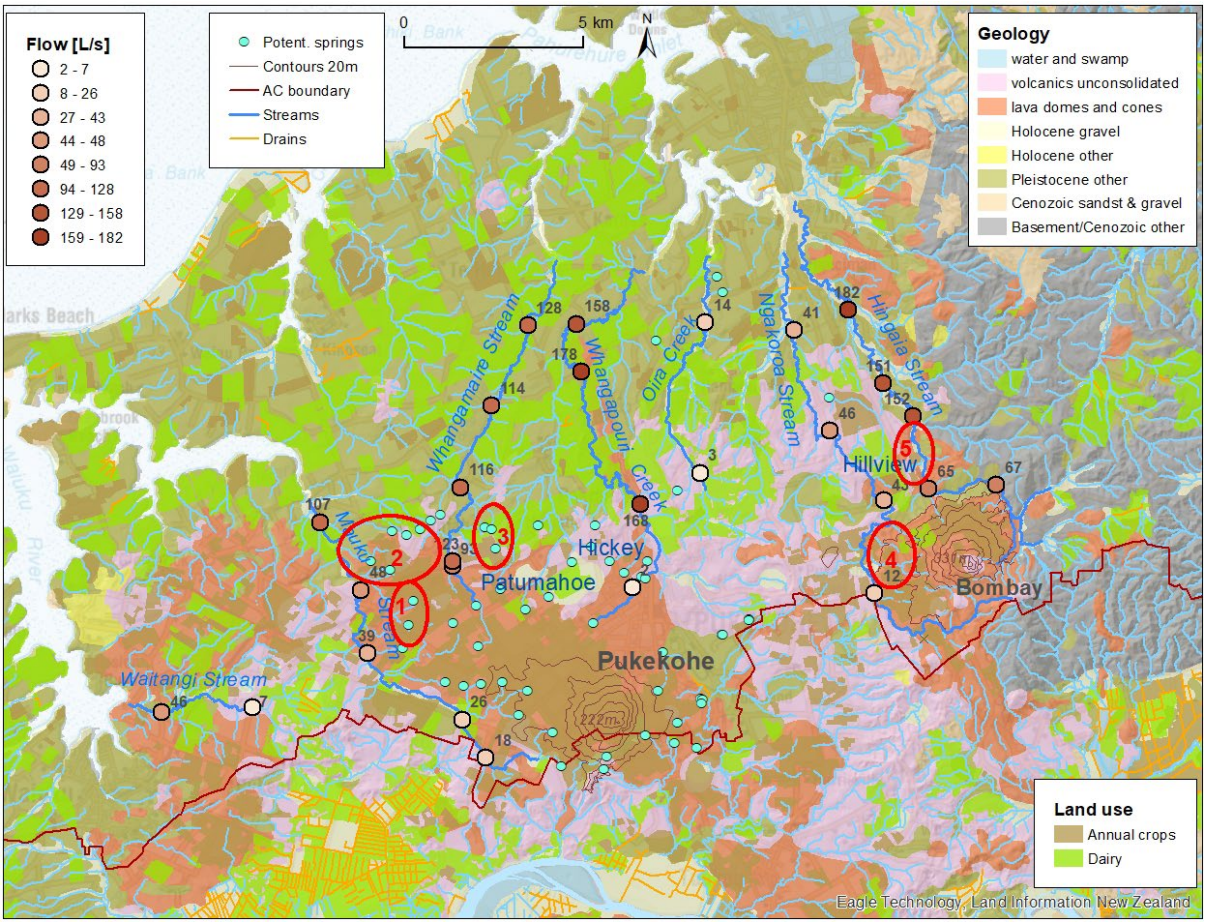

Figure 8.1 Areas with potential for groundwater nitrate attenuation (red numbered ellipses) and potential spring sites (teal circles, Viljevac [1996]).

To assist with finding access to suitable sampling locations, Figure 8.2. shows the areas of interest and potential spring sites in the topographic map.

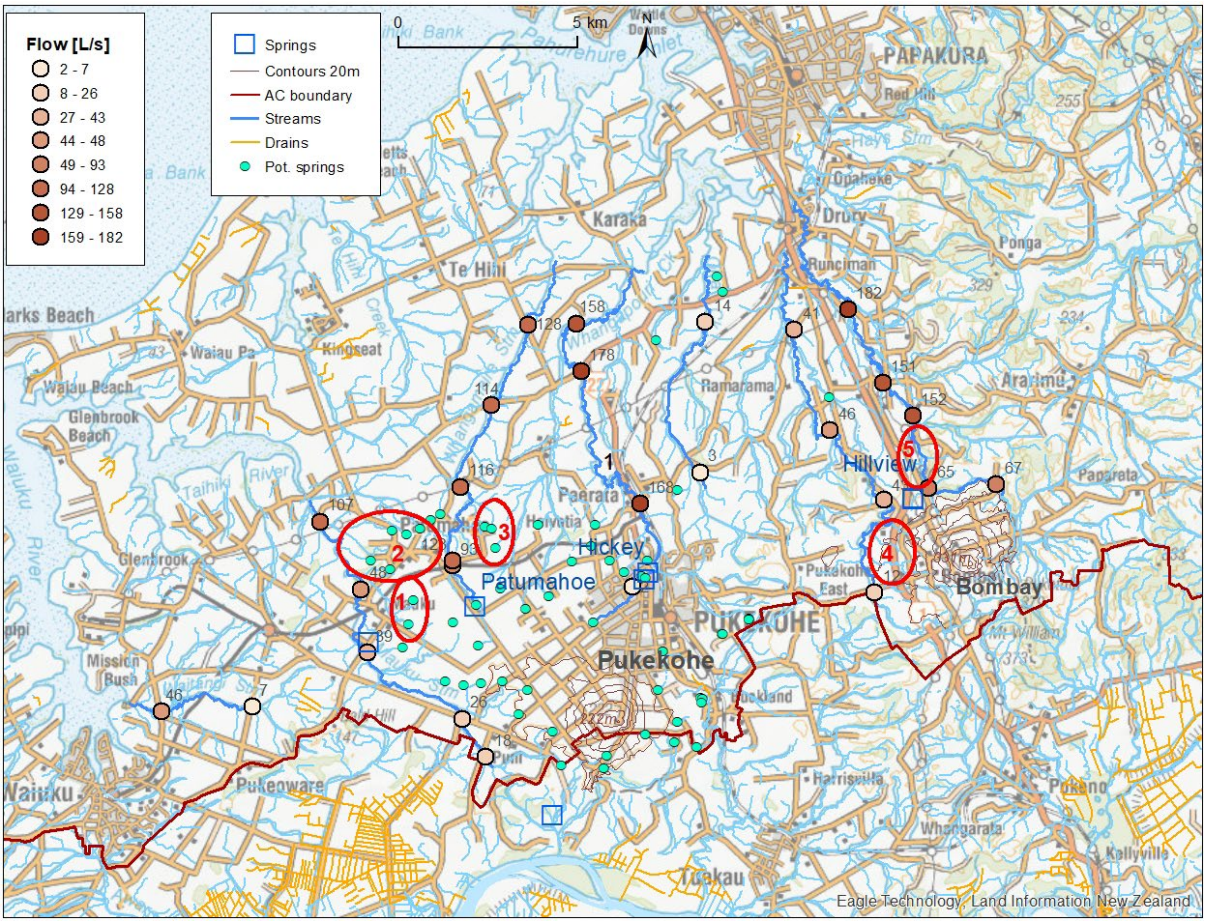

Figure 8.2 Topographic map of areas with potential for groundwater nitrate attenuation (red numbered ellipses) and potential spring sites (teal circles, Viljevac [1996]).

9.0 ACKNOWLEDGMENTS

This work was supported by Auckland Council funding (CW9929), the National Groundwater Monitoring Programme, age-tracer SSIF funding and the contestable programme Te Whakaheke o Te Wai (PROP-57536-ENDRP-GNS). We thank the Auckland Council hydrology and water quality teams for measuring stream flows and collecting samples, Auckland Council staff Coral Grant and Andrew Millar for thorough peer review, Biljana Lukovic for help with the ArcGIS figures, Catherine Cooper for editing and Kate Robb for formatting this report.

10.0 REFERENCES

Abascal E, Gómez-Coma L, Ortiz I, Ortiz A. 2022. Global diagnosis of nitrate pollution in groundwater and review of removal technologies. *Science of The Total Environment*. 810:152233. doi:10.1016/j.scitotenv.2021.152233.

Auckland Regional Council. 2010. State of the Auckland region. Auckland (NZ): Auckland Regional Council. 15 p.

Auckland Regional Water Board. 1989. A study of the Kaawa Formation aquifer system in the Manukau Lowlands. Auckland (NZ): Auckland Regional Water Board. 312 p. Technical Publication 85.

Baird R, Eaton AD, Rice EW, Bridgewater L, editors. 2017. Standard methods for the examination of water and wastewater. 23rd ed. Washington (DC): American Public Health Association, American Water Works Association, Water Environment Federation. 1 vol.

Barrell DJA, Bland KJ, Hill MP, Lee JM. 2021. Revised stratigraphic framework for the Pliocene to Holocene sedimentary deposits of the Auckland area. Lower Hutt (NZ): GNS Science. 25 p. (GNS Science report; 2020/05).

Berghuijs WR, Kirchner JW. 2017. The relationship between contrasting ages of groundwater and streamflow. *Geophysical Research Letters*. 44(17):8925–8935. doi:10.1002/2017gl074962.

Beyer M, Morgenstern U, van der Raaij R, Martindale H. 2017. Halon-1301 – further evidence of its performance as an age tracer in New Zealand groundwater. *Hydrology and Earth System Sciences*. 21(8):4213–4231. doi:10.5194/hess-21-4213-2017.

Bland KE, Townsend DB, Hill MP, Jones KE. 2023. Geology of the Pukekohe area. Lower Hutt (NZ): GNS Science. (GNS Science geological map; 12b). https://doi.org/10.21420/Y3CC-PB81

Briggs RM, Okada T, Itaya T, Shibuya H, Smith IEM. 1994. K-Ar ages, paleomagnetism, and geochemistry of the South Auckland volcanic field, North Island, New Zealand. *New Zealand Journal of Geology and Geophysics*. 37(2):143–153. doi:10.1080/00288306.1994.9514609.

Busenberg E, Plummer LN. 1992. Use of chlorofluorocarbons (CCl_3F and CCl_2F_2) as hydrologic tracers and age-dating tools: the alluvium and terrace system of central Oklahoma. *Water Resources Research*. 28(9):2257–2283. doi:10.1029/92wr01263.

Cartwright I, Morgenstern U. 2012. Constraining groundwater recharge and the rate of geochemical processes using tritium and major ion geochemistry: Ovens catchment, southeast Australia. *Journal of Hydrology*. 475:137–149. doi:10.1016/j.jhydrol.2012.09.037

Casanovas P, Goodwin E, Schattschneider J, Kamke J, Grant C, Ingley R, Fraser S, Young R. 2022. Dissolved oxygen and ecosystem metabolism in Auckland rivers 2004–2020: State of the Environment reporting. Auckland (NZ): Auckland Council. 142 p. Technical Report 2022/18.

Cook C, Briggs RM, Smith IEM, Maas R. 2004. Petrology and geochemistry of intraplate basalts in the South Auckland Volcanic Field, New Zealand: evidence for two coeval magma suites from distinct sources. *Journal of Petrology*. 46(3):473–503. doi:10.1093/petrology/egh084.

Crowcroft G, Bowden D. 2002. Auckland water resource quantity statement 2002: surface water and groundwater resource information, availability and allocation. Auckland (NZ): Auckland Regional Council. 44 p. Technical Publication 171.

Crush JR, Cathcart SN, Singleton P, Longhurst RD. 1997. Potential for nitrate leaching from different land uses in the Pukekohe area. *Proceedings of the New Zealand Grassland Association*. 59:55–58. doi:10.33584/jnzg.1997.59.2266.

Daughney CJ. 2007. Spreadsheet for automatic processing of water quality data: 2007 update. Lower Hutt (NZ): GNS Science. 15 p. (GNS Science report; 2007/17).

Daughney CJ, Jones A, Baker T, Hanson C, Davidson P, Zemansky GM, Reeves RR, Thompson M. 2006. A national protocol for state of the environment groundwater sampling in New Zealand. Wellington (NZ): Ministry for the Environment. 54 p. (GNS Science miscellaneous series; 5).

Daughney CJ, Randall M. 2009. National groundwater quality indicators update: state and trends 1995–2008. Lower Hutt (NZ): GNS Science. 55 p. + 1 CD. Consultancy Report 2009/145. Prepared for Ministry for the Environment.

Daughney CJ, Reeves RR. 2005. Definition of hydrochemical facies in the New Zealand National Groundwater Monitoring Programme. *Journal of Hydrology (New Zealand)*. 44(2):105–130.

Daughney CJ, Wall M. 2007. Groundwater quality in New Zealand: state and trends 1995–2006. Lower Hutt (NZ): GNS Science. 65 p. Consultancy Report 2007/23. Prepared for the Ministry for the Environment.

Earthtech Consulting Limited. 2013. TP133: South Auckland groundwater, Kaawa Aquifer recharge study: review comments. Pukekohe (NZ): Earthtech Consulting Ltd. 9 p. + appendices. Prepared for Auckland Council.

Edbrooke SW. 2001. Geology of the Auckland area [map]. Lower Hutt (NZ): Institute of Geological & Nuclear Sciences. 1 map + 74 p., scale 1:250,000. (Institute of Geological & Nuclear Sciences 1:250,000 geological map; 3).

Foster C, Johnson K. 2021. Groundwater quality state and trends in Tamaki Makaurau / Auckland 2010–2019: State of the Environment reporting. Auckland (NZ): Auckland Council, Research and Evaluation Unit (RIMU). 63 p. Technical Report 2021/03-2.

Güler C, Thyne GD, McCray JE, Turner KA. 2002. Evaluation of graphical and multivariate statistical methods for classification of water chemistry data. *Hydrogeology Journal*. 10(4):455–474. doi:10.1007/s10040-002-0196-6.

Heaton THE, Vogel JC. 1981. “Excess air” in groundwater. *Journal of Hydrology*. 50:201–216. doi:10.1016/0022-1694(81)90070-6.

Helsel DR, Hirsch RM, Ryberg KR, Archfield SA, Gilroy EJ. 2020. Statistical methods in water resources. In: *Hydrologic analysis and interpretation*. Reston (VA): U.S. Geological Survey. 458 p. (Techniques and methods; 4-A3).

Heron DW, custodian. 2020. Geological map of New Zealand [map]. 3rd ed. Lower Hutt (NZ): GNS Science. 1 USB, scale 1:250,000. (GNS Science geological map; 1).

Johnson K. 2021. Rainfall, river flow, and groundwater level state and trends in Tāmaki Makaurau / Auckland 2010–2019: State of the Environment reporting. Auckland (NZ): Auckland Council, Research and Evaluation Unit (RIMU). 77 p. + appendices. Technical Report 2021/06.

Jones KE, Strogen, DP, Hill MP. 2022. 3D geological model of the Pukekohe area. Lower Hutt (NZ): GNS Science. (GNS Science geological map; 12a). https://doi.org/10.21420/KA0P-SW95

Jurgens BC, Böhlke JK, Eberts SM. 2012. TracerLPM (Version 1): an Excel workbook® for interpreting groundwater age distributions from environmental tracer data. Reston (VA): U.S. Geological Survey. 60 p. Techniques and Methods Report 4-F3.

Kalbus E, Buckthought L, Perks A, Boyle JJ. 2017. State of the environment: groundwater state and trends in the Auckland region 2016. Auckland (NZ). 137 p. Technical Report 2017/34.

Lee L. 2022. Package 'NADA': nondetects and data analysis for environmental data. Version 1.6-1.1. Indianapolis (IN): R Foundation; [accessed 2023 Mar]. https://cran.r-project.org/web/packages/NADA/NADA.pdf

Lucas LL, Unterweger MP. 2000. Comprehensive review and critical evaluation of the half-life of tritium. *Journal of Research of the National Institute of Standards and Technology*. 105(4):541–549. doi:10.6028/jres.105.043.

Maiss M, Brenninkmeijer CAM. 1998. Atmospheric SF_6: trends, sources, and prospects. *Environmental Science & Technology*. 32(20):3077–3086. doi:10.1021/es9802807.

Małoszewski P, Zuber A. 1982. Determining the turnover time of groundwater systems with the aid of environmental tracers: 1. Models and their applicability. *Journal of Hydrology*. 57(3–4):207–231. doi:10.1016/0022-1694(82)90147-0.

Martindale H, van der Raaij RW, Knowling MJ, Morgenstern U. 2018. Quantifying groundwater discharge into New Zealand rivers using radon and concurrent flow gauging. Lower Hutt (NZ): GNS Science. 39 p. (GNS Science report; 2018/25).

McBride GB. 2019. Has water quality improved or been maintained? A quantitative assessment procedure. *Journal of Environmental Quality*. 48(2):412–420. doi:10.2134/jeq2018.03.0101.

MfE Data Service. 2012. LUCAS NZ Land Use Map 1990 2008 2012 2016 v01. Wellington (NZ) Ministry for the Environment; [updated 2022 Oct 3; accessed 2023 Mar]. https://data.mfe.govt.nz/layer/52375-lucas-nz-land-use-map-1990-2008-2012-2016-v011/

Milne J. 2019. Water quality part 1 – sampling, measuring, processing and archiving of discrete groundwater quality data. [Wellington] (NZ): National Environmental Monitoring Standards; [accessed 2023 Mar]. https://www.nems.org.nz/documents/water-quality-part-1-groundwater/

Ministry for the Environment. 2020. National Policy Statement for Freshwater Management 2020. Wellington (NZ): Ministry for the Environment. 70 p.

Mook WG. 2001. Environmental isotopes in the hydrological cycle: principles and applications Volume 1 – introduction: theory, methods, review. Paris (FR): UNESCO, IAEA. Chapter 8, Natural abundance of radioactive isotopes of C and H. p. 125–142. (Technical documents in hydrology; 39).

Moreau M, Daughney C. 2021. Defining natural baselines for rates of change in New Zealand's groundwater quality: dealing with incomplete or disparate datasets, accounting for impacted sites, and merging into state of the-environment reporting. *Science of The Total Environment*. 755(2):143292. doi:10.1016/j.scitotenv.2020.143292.

Moreau M, Riedi MA, Aurisch K. 2016. Update of national groundwater quality indicators: state and trends 2005–2014. Wairakei (NZ): GNS Science. 36 p. Consultancy Report 2015/107. Prepared for Ministry for the Environment.

Moreau-Fournier M, Daughney CJ. 2010. Procedure for checking laboratory water chemistry results prior upload to the Geothermal-Groundwater database. Wairakei (NZ): GNS Science. 62 p. Internal Report 2010/06.

Morgenstern U, Brown LJ, Begg JG, Daughney CJ, Davidson P. 2009. Linkwater catchment groundwater residence time, flow pattern, and hydrochemistry trends. Lower Hutt (NZ): GNS Science. 47 p. (GNS Science report; 2009/08).

Morgenstern U, Daughney CJ. 2012. Groundwater age for identification of baseline groundwater quality and impacts of land-use intensification – The National Groundwater Monitoring Programme of New Zealand. *Journal of Hydrology*. 456–457:79–93. doi:10.1016/j.jhydrol.2012.06.010.

Morgenstern U, Daughney CJ, Leonard G, Gordon D, Donath FM, Reeves R. 2015. Using groundwater age and hydrochemistry to understand sources and dynamics of nutrient contamination through the catchment into Lake Rotorua, New Zealand. *Hydrology and Earth System Sciences*. 19(2):803–822. doi:10.5194/hess-19-803-2015.

Morgenstern U, Stewart MK, Stenger R. 2010. Dating of streamwater using tritium in a post nuclear bomb pulse world: continuous variation of mean transit time with streamflow. *Hydrology and Earth System Sciences*. 14(11):2289–2301. doi:10.5194/hess-14-2289-2010.

Morgenstern U, Taylor CB. 2009. Ultra low-level tritium measurement using electrolytic enrichment and LSC. *Isotopes in Environmental and Health Studies*. 45(2):96–117. doi:10.1080/10256010902931194.

Morgenstern U, van der Raaij RW, Baalousha H. 2012. Groundwater flow pattern in the Ruataniwha Plains as derived from the isotope and chemistry signature of the water. Lower Hutt (NZ): GNS Science. 44 p. (GNS Science report; 2012/23).

Morgenstern U, van der Raaij RW, Trompetter VJ, McBeth K. 2008. The Marlborough Deep Wairau Aquifer sustainability review 2008: isotopic indicators. Lower Hutt (NZ): GNS Science. 18 p. (GNS Science report; 2008/33).

Murphy GK. 1991. Drury–Bombay groundwater investigation and interim management plan 1991. Auckland (NZ): Auckland Regional Council. Technical Publication 105.

Plummer LN, Busenberg E. 2000. Chlorofluorocarbons. In: Cook PG, Herczeg AL, editors. *Environmental tracers in subsurface hydrology*. Boston (MA): Kluwer Academic. p. 441–478.

Rogers KM, Buckthought LE. 2022. Nitrate source evaluation of surface water and groundwater in the Franklin area using a dual stable isotope approach. Lower Hutt (NZ): GNS Science. 30 p. (GNS Science report; 2022/02).

Rosen MR. 2001. Hydrochemistry of New Zealand's aquifers. In: Rosen MR, White PA, editors. *Groundwaters of New Zealand*. Wellington (NZ): New Zealand Hydrological Society. p. 77–110.

Schofield JC. 1958. Notes on volcanism and structure in Franklin County. *New Zealand Journal of Geology and Geophysics*. 1(3):541–559. doi:10.1080/00288306.1958.10422787.

Seltzer AM, Stute M, Morgenstern U, Stewart MK, Schaefer JM. 2015. Mean annual temperature in New Zealand during the last glacial maximum derived from dissolved noble gases in groundwater. *Earth and Planetary Science Letters*. 431:206–216. doi:10.1016/j.epsl.2015.09.032.

Snelder T, Fraser C. 2021. The LWP-Trends library. Version 2101. Christchurch (NZ): Land Water People. 37 p.

Snelder TH, Larned ST, McDowell RW. 2018. Anthropogenic increases of catchment nitrogen and phosphorus loads in New Zealand. *New Zealand Journal of Marine and Freshwater Research*. 52(3):336–361. doi:10.1080/00288330.2017.1393758.

Stenger R, Park J, Morgenstern U, Hadfield J, Rivas A, Clague J. 2022. Combining surface water monitoring, age-dating, and parsimonious modelling to unravel water and contaminant pathways through catchments. In: Christensen CL, Horne DJ, Singh R, editors. *Adaptive strategies for future farming*. Palmerston North (NZ): Massey University, Farmed Landscapes Research Centre. 9 p. (Occasional report; 34).

Stewart MK, Morgenstern U. 2001. Age and source of groundwater from isotope tracers. In: Rosen MR, White PA, editors. *Groundwaters of New Zealand*. Wellington (NZ): New Zealand Hydrological Society. p. 161–183.

Townsend DB, Jones, KE, Bland KJ. In prep. Geomorphology map of the Pukekohe area. Lower Hutt (NZ): GNS Science. (GNS Science geological map; 12c). doi:10.21420/6G7F-R243.

van der Raaij RW. 2003. Age-dating of New Zealand groundwaters using sulphur hexafluoride [MSc thesis]. Wellington (NZ): Victoria University of Wellington. 122 p.

van der Raaij RW. 2015. Groundwater residence times and chemistry of the Pukekohe and Bombay basalt aquifers. Lower Hutt (NZ): GNS Science. 50 p. (GNS Science report; 2015/11).

Viljevac Z. 1996. A model of recharge to Pukekohe volcanic aquifers, South Auckland: preliminary study. Auckland (NZ): Auckland Regional Council Environment Water Resources. 58 p. Technical Publication 77.

Viljevac Z, Murphy G, Smaill A, Crowcroft G, Bowden D. 2002. South Auckland groundwater, Kaawa aquifer recharge study and management of the volcanic and Kaawa aquifers. Auckland (NZ): Auckland Council. 85 p. Technical Publication 133.

Ward JH. 1963. Hierarchical grouping to optimize an objective function. *Journal of the American Statistical Association*. 58(301):236–244. doi:10.1080/01621459.1963.10500845.

Water Services (Drinking Water Standards for New Zealand) Regulations 2022; [accessed 2023 Mar]. https://www.legislation.govt.nz/regulation/public/2022/0168/latest/whole.html

White PA, Moreau M, Mourot F, White JT, Johnson K, Hill MP. 2019. Groundwater in the Franklin area. Wairakei (NZ): GNS Science. 105 p. Consultancy Report 2019/81. Prepared for Auckland Council, Waikato Regional Council.

Woodward SJR, Stenger R, Bidwell VJ. 2013. Dynamic analysis of stream flow and water chemistry to infer subsurface water and nitrate fluxes in a lowland dairying catchment. *Journal of Hydrology*. 505:299–311. doi:10.1016/j.jhydrol.2013.07.044.

APPENDICES

This page left intentionally blank.

APPENDIX 1 DETERMINATION OF GROUNDWATER RESIDENCE TIME USING TRITIUM, CFCS AND SF_6

A1.1 Tritium, CFCs and SF_6 Methods

Tritium is produced naturally in the atmosphere by cosmic rays, but large amounts were also released into the atmosphere in the early 1960s during atmospheric thermonuclear bomb tests, giving rain and surface water high tritium concentration at this time (Figure A1.1). Surface water becomes separated from the atmospheric tritium source when it infiltrates into the ground, and the tritium concentration in the groundwater then decreases over time due to radioactive decay. Tritium concentration in groundwater is therefore a function of the time that the water has been underground. Groundwater dating using tritium is described in more detail in Morgenstern and Daughney (2012).

Tritium is a conservative tracer in groundwater. It is not affected by chemical or microbial processes or by reactions between the groundwater, soil sediment and aquifer material. Tritium is a component of the water molecule, and age information is therefore not distorted by any processes occurring underground. Tritium is an ideal tracer for understanding groundwater flow.

As a result of the superimposed atmospheric tritium bomb peak in the 1960s, ambiguous ages have occurred with single tritium determinations before around 2015 in the groundwater age range of 15–40 years (i.e. the tritium concentration could indicate any of several possible groundwater ages). This ambiguity could be overcome by using a second tritium determination after about three years or combining age interpretation of tritium data and data from other dating methods, such as atmospheric gases SF_6 or CFCs, whose atmospheric concentrations have risen steadily since the 1960s and therefore could resolve tritium ambiguity, if these gas tracers are not altered in the aquifer (see below). On the other hand, due to the global tritium bomb spike, the tritium method is very sensitive for identifying mixing of groundwater from short and long flow paths (Section A1.3).

Chlorofluorocarbons (CFCs) are entirely man-made contaminants. They were mainly used as refrigerants, propellants, blowing agents for foams and packing materials, and solvents. Their global atmospheric concentrations gradually increased over time until the 1990s, when they began to be phased out of industrial use (Figure A1.1) due to their contribution to ozone depletion in the upper atmosphere. CFCs are relatively long-lived and slightly soluble in water, and therefore they enter groundwater systems with groundwater recharge. Their concentrations in groundwater record the atmospheric concentrations when the water was recharged, allowing determination of the recharge date of the water. However, after production was phased out, rates of increase in atmospheric CFC concentrations slowed greatly in the 1990s and subsequently decreased (Figure A1.1), meaning that CFCs are not effective for dating water recharged after 1990.

A number of factors can modify CFC concentrations in aquifers (Plummer and Busenberg 2000), including microbial degradation of CFCs in anaerobic environments (CFC-11 is more susceptible than CFC-12) and CFC contamination from local anthropogenic sources (CFC-12 is more susceptible to this). CFC-11 has been found to be less susceptible to local contamination in New Zealand compared to CFC-12, and CFC-11 age estimates generally agree better with those from tritium. Note that CFC and SF_6 ages do not take into account travel time through unsaturated zones.

Sulphur hexafluoride (SF_6) is primarily anthropogenic in origin but can also occur in some volcanic and igneous fluids. In the 1960s, SF_6 began to be significantly produced for use in high-voltage electrical switches, leading to increasing atmospheric concentrations (Figure A1.1). The residence time of SF_6 in the atmosphere is extremely long (800–3200 years). It holds considerable promise as a dating tool for post-1990s groundwater because, unlike CFCs, atmospheric concentrations of SF_6 have continued increasing over recent decades (Figure A1.1). The recent more-than-linear increase over the last two decades makes SF_6 a very sensitive tool for dating young groundwater.

Halon-1301 ($CBrF_3$) holds promise to remain a more efficient age tracer than the CFCs, with still slightly increasing concentrations in the atmosphere (Figure A1.1) and absence of local contamination sources that interfere with dating (Beyer et al. 2017). Halon-1301 was used as a refrigerant gas and fire-suppressing agent in the mid-1990s but also faces production restrictions due to its ozone-depleting effect.

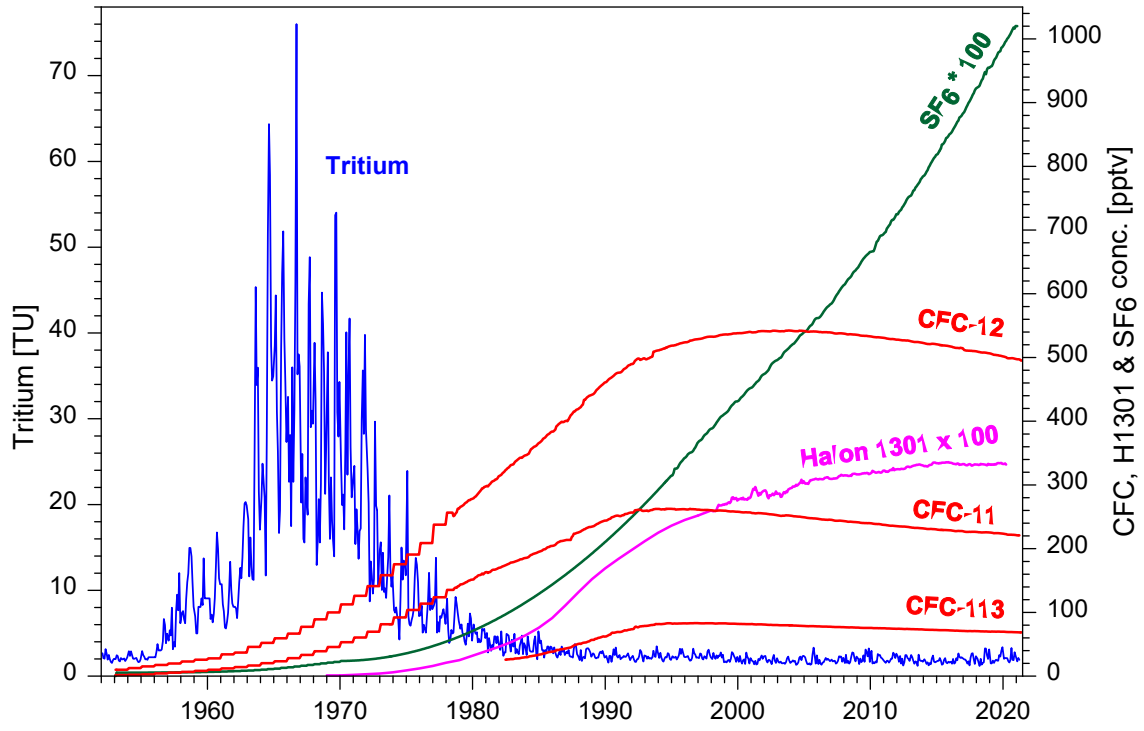

Figure A1.1 Tritium, CFCs, Halon-1301 and SF_6 input for New Zealand rain. Tritium concentrations are in rain at Kaitoke, 40 km north of Wellington (monthly samples); and CFCs, Halon-1301 and SF_6 concentrations are for southern hemispheric air. TU = 1 represents a $^3H/^1H$ ratio of 10^{-18}, and 1 ppt is one part per trillion by volume of CFCs, Halon-1301 or SF_6 in air, or 10^{-12}. Pre-1978 CFC data are reconstructed using the methods of Plummer and Busenberg (2000) and scaled to the southern hemisphere by a factor of 0.83 (CFC-11) and of 0.9 (CFC-12). Post-1978 CFC data are from Tasmania. Pre-1970 SF_6 data are reconstructed (USGS, Reston), 1970–1995 data are from Maiss and Brenninkmeijer (1998) and post-1995 data were measured in Tasmania. Halon-1301 data are from Beyer et al. (2017).

Radon-222 (^{222}Rn) gas is a radioactive decay product of uranium, which is ubiquitous in almost all rocks and soils. Groundwaters that are in a closed system in contact with these rocks accumulate ^{222}Rn released from the minerals, resulting in elevated ^{222}Rn concentrations in the groundwater. These concentrations are a result of equilibrium between ^{222}Rn delivery and radioactive decay (half-life 3.8 days) and can vary considerably depending on the uranium content and ^{222}Rn emanation potential of the aquifer material. In surface waters, ^{222}Rn concentrations are low because of limited contact with its source and because of decay and degassing into the air. This tracer informs on the presence of young (up to weeks) groundwater.

This contrast between high ^{222}Rn concentrations in groundwater and low concentrations in surface water allows the identification of groundwater seepage into surface water, as indicated by elevated ^{222}Rn concentrations in the river water (Martindale et al. 2018). Conversely, recent river-water recharge into groundwater systems is indicated by low ^{222}Rn concentrations in groundwater, as it takes approximately three weeks (5–6 half-lives) for the ^{222}Rn to equilibrate to the ambient concentration of the groundwater.

A1.2 Groundwater Mixing Models

Groundwater at its discharge point is a mixture of water from short and long flowlines, and therefore has a distribution of ages rather than a single age. Various transfer functions describe the distribution of ages within the water sample. Lumped parameter models (LPMs), which are mathematical models of water transport based on simplified aquifer geometry and flow configuration, can account for such mixing of groundwater of different age, usually representing the age distribution with two parameters, the mean residence time and the mixing parameter.

Various mixing models with different age distributions describe different hydrogeological situations (Małoszewski and Zuber 1982). The piston-flow model describes systems with little mixing (such as confined aquifers and river recharge), while the exponential model describes fully mixed systems (more like unconfined aquifers and local rain recharge). Real groundwater systems, which are partially mixed, lie between these two extremes. They can be described by a combination of the exponential and piston-flow models representing the recharge, flow and discharge parts of a groundwater system, respectively. The output tracer concentration can be calculated by solving the convolution integral, and the mean residence time (MRT) can be obtained from the tracer output that gives the best match to the measured data. If the second parameter in the age-distribution function, the fraction of mixed flow, cannot be estimated from hydrogeological information, then two independent tracers (tritium and CFC/SF_6) or two tritium measurements over time are necessary.

Schematic groundwater flow situations are shown in Figure A1.2. An unconfined aquifer situation is described by the exponential model (EM). Flow lines of different length containing water of different ages converge in the well or the stream, and the abstracted water has a wide range of ages with an exponential age distribution. A confined aquifer situation is described by the piston flow model (PM) with a narrow range of ages. A partly confined aquifer situation is described by the exponential piston flow model (EPM). The second parameter is the fraction of exponential flow within the total flow volume (represented by E%PM, where the fraction is given in %), or the ratio *f* of the total flow volume to the volume of the exponential part. The water has a wide range of ages, but, because part of the flow is piston flow, the age distribution has a minimum age (no water can be younger than the time necessary to pass through the piston flow part). The piston flow part can be represented by a partly confined flow with no vertical input of young water from the surface, or it can be represented by a significant unsaturated zone with vertical piston flow towards the water table and mixing of different ages below the water table.

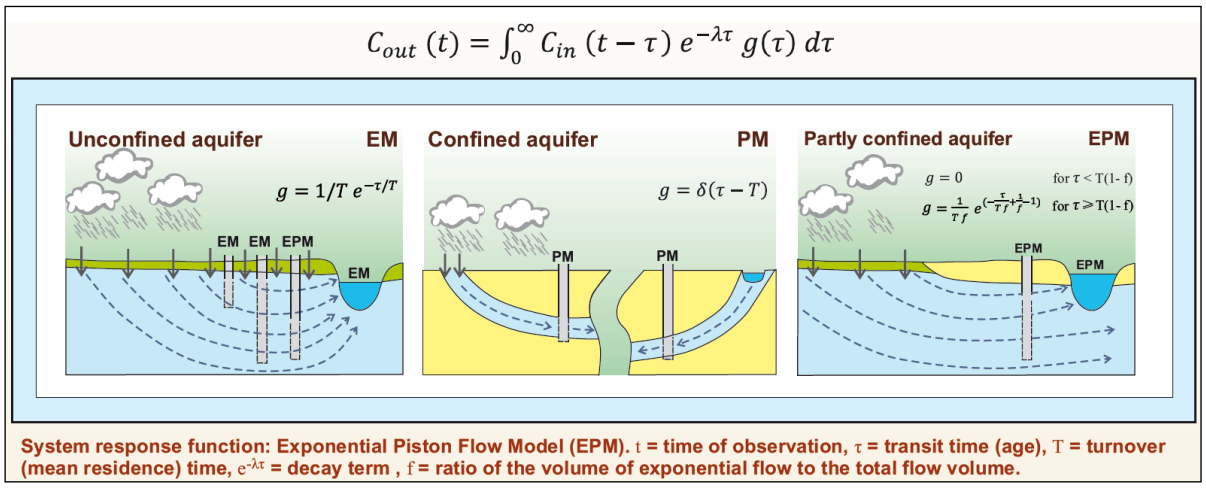

Figure A1.2 Schematic groundwater flow scenarios and corresponding age distribution functions (see Małoszewski and Zuber [1982] for theoretical background).

As an example, the age distribution for an EPM for different fractions of mixed flow is shown in Figure A1.3 for water with a MRT of 50 years. Water with a high fraction of exponential flow of 90% has a wide range of ages, starting at five years, and still significant contributions of old water with ages over 150 years. Despite the MRT of 50 years, most of the water is younger than 50 years. The water can therefore be partly contaminated before the MRT of 50 years has elapsed. About 2% of the water can already be contaminated after five years. With each further year, these young fractions accumulate and increasingly contaminated water arrives at the spring or well. The total fraction of water within a certain age range can be obtained by integrating the age distribution over the specified age range. This is equal to the area below that part of the curve, with the total area below the whole curve being the 100% water fraction. The fraction of water that is younger than a specified age is called the young water fraction (yf). The young water fraction younger than 55 years is about 80% in the example in Figure A1.3 (hatched area).

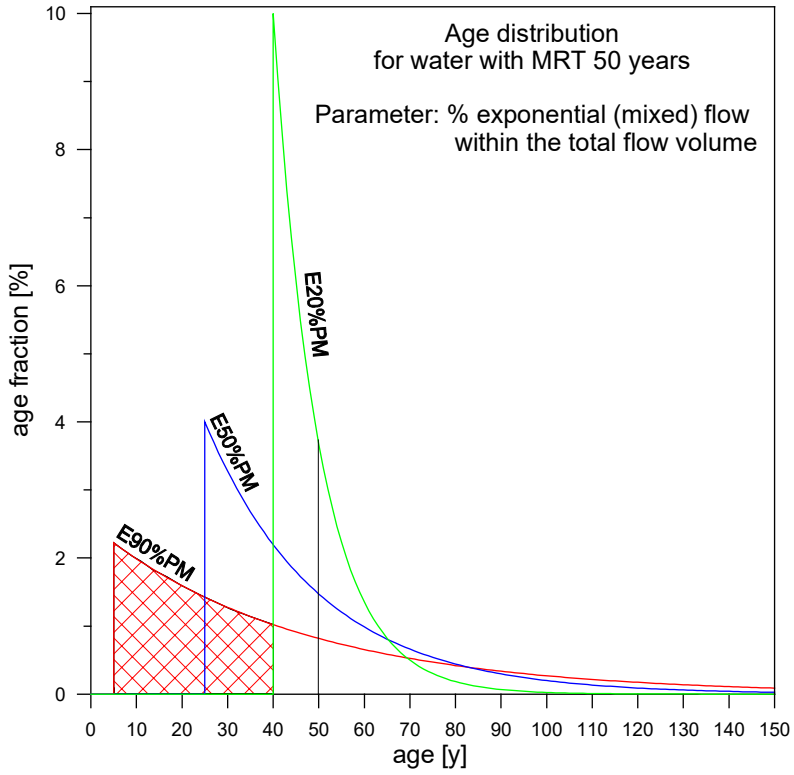

Figure A1.3 Age distributions for the exponential piston flow model.

In a flow situation with less exponential flow, the age distribution of the water has a narrower spread. At 50% exponential flow, the minimum age is 25 years, and the water does not contain significant fractions older than 150 years. At only 20% exponential flow, the age distribution is relatively peaked around the MRT. The minimum age is 40 years, and there is an insignificant amount of water older than 100 years. This water would just start to show a contaminant introduced 40 years ago, but this contaminant would arrive in a relatively sharp front, with a 10% contribution in the first year of arrival after 40 years' time.

A1.3 Constraining Complex Age Distributions

Simple LPMs can often match well with the measured time-varying age-tracer concentrations and are therefore a good representation of the groundwater mixing at these sites. Usually a few tracer data (time-series and/or multi-tracer) can constrain both parameters.

However, with larger datasets of age-tracer data throughout New Zealand becoming available now – including tritium, SF_6, CFCs and, recently, Halon-1301, as well as time-series of these tracers – for a number of wells the groundwater ages using a simple LPM are inconsistent between the different tracer methods. Contamination or degradation of individual tracers is unlikely because the different tracers show consistent trends over years and decades. This points toward more complex mixing of groundwaters with different ages for such wells than represented by the simple LPMs.

Binary (or compound) mixing models are able to represent a more complex mixing, with mixing of water of two different age distributions. The problem related to these models is that they usually have five parameters, which makes them data-hungry and therefore difficult to constrain all parameters. Two or more age tracers with different input functions, with multiple measurements over time, can provide the required information to constrain the parameters of the binary mixing model. Figure A1.4 shows an example for a well in the Heretaunga Plains aquifer for which tritium time-series encompassing the passage of the bomb-tritium through the aquifer, and SF_6 with its steep gradient currently in the input, have been able to constrain the five parameters of a binary mixing model.

The tritium time series (1–5) can be matched with the EPM mixing model, commonly applied to such hydrogeological settings, with an MRT of 42 years (blue curve). However, the 2016 tritium data point (6) indicates that this model is not sufficient. Tritium no longer matches the proposed EPM model, as indicated by the mismatch of the model output (blue line) with the measured data (red points). The measured tritium in 2016 is too high for this model. Using a simple EPM model, the 2016 tritium concentration (6) indicates that the water is younger (pink curve). Furthermore, the SF_6 data (7+8) do not match the blue model curve in this example. SF_6 concentrations are too high to be consistent with such old water. The measured SF_6 concentrations (7+8) would also not match a younger EPM age model (pink curve). However, the consistent trend of the SF_6 data indicated that the SF_6 data are not affected by contamination and can be considered robust.

Only by using more complex binary mixing models, with a parallel connection of two EPMs, was it possible to obtain good fits between the model outputs and the measured data. Such a model is able to match all the data 1–8 (green curve), tritium time-series and SF_6. The hydrogeological explanation for such binary mixing models is that, in some wells, young water from shallow aquifers is mixed with older water from deeper aquifers due to two screens.

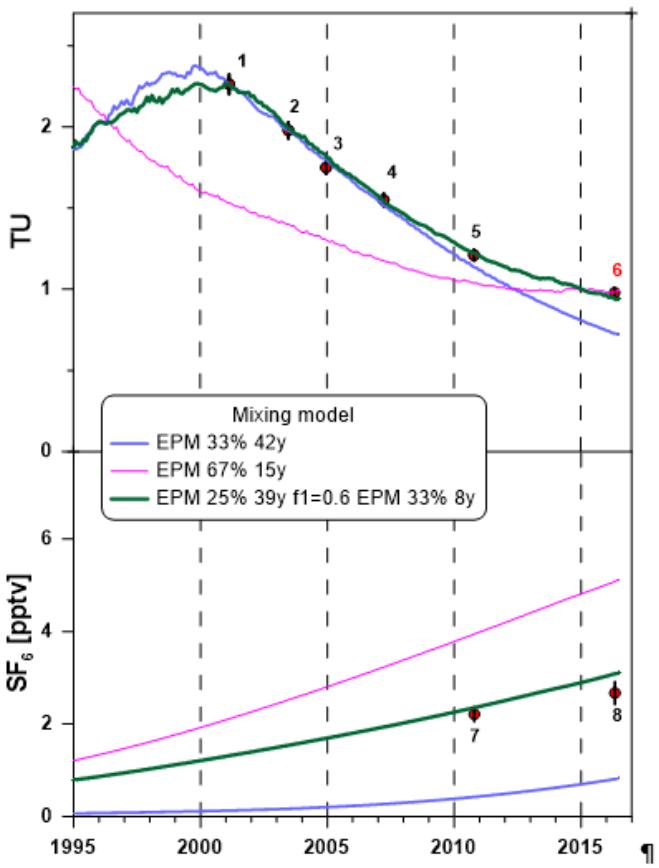

Figure A1.4 Age interpretation of Hastings District Council drinking water bore at Tucker Lane, Clive.

APPENDIX 2 AGE-TRACER RESULTS REPORTS

The following age-tracer results are provided as file attachments to the PDF of this report:

- GNS SR2022-63 – CFC Analysis
- GNS SR2022-63 – Radon Analysis
- GNS SR2022-63 – SF_6 Analysis
- GNS SR2022-63 – Tritium Analysis.

www.gns.cri.nz

Principal Location

1 Fairway Drive, Avalon
Lower Hutt 5010
PO Box 30368
Lower Hutt 5040
New Zealand
T +64-4-570 1444
F +64-4-570 4600

Other Locations

Dunedin Research Centre
764 Cumberland Street
Private Bag 1930
Dunedin 9054
New Zealand
T +64-3-477 4050
F +64-3-477 5232

Wairakei Research Centre
114 Karetoto Road
Private Bag 2000
Taupo 3352
New Zealand
T +64-7-374 8211
F +64-7-374 8199

National Isotope Centre
30 Gracefield Road
PO Box 30368
Lower Hutt 5040
New Zealand
T +64-4-570 1444
F +64-4-570 4657